SYNTHESIS AND INVESTIGATION OF ORGANOFLUOROSILICATE AND ORGANOFLUOROGERMANATE SPECIES

Jan Gnidovec

Doctoral Dissertation
Jožef Stefan International Postgraduate School
Ljubljana, Slovenia

Supervisor: Assoc. Prof. Dr. Gašper Tavčar, Jožef Stefan International Postgraduate School and Jožef Stefan Institute, Ljubljana, Slovenia

Evaluation Board:
Asst. Prof. Dr. Evgeny Goreshnik, Chair, Jožef Stefan International Postgraduate School and Jožef Stefan Institute, Ljubljana, Slovenia

Prof. Dr. Uroš Grošelj, Member, Faculty of Chemistry and Chemical Technology, University of Ljubljana, Ljubljana, Slovenia

Prof. Dr. David Vicic, Member, Lehigh University, Bethlehem, Pennsylvania, USA

MEDNARODNA PODIPLOMSKA ŠOLA JOŽEFA STEFANA
JOŽEF STEFAN INTERNATIONAL POSTGRADUATE SCHOOL

Jan Gnidovec

SYNTHESIS AND INVESTIGATION OF ORGANOFLUOROSILICATE AND ORGANOFLUOROGERMANATE SPECIES

Doctoral Dissertation

SINTEZA IN RAZISKAVA ORGANOFLUOROSILIKATNIH IN ORGANOFLUOROGERMANATNIH ZVRSTI

Doktorska disertacija

Supervisor: Assoc. Prof. Dr. Gašper Tavčar

Ljubljana, Slovenia, April 2025

Acknowledgments

I am deeply grateful to my family and friends for their love and support throughout my doctoral journey. Your encouragement, understanding and belief in me have motivated me to complete this journey. Your presence reminds me of the important things in life, and I am eternally grateful for your presence in my life.

I would also like to express my sincere gratitude to my dedicated mentor and supportive coworkers. Their guidance and encouragement throughout my studies have been invaluable. Their willingness to share their knowledge with me, engage in thoughtful discussions and provide constructive feedback has also enriched my learning experience. I am very grateful for their professional support and the invaluable contributions they have made to my academic journey.

Abstract

Fluorine, though abundant on Earth, is not readily available in a form suitable for organic synthesis. While fluoride salts like fluorite exist, they have limited reactivity due to solubility properties. Converting fluorite to hydrofluoric acid (HF) or fluorine gas (F_2) increases reactivity but introduces significant safety concerns due to the corrosive and toxic natures of their products.

A more practical approach to fluorination is to use pre-fluorinated starting materials. However, these are often limited in availability and scale. Late-stage fluorination methods offer an alternative but can suffer from low atom economy and functional group compatibility issues. Therefore, developing new, efficient, and selective fluorination methods remains a crucial goal in organic synthesis.

This dissertation aims to expand the knowledge of nucleophilic fluorination reagents, especially those based on masked fluoride compounds such as organofluorosilicates and organofluorogermanates. While organofluorosilicates have been extensively studied, organofluorogermanates are still relatively unexplored as only a few structurally characterised compounds are known. In addition, most known organofluorogermanates contain strongly electron-withdrawing groups, which limits their potential as fluorinating agents. This research aims to fill this gap by synthesising new organofluorosilicate and organofluorogermanate species with different structural features.

In the first part of this study, we prepared new discrete organofluorosilicate and organofluorogermanate species with an imidazolium countercation. The target compounds were synthesised from commercially available organochlorosilanes and organochlorogermanes with a focus on compounds containing more electron-donating substituent groups to increase fluoride-donating potential. Using alkali metals and imidazolium fluoride reagents, five new organofluorosilicates and two new organofluorogermanate salts were successfully synthesised and structurally characterised.

In the study of imidazolium-based organofluorosilicates and organofluorogermanates, we observed unexpectedly low yields in reactions of organochlorosilanes and organochlorogermanes with alkali metal fluorides. Further investigations, including NMR spectroscopy and single-crystal X-ray diffraction, revealed the formation of polymeric alkali metal-based organofluorosilicates and organofluorogermanates as by-products.

The second part of this study focussed on the investigation of the conditions for this reaction and the synthesis of new such species, which had previously been reported only once for an organofluorosilicate compound. Detailed NMR studies showed that alkali metal fluorides are differently reactive, with heavier metal fluorides generally exhibiting higher reactivity. In addition, we have successfully isolated new polymeric organofluorosilicate and organofluorogermanate compounds and structurally characterised them using X-ray diffraction.

Povzetek

Fluor, čeprav je na Zemlji zelo razširjen, ni v naravi na voljo v obliki, primerni za organsko sintezo. Čeprav obstajajo fluoridi, kot je kalcijev fluorid, pogosto niso dovolj reaktivni za potrebe organske sinteze. Pretvorba fluorita v fluorovodikovo kislino (HF) ali plinast fluor (F_2) poveča reaktivnost, vendar prinaša velike varnostne težave zaradi njihove korozivnosti in toksičnosti.

Bolj praktičen pristop je uporaba že fluoriranih izhodnih materialov. Na žalost so ti materiali pogosto nedostopni v zadostnih količinah. Metode poznega fluoriranja so privlačna alternativa, ki pa ni ugodna zaradi nizke atomske ekonomije in težav s kompatibilnostjo funkcionalnih skupin. Zato ostaja razvoj novih učinkovitih in selektivnih metod fluoriranja ključnega pomena v organski sintezi.

Namen te disertacije je razširiti znanje o nukleofilnih fluorirnih reagentih, zlasti tistih, ki temeljijo na maskiranih fluoridih, kot so organofluorosilikati in organofluorogermanati. Medtem ko so organofluorosilikati obsežno preučeni, so organofluorogermanati še vedno relativno neraziskani, saj je znanih le nekaj strukturno karakteriziranih spojin. Poleg tega večina znanih organofluorogermanatov vsebuje močno elektron-privlačne skupine, ki jih stabilizirajo in s tem omejujejo njihov potencial za uporabo pri fluoriranju. Ta raziskava si prizadeva zapolniti to vrzel s sintezo novih organofluorosilikatnih in organofluorogermanatnih zvrsti.

V prvem delu te raziskave so bile pripravljene nove diskretne organofluorosilikatne in organofluorogermanatne zvrsti z imidazolijevim kationom. Ciljne spojine so bile sintetizirane iz komercialno dostopnih organoklorosilanov in organoklorogermanov s poudarkom na spojinah, ki vsebujejo več elektrondonorskih skupin za povečanje potenciala za doniranje fluorida. Z uporabo alkalijskih kovin in imidazolijevih fluoridnih reagentov je bilo uspešno sintetiziranih in strukturno karakteriziranih pet novih organofluorosilikatov in dve novi organofluorogermanatni soli.

Pri preučevanju imidazolijevih organofluorosilikatov in organofluorogermanatov so bili opaženi nenavadno nizki izkoristki pri reakcijah organoklorosilanov in organoklorogermanov z alkalijskimi fluoridi. Nadaljnje preiskave, vključno z NMR spektroskopijo in rentgensko difrakcijo, so pokazale nastanek polimernih organofluorosilikatov in organofluorogermanatov z alkalijskimi kovinami kot protiioni.

Drugi del te študije se je osredotočil na preučevanje reakcijskih pogojev za to reakcijo in sintezo novih takšnih polimernih zvrsti. Doslej je bila objavljena le ena taka organofluorosilikatna spojina. Podrobne raziskave s pomočjo NMR spektroskopije so pokazale, da so alkalijski fluoridi različno reaktivni, pri čemer težji kovinski fluoridi na splošno kažejo višjo reaktivnost. V sklopu tega dela je bila uspešna izolacija treh novih polimernih organofluorosilikatov in organofluorogermanatov in njihova strukturna karakterizacija z rentgensko difrakcijo.

Contents

List of Figures

List of Schemes

List of Tables

Abbreviations

Acetone-d_6 ... deuterated acetone
Bu ... butyl group
C_6D_6 ... deuterated benzene
CD_2Cl_2 ... deuterated dichloromethane
CD_3CN ... deuterated acetonitrile
$CDCl_3$ ... deuterated chloroform
DAST ... diethylaminosulfur trifluoride
DFT ... density functional theory
DMSO-d_6 ... deuterated dimethyl sulfoxide
Et ... Ethyl group
FEP ... fluorinated ethylene propylene
i-Pr ... isopropyl group
IPr ... 1,3-bis(2,6-diisopropylphenyl)imidazol-2-ylidene
IUPAC ... International Union of Pure and Applied Chemistry
Me ... methyl group
MeCN ... acetonitrile
MeOD-d_4 ... deuterated methanol
NFPy ... *N*-fluoropyridinium salts
NFSI ... *N*-fluorobenzenesulfonimide
NMR ... nuclear magnetic resonance
PET ... positron emission tomography
Ph ... phenyl group
pKa ... acid dissociation constant
PP ... polypropylene
PTFE ... polytetrafluoroethylene
SPS ... solvent purification system
TBAF ... tetraalkylammonium fluoride
TBAT ... tetrabutylammonium difluorotriphenylsilicate
THF ... tetrahydrofuran
THF-d_8 ... deuterated tetrahydrofuran
TMS ... tetramethylsilane

Symbols

M ... metal or metalloid (alkali metal fluorides, Si, Ge)
n ... number
R ... alkyl or aryl group
X ... leaving group (halide or sulfonate)
$t_{1/2}$ ... half-life

Chapter 1

Introduction

1.1 Omnipresence of Fluorine

Since its first isolation, fluorine has played an important role in the development of our civilisation, even though it is dangerous to handle and difficult to use in its elemental form. Mankind's expertise in handling fluorine in many of its forms has led to the widespread use of fluorine compounds in various commercial applications, from steelmaking and nuclear engineering to the polymer, pharmaceutical and agrochemical industries. More recently, the use of fluorine has also opened up numerous other technologically advanced areas such as medicine and solar cell technology.

In the pharmaceutical and agrochemical industries, the incorporation of fluorine into drugs and agrochemicals imparts many desirable properties such as metabolic stability, hydrophobicity, pKa and conformational control [1]–[4].

Once drugs enter the body, they are subject to physiological reactions leading to the elimination of the drug compound from the body. Although drugs can be excreted in unchanged form, they are more often metabolised first. One group of enzymes often responsible for metabolising drugs are the cytochrome P450 monooxygenases, which oxidise their substrates, making them less lipophilic and consequently accelerate their elimination from the body. For drugs to work well, they need time to cause the desired effect. As such, the metabolic stability of these compounds is of great importance. Metabolic stability can be increased by replacing labile functional groups with fluorine [2].

Hydrophobicity is another important characteristic for orally administered drugs. Ingested drugs are absorbed and distributed by active or passive transport. The more common passive transport depends on the permeability of cell membranes. Drugs must be hydrophobic enough to pass through cell membranes and be absorbed, but not too high to become trapped in fatty lipid particles. [2] Generally, fluorination is expected to increase the hydrophobicity of a molecule, although this is not always the case. It has been shown that monofluorination or trifluoromethylation of saturated alkyl groups can sometimes lead to lower hydrophobicity due to the introduction of a strongly electron-withdrawing group [5].

Like hydrophobicity, the pKa value also has an effect on the absorption process. Therefore, drugs can be modified with fluorine to improve their bioavailability, and by adjusting the pKa value, the pharmacokinetic properties of drug molecules can be significantly improved. Since fluorine has a strong modifying effect on the acidity and basicity of neighbouring functional groups, it can be used to regulate the pKa and thus increase the absorption of orally ingested drugs [6].

Finally, newly introduced fluorine-containing groups can have steric or electronic effects on the drug molecule, leading to changes in the preferred molecular conformation. This can be utilised to trigger more efficient binding to the target protein [7].

All the above properties make organofluorine compounds highly desirable chemical raw materials for the development of new drugs. Unfortunately, almost all terrestrial fluorine is in insoluble form, making it unavailable to bioorganisms. Due to the lack of readily available raw materials, the first fluorine-containing drugs were not developed until late 1950s. Since then, the share of fluorine-containing pharmaceuticals and agrochemicals has grown rapidly and accounted for more than a quarter of the market for pharmaceuticals and agrochemicals [8]–[10]. In recent years, this share is likely to increase even further, as around one third of new small molecule drugs approved for treatment by the Food and Drug Administration (FDA) contain fluorine [11]. Some examples are shown in Figure 1.1.

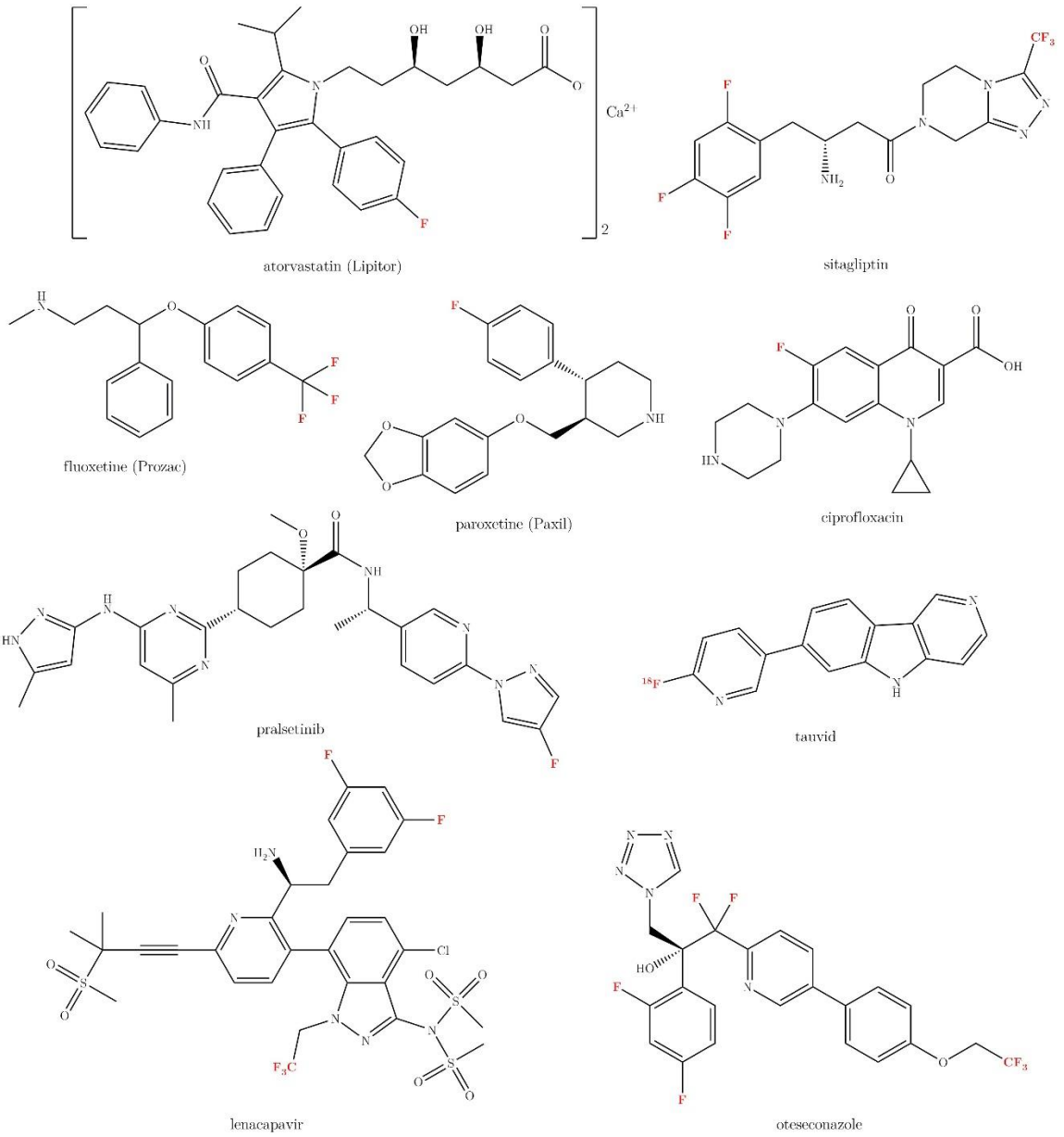

Figure 1.1: Fluorine containing pharmaceuticals.

These include atorvastatin (for the treatment of cardiovascular disease) [12], ciprofloxacin (antibacterial) [13], fluoxetine (antidepressant) [14], pralsetinib (for the treatment of metastatic lung cancer) [15], tauvid (positron emission tomography imaging probe for the treatment of Alzheimer's disease) [16], lenacapavir (HIV antiretroviral) [17] and oteseconazole (antifungal) [18]. The drugs mentioned above are an example of the wide range of great successes of fluorinated medical drugs.

The introduction of fluorine into organic frameworks is of increasing interest, not only for the improvement of active substances, but also for analytical purposes through the use of the radionuclide ^{18}F in positron emission tomography (PET). This is a non-invasive medical imaging procedure in which radioactive substances are used to monitor metabolic processes in *vivo* [19], [20]. The radionuclides used in PET are relatively short-lived, with the average half-life measured in minutes: $^{11}C(t_{1/2} = 20$ min), $^{13}N(t_{1/2} = 10$ min), $^{15}O(t_{1/2} = 2$ min), and $^{18}F(t_{1/2} = 110$ min) [2]. Before these radioisotopes can be incorporated into tracer molecules, they are first produced in cyclotrons. A major advantage of ^{18}F radiotracers is the significantly longer half-life of ^{18}F compared to other commonly used radioisotopes, which makes them easier to handle.

This brief overview of fluorinated compounds in medicinal chemistry demonstrates the importance of progress in the field of fluorine chemistry. Although massive progress has been made, mastering the introduction of fluorine into new organic compounds can still be considered very important for human development.

1.1.1 Fluorination reagents

When considering incorporating fluorine into new compounds, it is best to consider the fluorine sources from which fluorine-containing functional groups are introduced. Although fluorine is the 13th most abundant element on earth, there are very few natural biological processes that include fluorine, and as such, organofluorine compounds are very rare [21]. Thus, fluorine occurs in nature exclusively in the form of fluoride salts such as cryolite (Na_3AlF_6), fluorapatite ($Ca_5(PO_4)_3F$) and calcium fluoride (CaF_2), also known as fluorite or fluorspar [22]–[24]. Although it is a strategic material, more than 90% of fluorspar is produced in China, Mexico and Mongolia.

Fluorite itself however, is not a suitable as a reagent in synthetic chemistry due to its lack of reactivity. To improve reactivity, the fluorite is reacted with a strong acid such as sulfuric acid to generate hydrofluoric acid (HF), which is produced in large quantities for many industrial applications [25]. Regrettably, HF is not an ideal reagent due to its high reactivity, corrosiveness and toxicity; it reacts with glass, penetrates the skin and causes severe burns [26].

Fluorine gas (F_2) is an alternative source of fluorine, but like the hydrofluoric acid from which it is made, fluorine gas is highly toxic and requires specialised equipment to handle, so it is rarely used outside of specialised laboratories and manufacturing facilities.

A good way to introduce fluorine into complex compounds is to start the synthesis with compounds that already contain desirable fluorinated functional groups. Unfortunately, starting materials are not always available in the quantities required for industrial scale. To avoid this problem, many late stage fluorination methods have been developed to allow the fluorination of complex compounds. Unfortunately, current methods for this type of fluorination suffer from poor atom economy and other green chemistry criteria. In addition, fluorination is further complicated for complex molecules with numerous functional groups.

For this reason, the search for new practical synthesis methods with high yields and good tolerance to a large number of functional groups is still ongoing. This is of crucial importance as the purification of fluorinated compounds is difficult when they are present in a mixture with their non-fluorinated precursor.

In organic chemistry, there are three commonly used pathways for the formation of carbon-fluorine bonds and the introduction of fluorine into organic compounds: nucleophilic, electrophilic and radical fluorination [27].

1.1.2 Nucleophilic fluorination

Nucleophilic fluorination is a reaction between the nucleophilic fluoride ion and the electrophilic substrate. A general reaction scheme of the reaction is shown in Scheme 1.1.

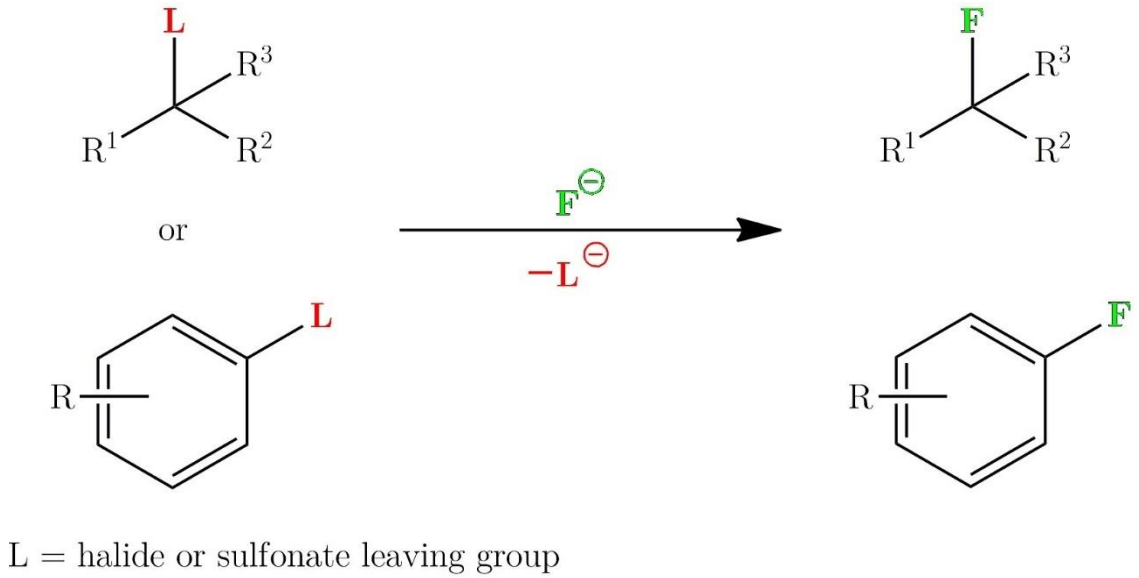

Scheme 1.1: General nucleophilic fluorination reaction scheme.

Nucleophilic fluorination involves the nucleophilic attack of a fluoride anion on an electrophilic substrate. The substrate, often an alkyl or aryl compound bearing a suitable leaving group, is substituted by the fluoride anion. The most commonly used sources of fluoride anions are alkali metal fluorides (especially KF and CsF), HF-containing reagents (KHF_2, $Et_3N{\cdot}3HF$), tetraalkylammonium fluorides. (e.g. TBAF – tetraalkylammonium fluoride), hypervalent fluorosilicates (e.g. TBAT – tetrabutylammonium difluorotriphenylsilicate) and fluorostannates. A list of examples can be found in Figure 1.2.

An alternative form of nucleophilic fluorination, in which alcohols are substituted with fluorine, is called deoxyfluorination. A general reaction process is shown in Scheme 1.2.

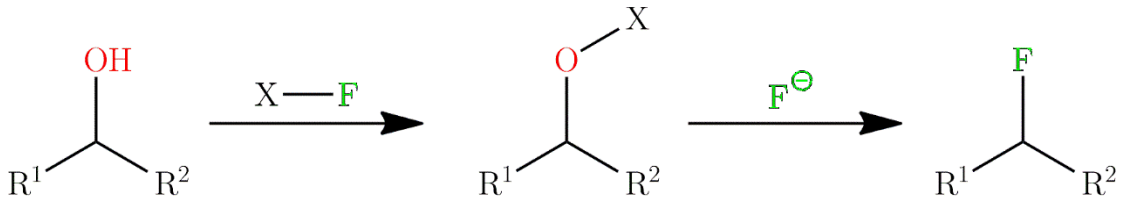

Scheme 1.2: General reaction scheme of deoxyfluorination.

Deoxyfluorination is a nucleophilic fluorination reaction in which the nucleophilic hydroxyl group of the alcohol attacks the electrophilic part of the deoxofluorinating agent, resulting in the formation of an activated alcohol intermediate and a fluoride anion. In the second step, the released fluoride ion acts as a nucleophile and displaces the leaving group

from the activated alcohol, leading to the formation of the desired alkyl fluoride. Common reagents for this reaction are DAST [28] and Deoxo-Fluor [29], as well as the recently developed PyFluor [30], AlkylFluor [31] and PhenoFluorMix [32], which are also shown in Figure 1.2.

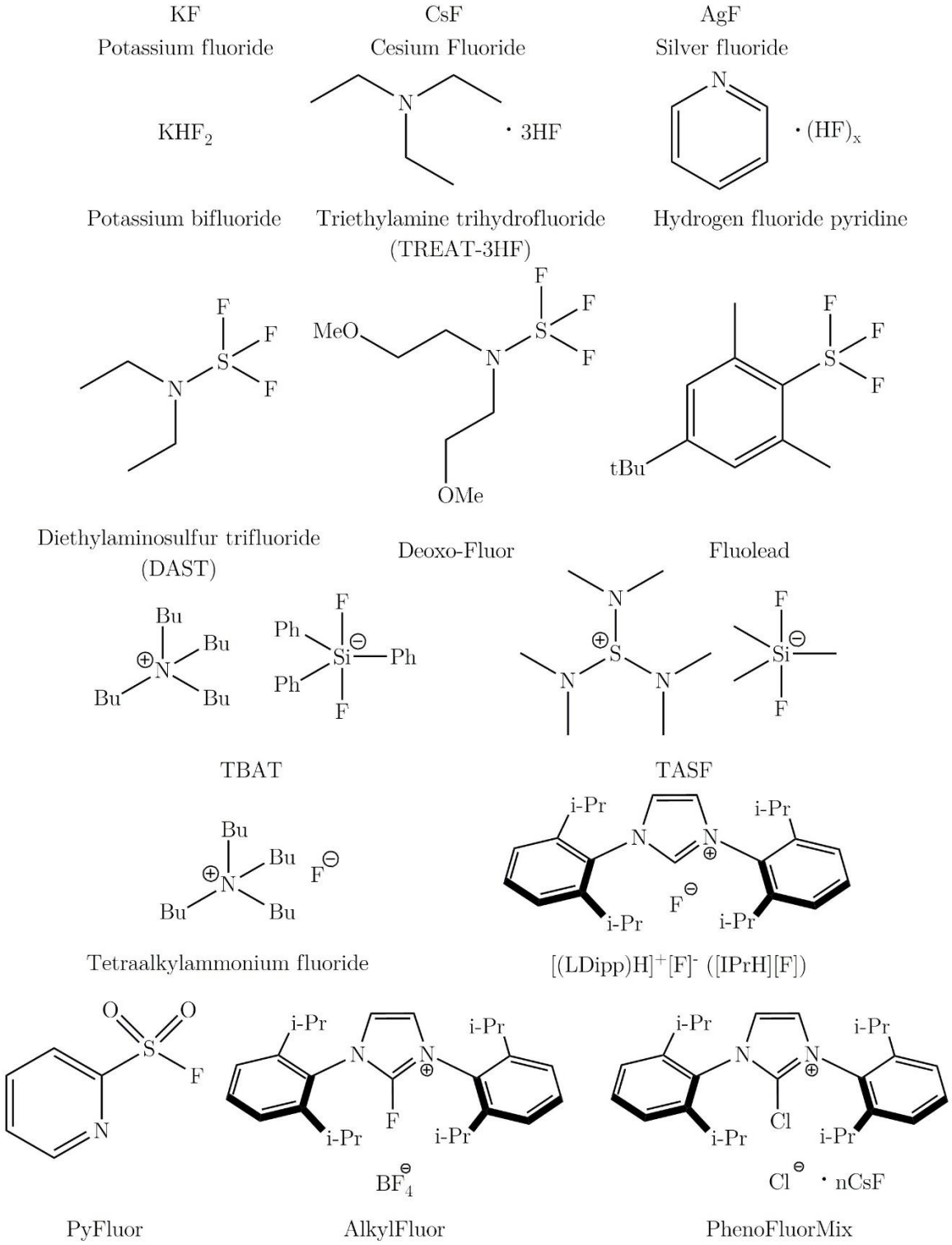

Figure 1.2: Examples of nucleophilic fluoride sources: Metal fluorides, HF-containing reagents, sulphur trifluorides, organofluorosilicates, organic fluoride salts and commercially available deoxyfluorination reagents.

1.1.3 Electrophilic fluorination

In electrophilic fluorination, the roles of substrate and fluorine source are reversed: During the reaction, a nucleophilic substrate attacks an electrophilic fluorine source ("F^+"). The substrate can be a carbanion, an electron-rich unsaturated compound such as an arene, alkene or alkyne or a compound with a weak bond such as C—Si, C—Sn or C—B, which can be easily broken [33]. General reaction procedures are shown in Scheme 1.3.

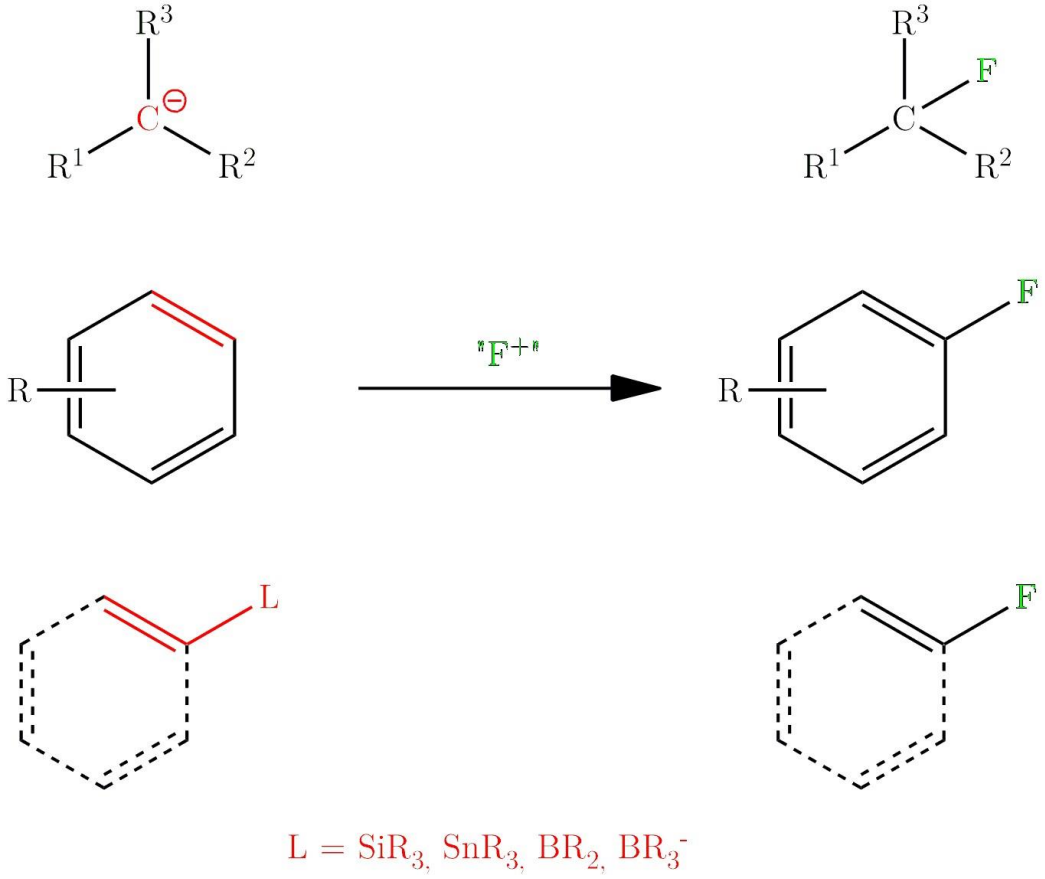

Scheme 1.3: General reaction procedures of electrophilic fluorination.

Despite the term "electrophilic fluorine", an F^+ species is not known, and the reaction mechanism occurs via a single-electron transfer or via an S_N2 mechanism. This depends on the reaction conditions used as well as the substrate and the electrophilic fluorine source used in the reaction.

Early electrophilic fluorinating agents, such as those containing O—F or Xe—F bonds (e.g. CF_3OF [34], ClO_3F [35], CF_3COOF [36], $CsSO_4F$ [37] and XeF_2 [38]), were often too reactive and consequently unselective or difficult to handle. Elemental fluorine (F_2) is effective in these types of reactions, but its safe handling requires specialised techniques and equipment, making it less accessible for widespread use.

A significant advancement in this field was the development of bench-stable *N*-F reagents [39]. These reagents are selective, easy-to-handle sources of electrophilic fluorine, many of which are commercially available and, unlike the examples listed above, do not require special handling and can be used safely in glassware. Prominent examples of this class of reagents are NFPy (*N*-fluoropyridinium salts) [40], NFSI (*N*-fluorobenzenesulfonimide) [41], Selectfluor [42] and its analogue Accufluor [43], which are shown in Figure 1.3 along with other examples of electrophilic fluorine sources.

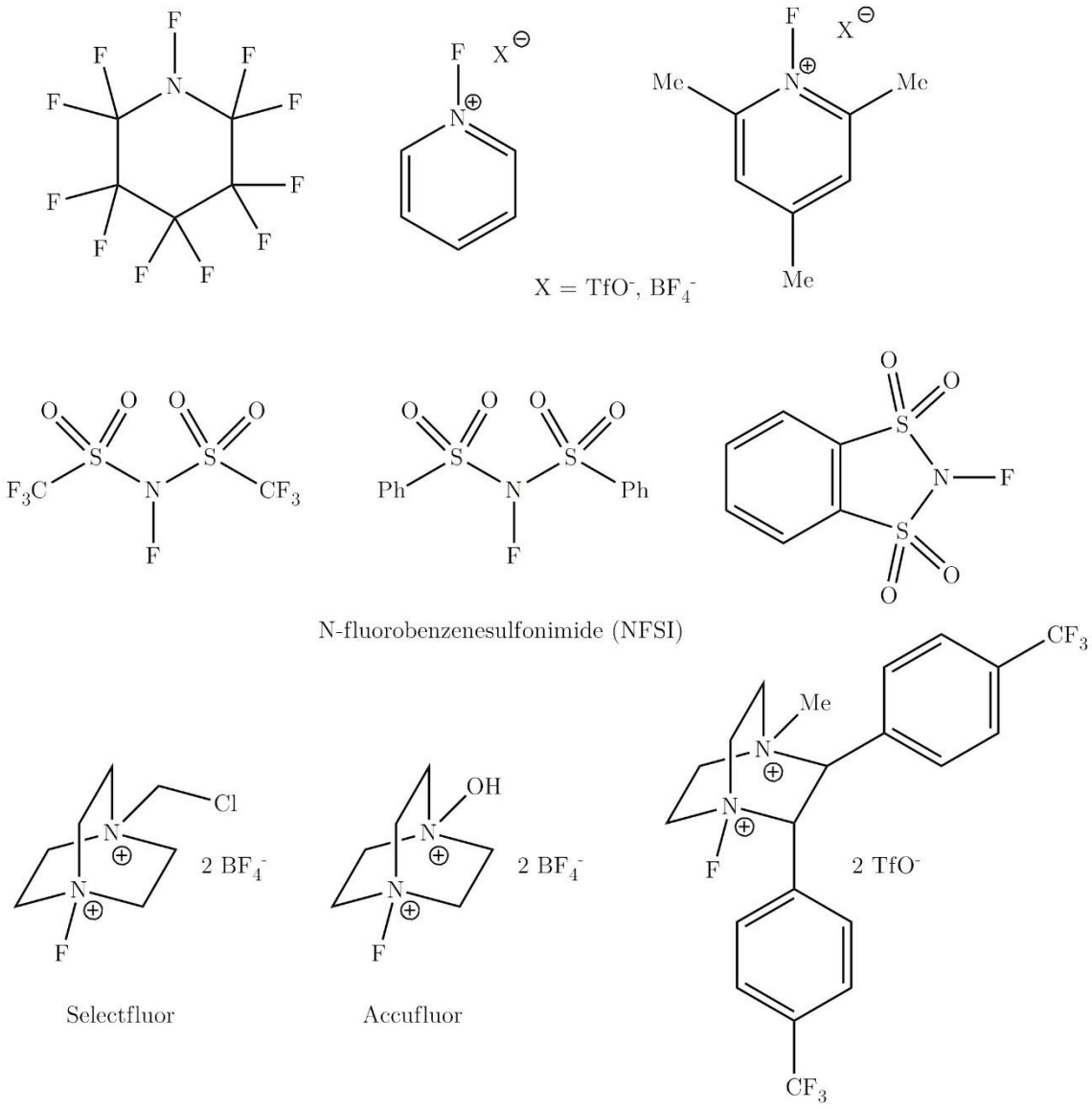

Figure 1.3: Examples of N−F electrophilic fluoride sources: *N*-fluoropyridinium salts, *N*-fluorosulfonimides and Selectfluor and its derivatives.

1.1.4 Radical fluorination

Radical fluorination is a fluorination method in which an atomic fluorine species reacts with a carbon-based radical, resulting in the formation of a C−F bond [44]. Compared to the two previously described methods, radical fluorination is rarely encountered as the atomic fluorine sources are limited to hypofluorites, molecular F_2 and XeF_2 [45]–[47]. These reagents are often unsuitable due to their price, low selectivity or hazardous properties.

More recently, it has been shown that some N−F electrophilic fluorine sources [48] and fluorinated solvents [49] can also act as fluorine transfer agents, drastically improving the prospects of this method. Unfortunately, these second-generation radical fluorination reagents often have the disadvantage that they require transition metal catalysts and can be limited by their highly electrophilic and oxidative nature. Research in this area is ongoing as a third generation of reagents that function under mild reaction conditions is being developed [50].

1.2 Organofluorosilicates

Organofluorosilicates, silicon-based anions with the general formula $[R_{5-n}SiF_n]^-$ or $[R_{6-n}SiF_n]^{2-}$, where n ranges from 1 to 5, have a central silicon atom surrounded by up to six carbon and fluorine ligands. Depending on the number of ligands, these anions can be divided into two categories:

Pentacoordinated organofluorosilicates: these anions have a trigonal bipyramidal geometry and carry a −1 charge. In this configuration, the fluorine atoms normally occupy the axial positions. Approximately 80 structurally characterised compounds belong to this category.

Hexacoordinated organofluorosilicates: These anions have an octahedral geometry and carry a −2 charge. Only seven such compounds have been structurally characterised [51]–[54].

While pentacoordinated organofluorosilicates are more common, both types offer unique structural and chemical properties. With their loosely bound fluoride anion, organofluorosilicates are attractive fluoride ion donors for nucleophilic fluorination reactions [55], [56]. Recent studies have also shown the potential of organofluorosilicates as promising precursors for coupling and oxidation reactions [57], [58]. Examples of penta- and hexacoordinated organofluorosilicate anions are listed in Figure 1.4.

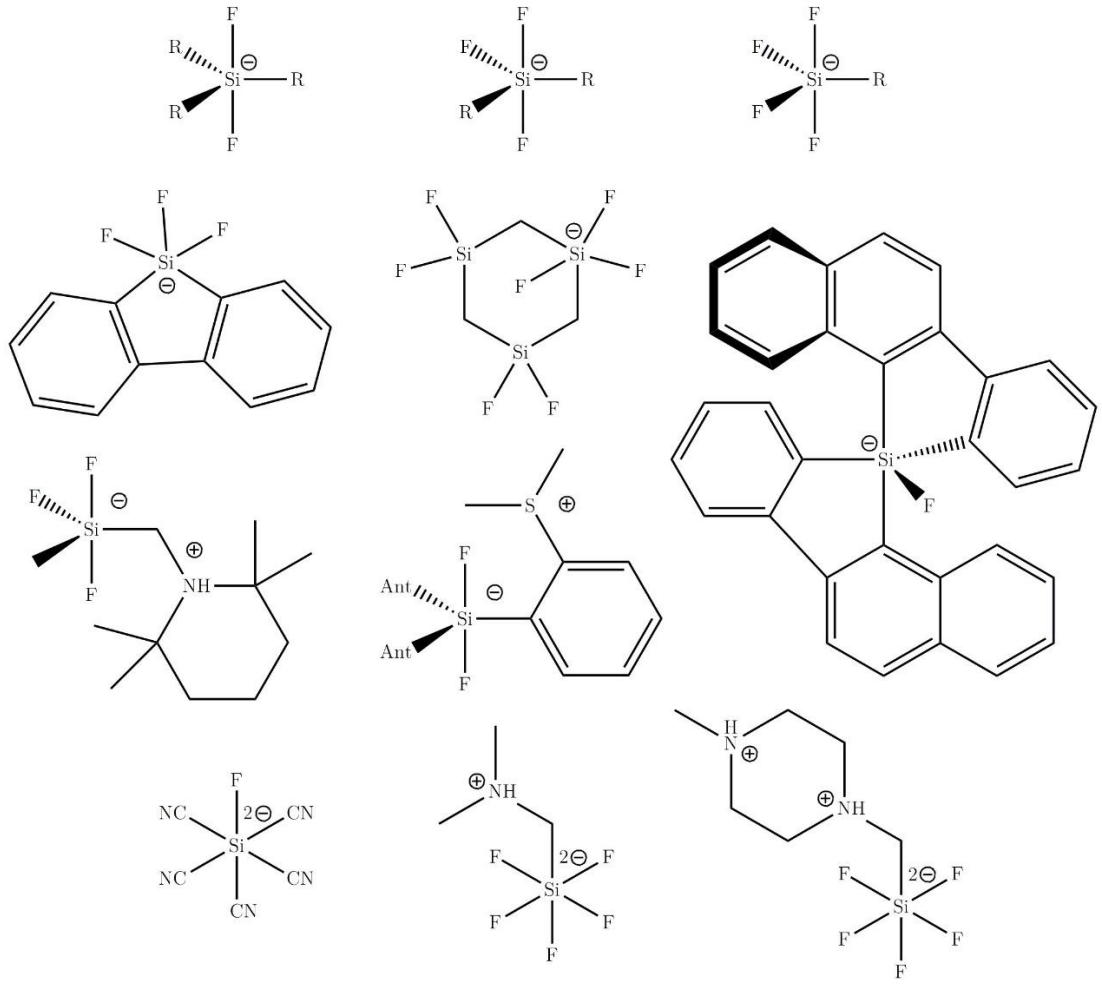

Figure 1.4: Diagrams of different structurally characterised penta- and hexacoordinated organofluorosilicates.

As can be seen from Figure 1.4, organofluorosilicates are generally anionic species, although they can also be neutral, as is the case with zwitterionic organofluorosilicates [59]. As previously mentioned, pentacoordinated organofluorosilicates always have a trigonal bipyramidal structure, with the fluorine atoms generally occupying the axial positions. In one case where the silicon centre was surrounded by bulky bidentate ligands, the fluorine atom was forced into the equatorial position [60]. These compounds contain 1 to 4 fluorine atoms, with the remaining positions occupied by various organic substituents, usually simple alkyl or aryl groups. With more complex ligands, silicon can form heterocyclic structures with bidentate ligands [60]–[63]. In addition, a rather unique organofluorosilicate structure was discovered by Pietschnig and Merz: a polymer with a fluorosilicate backbone and a non-polar shell [64].

Since hexacoordinated organofluorosilicates contain an additional atom in the silicon sphere, the resulting structure takes on an octahedral geometry. Therefore, we can no longer distinguish between axially and equatorially bound ligands. Since there are only 7 structurally characterised hexacoordinated organofluorosilicates, the structural diversity between them is low. In all cases, most if not all ligands consist of strong electron-withdrawing groups such as fluoride or the pseudohalogen cyanide anion. The remaining positions are occupied by organic substituents, some of which contain positively charged groups and thus reduce or completely neutralise the negative charge of the compound [51]–[53].

1.3 Organofluorogermanates

In contrast to organofluorosilicate chemistry, organofluorogermanates with the general formula $[R_{5-n}GeF_n]^-$ or $[R_{6-n}GeF_n]^{2-}$, where n ranges from 1 to 5 have been much less researched. So far, only a few structurally characterised organofluorogermanates such as $[C_{23}H_{17}O][(CF_3CF_2)_3GeF_2]$ [65], $[(CH_3)_4N][(CF_3)_3GeF_2]$ [66] and $K_2[cis\text{-}(CF_3)_2GeF_4]$ [67] have been reported. All structurally characterised cases of organofluorogermanate anions are shown in Figure 1.5.

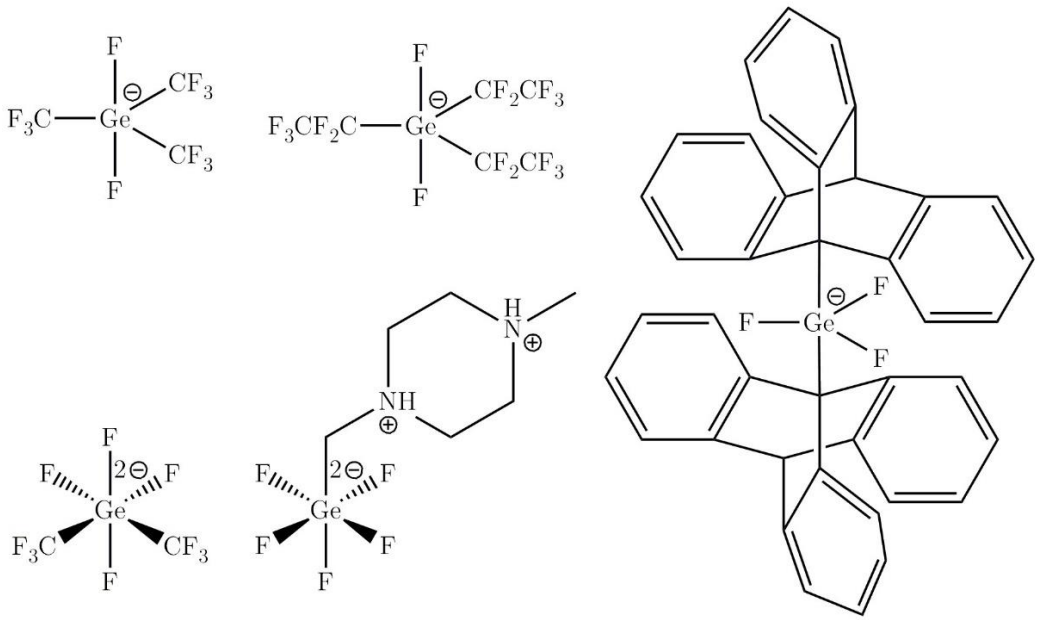

Figure 1.5: Structures of all organofluorogermanate anions structurally characterised so far.

Figure 1.5 describes some known penta- and hexacoordinated organofluorogermanates. Most of the reported anions contain strongly electron-withdrawing groups, such as fluoride and perfluorinated alkyl groups. Similar to organofluorosilicates, organofluorogermanates adopt a trigonal bipyramidal and octahedral geometry for penta- and hexacoordinated compounds, respectively. In trigonal bipyramidal structures, fluorine substituents typically occupy axial positions unless sterically bulky substituents force them into equatorial positions, as shown in the structure with bulky bicyclic substituents in Figure 1.5. In contrast to organofluorosilicates, no polymeric structures similar to the structure reported by Pietschnig and Merz [64] have been observed for organofluorogermanates.

Chapter 1

Aims and Hypothesis

The main objective of this work was the synthesis of new organofluorosilicate and organofluorogermanate species that show promise as nucleophilic fluorinating agents. While organofluorosilicates have been extensively studied, research on organofluorogermanates remains limited as there are few structurally characterised compounds. In addition, most known organofluorogermanates contain strong electron-withdrawing groups, which while enhancing stability, by helping disperse the negative charge of the anion may reduce their fluoride-releasing ability. The aim of this part of research was to test the following hypotheses:

Hypothesis 1: Organofluorosilicate anions become more stable as the number of electron-withdrawing groups (including fluorine) increases.

Hypothesis 2: Despite the lack of structurally characterised organofluorogermanates, the synthesis of new organofluorogermanate salts is possible, even without the use of strongly electron-withdrawing substituents that stabilise the anionic species by reducing the electron density at the central atom.

Alkali metal fluorides, which are readily available and inexpensive, are often used as nucleophilic fluorinating reagents. However, their low solubility can limit their application, so that chelating agents such as crown ethers or cryptands often have to be used. Despite this limitation, they remain popular for halide exchange reactions, where they efficiently replace other halogens with fluorine, regardless of the metal present in the compound.

In this research, unexpectedly low yields were observed in reactions with alkali metal fluorides. Further investigation revealed that these fluorides reacted further with organofluorosilanes and organofluorogermanes, leading to the formation of polymeric organofluorosilicate or organofluorogermanate species.

The final aim of this study was to test the following hypothesis:

Hypothesis 3: Reactions between nucleophilic alkali fluoride reagents and certain inorganic species, especially organochlorosilanes and organochlorogermanes, can lead not only to substitution reactions but also to addition of the fluoride anion, resulting in the formation of organofluorosilicate and organofluorogermanate species.

Chapter 2

Methodology

3.1 General Information

The silicon and germanium compounds used and prepared in this work are sensitive to moisture. For this reason, all manipulations, including synthesis, purification and storage, were carried out under an inert atmosphere of dry argon. The samples were stored in a glovebox (M. Braun). Samples were stored in PP or PTFE containers due to concerns about the reactivity of fluorine-containing compounds with glass. The reactions were carried out in custom-made FEP reaction vessels with PTFE valves. Glassware and stir bars were oven dried at 150 °C, while plastic vessels and PTFE filters were dried overnight at 60 °C and vacuum dried before use.

Solvents were purchased from Acros Organics, Carlo Erba, Deutero, Honeywell, Merck and Sigma-Aldrich. All solvents were degassed and dried before use. Acetonitrile and tetrahydrofuran were purified using a solvent purification system (SPS – Vigor). Other solvents were dried with molecular sieves or distilled from a sodium and benzophenone mixture and degassed by freeze-vacuum-thaw cycles. All solvents except acetone were stored over molecular sieves.

Commercially available chemicals were purchased from Acros Organics, Sigma-Aldrich or Tokyo Chemical Industry (TCI) and were used as received unless otherwise stated. Alkali metal fluorides (LiF, NaF, KF, RbF and CsF) were dried overnight in vacuum at 150 °C. All chemicals were stored in a glovebox (M. Braun).

Reagents not commercially available were prepared as described in the literature: [IPrH][F] [68].

Synthetic procedures and characterisation results for each compound prepared can be found in Appendix A.2.

3.2 NMR Spectroscopy

Samples for NMR analysis were prepared in a glovebox under inert atmosphere with deuterated solvents: CD_3CN, THF-d_8, C_6D_6, MeOD-d_4, DMSO-d_6 and acetone-d_6. Fluorine-containing samples were measured using custom-made FEP inlays for NMR tubes to prevent possible reactions with glass. ^{1}H, ^{13}C and ^{19}F NMR spectra were recorded at the Slovenian NMR Centre (National Institute of Chemistry), using a Bruker AVANCE NEO 400 or 600 MHz NMR spectrometer. The spectra were recorded at 298 K, unless otherwise stated. The chemical shifts of ^{1}H and ^{13}C were referenced to the residual signals of the deuterated solvent and are given relative to tetramethylsilane (TMS). The ^{19}F references were calculated according to IUPAC guidelines and are given relative to $CFCl_3$ in deuterated water [69].

3.3 Raman Spectroscopy

Samples for Raman analysis were prepared under an inert atmosphere in a glovebox. Solid samples were placed in 0.3 mm quartz capillaries and sealed with silicone grease to prevent contact with air. Raman spectra were recorded at room temperature using a Horiba Jobin Yvon Labram-HR spectrometer coupled to an Olympus BXFM-ILHS microscope. The samples were excited with the 633 nm emission line of the He-Ne laser. Before use, the device was calibrated to the peak of the silicon wafer.

3.4 Crystal Structure Determination

Single crystals suitable for X-ray analysis were prepared under an inert atmosphere by slowly evaporating the solvent under static vacuum. The crystals formed were covered with silicon oil to prevent contact with air. Single crystals suitable for X-ray analysis were handpicked under a microscope with a looped pin and mounted onto the diffractometer.

Crystal data were collected on a Gemini A diffractometer equipped with an Atlas CCD detector using graphite monochromated Cu Kα (λ = 1.54184 Å).and Mo Kα radiation (λ = 0.71069 Å). All crystal data were collected at 150 K unless otherwise stated. The data were processed using the CrysAlisPro software package [70]. Analytical absorption correction was applied to all data sets [71]. Structures were solved with the intrinsic phase method using the SHELXT programme [72]. Structure refinement was performed using the SHELXL software implemented in the Olex2 programme package [73], [74]. All non-hydrogen atoms were refined anisotropically. Hydrogen atoms except hydride substituents were assigned ideal positions and refined with a rigid model. The figures were created with Diamond 4.6.4 [75]. The crystallographic data for all compounds is given in Appendix A.3.

3.5 Molecular Calculations

Molecular gas-phase calculations were performed with the programme Gaussian 16 [76] using the Perdew–Burke–Ernzerhof (PBE) exchange-correlation functional [77] and an empirical D3 dispersion correction of Grimme [78] with Becke-Johnson damping [79]. The electrons were described with all electron basis sets. We used the triple-ζ basis set with polarisation functions, in particular Def2-TZVP [80], [81]. We calculated stand-alone $[R_{4-n}SiF_{n+1}]^-$ and $[R_{4-n}GeF_{n+1}]^-$ anions (n = 1−3, R = Et, Ph) as described above. The calculated electronic energies and the calculated reaction energies are shown in Appendix A.3.

Chapter 3

Results and Discussion

4.1 Imidazolium-Based Organofluorosilicate and Germanate salts

This chapter is based on the article "Synthesis of imidazolium-based pentacoordinated organofluorosilicate and germanate salts" in *Dalton Transactions* from 2023 [82] and other so far unpublished results.

In this chapter, the reactivity of organofluorosilanes and organofluorogermanes with imidazolium fluoride reagent [IPrH][F] is presented. A series of organofluorosilicates [IPrH][$R_{4-n}SiF_{n+1}$] (n = 1-3, R = Et, Ph) and organofluorogermanates [IPrH][$Ph_{4-n}GeF_{n+1}$] (n = 1-2) were synthesised by exchanging halides atoms of organochlorosilanes and organochlorogermanes with potassium fluoride, followed by fluorination of organofluorosilanes and organofluorogermanes with imidazolium fluoride [IPrH][F]. Where possible, the products were characterised by X-ray structural analysis and NMR spectroscopy. Structural features of characterised compounds were compared with DFT calculations of structurally optimised organofluorosilicate and organofluorogermanate salts.

4.1.1 Synthesis and crystal structure determination

The detailed synthetic procedures of all compounds are listed in Appendix A.2, along with their characterisation data.

4.1.1.1 [IPrH][Ph_3SiF_2] (1)

In the first step, Ph_3SiCl was added to the acetonitrile suspension of 5 equivalents of KF to ensure the exchange of chlorine with fluorine and generate Ph_3SiF. The reaction mixture was stirred for 24 hours at room temperature. The suspension was filtered and added to a solution of [IPrH][F] in acetonitrile. The reaction mixture was stirred for a further 24 hours. The volatiles were removed under vacuum and crystals of [IPrH][Ph_3SiF_2] (**1**) were formed. The complete synthesis procedure is shown in Scheme 4.1. The crystals were collected and used for X-ray structural analysis, NMR spectroscopy, Raman spectroscopy and mass spectroscopy.

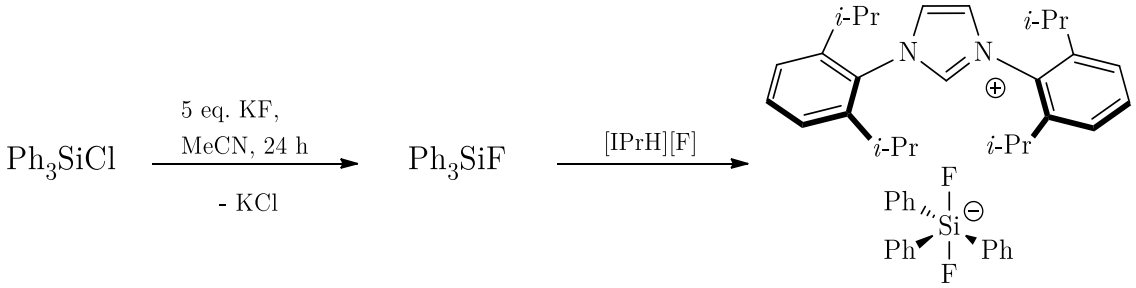

Scheme 4.1: The synthetic procedure for preparation of [IPrH][Ph_3SiF_2] (**1**).

Single crystals of [IPrH][Ph_3SiF_2] (**1**) were formed by slow evaporation of the acetonitrile solvent under static vacuum conditions. It crystallises in the monoclinic space group $P2_1/c$ and its crystal structure is shown in Figure 4.1.

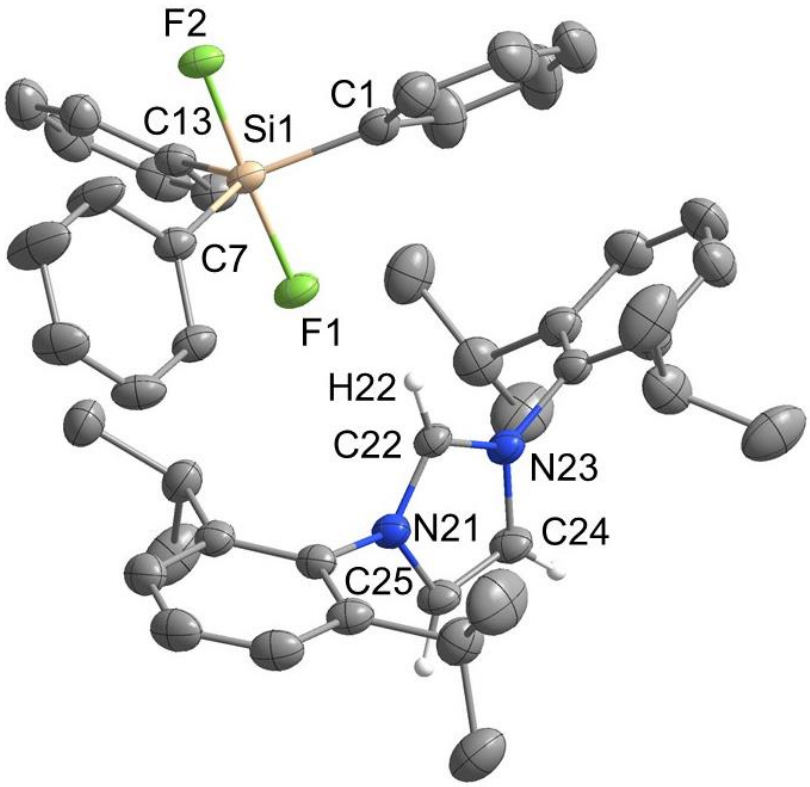

Figure 4.1: The crystal structure of [IPrH][Ph_3SiF_2] (**1**). The ellipsoids are drawn at 50% probability. All hydrogen atoms are omitted except for those on the imidazolium ring.

The asymmetric unit contains an imidazolium cation $[IPrH]^+$ and a triphenyldifluorosilicate anion $[Ph_3SiF_2]^-$, which, as expected, adopts a trigonal bipyramidal geometry with the fluorine atoms occupying the axial positions. The two Si—F bond distances are very similar. Si(1)—F(1) has a bond distance of 1.743(1) Å, while Si(1)–F(2) has a distance of 1.746(1) Å. In other crystal structures this difference is slightly larger: 1.734(1) and 1.721(1) Å [84]; 1.753(2) and 1.718(2) Å [85]; 1.732(1) and 1.726(1) Å [86]. This effect could be due to the similar strong hydrogen bonding interactions formed by the two fluorine atoms with the $[IPrH]^+$ cation. The $[Ph_3SiF_2]^-$ anion has two hydrogen bonds with two neighbouring imidazolium cations, each with separate fluorine atoms. The first hydrogen bond forms between F(1) and the hydrogen atom at the C2 position of the imidazolium cation C(22)–H(22)···F(1) with an H···F distance of 2.0841(9) Å, while the other hydrogen bond forms between F(2) and the hydrogen atom at the backbone of the symmetrically generated imidazolium cation C(24). C(24)–H(24)···F(2) with an H···F distance of 2.0383(9) Å.

4.1.1.2 [IPrH][Et_3SiF_2] (2)

The synthesis of [IPrH][Et_3SiF_2] was attempted under the same reaction conditions used for the preparation of [IPrH][Ph_3SiF_2] (**1**), as shown in Scheme 4.2. All attempts of synthesis under these conditions were unsuccessful.

Scheme 4.2: The synthetic procedure for the attempted preparation of [IPrH][Et_3SiF_2] (**2**).

NMR spectroscopy was used to observe the course of the reaction between [Et_3SiF] and [IPrH][F]. No product formation was observed, as only signals for [IPrH][F] (−148 ppm) and Et_3SiF (−175 ppm) were visible in the reaction mixture (Figure 4.2).

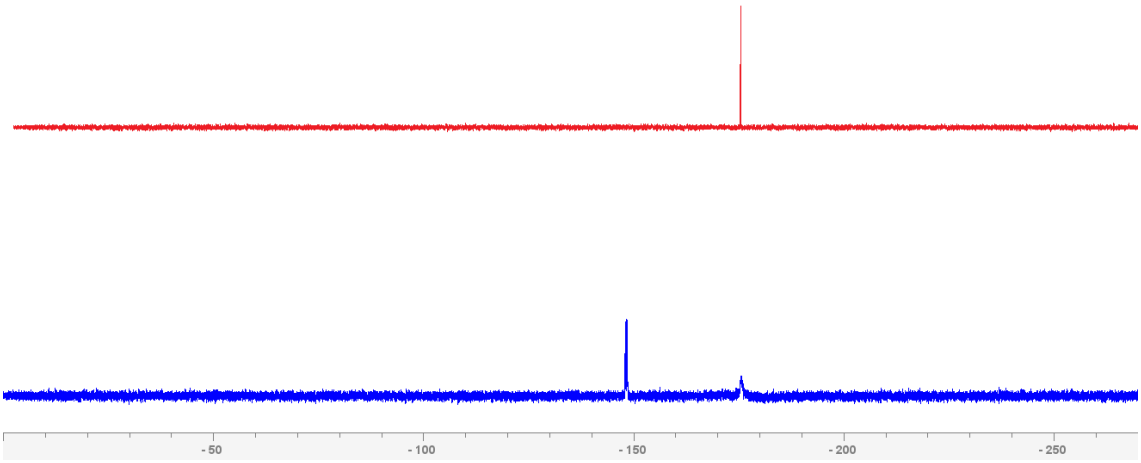

Figure 4.2: ^{19}F NMR spectrum of Et_3SiF + [IPrH][F] reaction mixture (blue) in comparison with ^{19}F NMR spectrum of Et_3SiF starting compound (red) in acetonitrile solvent. The only additional signal at −148 ppm belongs to the [IPrH][F] fluorination reagent.

4.1.1.3 [IPrH][Ph_2SiF_3] (3)

In the first step, Ph_2SiCl_2 was added to the acetonitrile suspension of 5 equivalents of KF to ensure the exchange of chlorine with fluorine and generate Ph_2SiF_2. The reaction mixture was stirred for 24 hours at room temperature. The suspension was filtered and added to a solution of [IPrH][F] in acetonitrile. The reaction mixture was stirred for a further 24 hours. The volatiles were removed under vacuum and crystals of [IPrH][Ph_2SiF_3] (**3**) were formed. The complete synthesis procedure is shown in Scheme 4.3. The crystals were collected and used for X-ray structural analysis, NMR spectroscopy, Raman spectroscopy and mass spectroscopy.

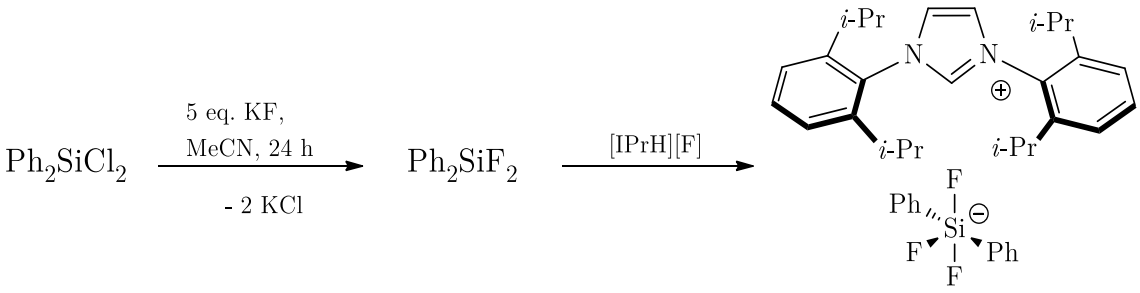

Scheme 4.3: The synthetic procedure for preparation of [IPrH][Ph_2SiF_3] (**3**).

Single crystals of [IPrH][Ph_2SiF_3] (**3**) were formed by slow evaporation of the acetonitrile solvent under static vacuum conditions. It crystallises in the monoclinic space group $P2_1/c$ and its crystal structure is shown in Figure 4.3.

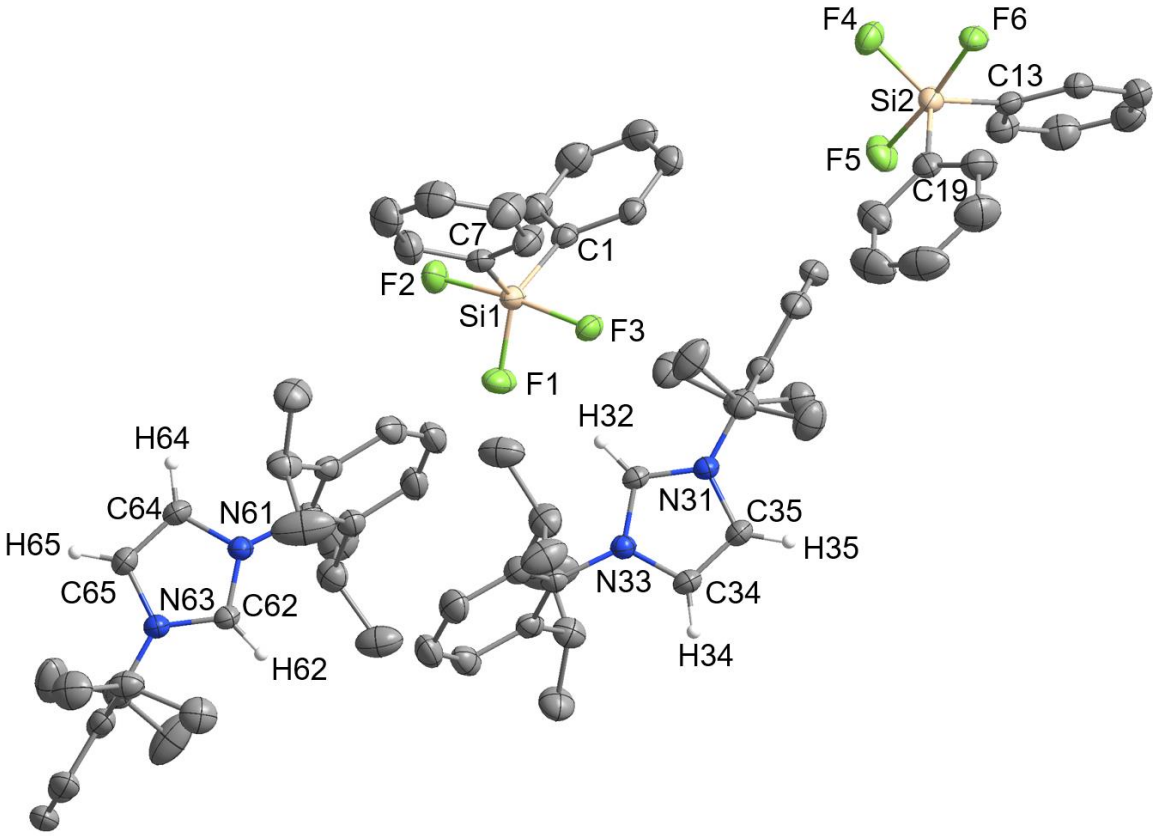

Figure 4.3: The crystal structure of [IPrH][Ph_2SiF_3] (**3**). The ellipsoids are drawn at 50% probability. All hydrogen atoms are omitted except for those on the imidazolium ring.

The asymmetric unit of **3** contains two ion pairs: two imidazolium $[IPrH]^+$ cations and two diphenyltrifluorosilicate $[Ph_2SiF_3]^-$ anions. The anions adopt a trigonal bipyramidal configuration with the axial positions occupied by fluorine atoms. The remaining fluorine atom and two phenyl groups occupy the positions in the equatorial plane around the silicon centre. As expected, the fluorine atom in the equatorial plane has a significantly shorter Si–F bond with a Si(1)–F(1) bond length of 1.645(1) Å, compared to axially positioned fluorine atoms with bond lengths of 1.691(1) and 1.711(1) Å for Si(1)–F(2) and Si(1)–F(3) respectively. The two anions in the asymmetric unit each form three interactions with imidazolium cations. Two hydrogen bonds are formed between the hydrogen atom in the C2 position of the imidazolium ring and the two nearest fluorine atoms. The lengths of the hydrogen bonds of the fluorine atoms in the axial position F(3)···H(32) 2.233(1) Å and F(6)···H(62) 2.226(1) Å are similar to those in the equatorial plane F(1)···H(32) 2.298(1) Å and F(4)···H(62) 2.343(1) Å. This trend is observed for both anions of the asymmetric unit. In addition to the hydrogen bonds mentioned above, the fluorine atoms in the equatorial plane also interact with hydrogen atoms on the neighbouring phenyl rings: F(1)···H(69) 2.368(1) Å and F(4)···H(52) 2.424(1) Å.

4.1.1.4 [IPrH][Et_2SiF_3] (4)

In the first step, Et_2SiCl_2 was added to the acetonitrile suspension of 5 equivalents of KF to ensure the exchange of chlorine with fluorine and generate Et_2SiF_2. The reaction mixture

was stirred for 24 hours at room temperature. The suspension was filtered and added to a solution of [IPrH][F] in acetonitrile. The reaction mixture was stirred for a further 24 hours. The volatiles were removed under vacuum and crystals of [IPrH][Et_2SiF_3] (**4**) were formed. The complete synthesis procedure is shown in Scheme 4.4. The crystals were collected and used for X-ray structural analysis, NMR spectroscopy, Raman spectroscopy and mass spectroscopy.

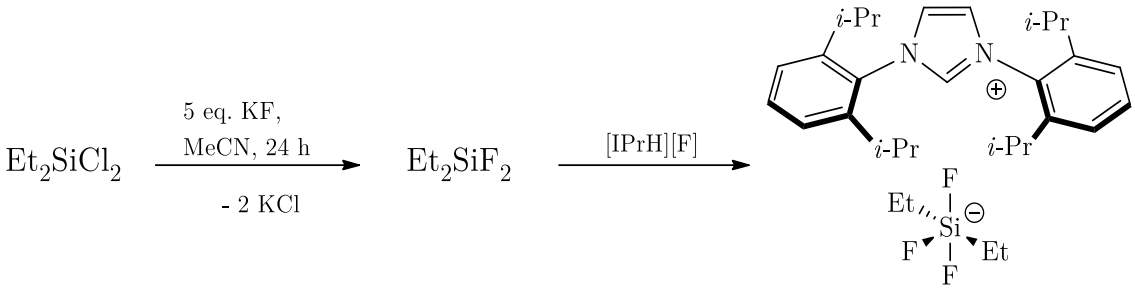

Scheme 4.4: The synthetic procedure for preparation of [IPrH][Et_2SiF_3] (**4**).

Single crystals of [IPrH][Et_2SiF_3]·MeCN (**4**·MeCN) were formed by slow evaporation of the acetonitrile solvent under static vacuum conditions. It crystallises in the monoclinic space group $P2_1/n$ in the form of a solvate with acetonitrile. The crystal structure is shown in Figure 4.4.

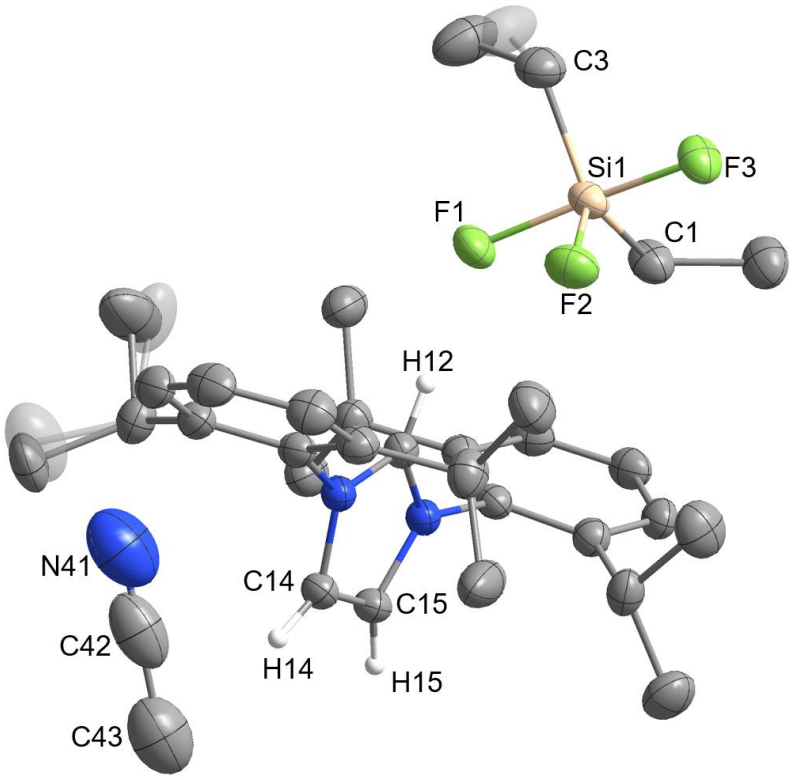

Figure 4.4: Crystal structure of the asymmetric unit of [IPrH][Et_2SiF_3]·MeCN (**4**·MeCN). The ellipsoids are drawn at 50% probability. The positions of disordered atoms are shown in domains A and B. For clarity, domain B is shaded and all hydrogen atoms are omitted except for those on the imidazolium ring.

The asymmetric unit of **4** contains a single ion pair of imidazolium cation $[IPrH]^+$ and diethyltrifluorosilicate anion $[Et_2SiF_3]^-$ and a molecule of acetonitrile. The anion adopts the expected trigonal bipyramidal structure, with the axial positions occupied by fluorine atoms. The remaining fluorine atom and the two ethyl groups are arranged around the silicon centre in the equatorial plane. As expected, the equatorial fluorine has a shorter bond distance Si(1)–F(2) 1.648(1) Å compared to the bond lengths of the axially bonded fluorine atoms (Si(1)–F(1) 1.733(1) Å, Si(1)–F(3) 1.729(1) Å). Similar to the crystal structure of $[IPrH][Ph_2SiF_3]$ **3**, the anion in $[IPrH][Et_2SiF_3]$ **4** also forms three hydrogen bonds. However, in this case, all interactions are between fluorine atoms of the anion and hydrogen atoms on the imidazolium ring. The first hydrogen bond is formed between the hydrogen atom at the C2 position and the nearest fluorine atom in the axial position (F(1)···H(12) 2.058(1) Å). The remaining two hydrogen bonds are formed between the other two fluorine atoms and the hydrogen atoms on the backbone of the symmetrically generated imidazolium ring (F(2)···H(15)I 2.307(1) Å and F(3)···H(14) 2.507(1) Å).

4.1.1.5 [IPrH][PhSiF$_4$] (5)

In the first step, $PhSiCl_3$ was added to the acetonitrile suspension of 5 equivalents of KF to ensure the exchange of chlorine with fluorine and to generate $PhSiF_3$. The reaction mixture was stirred for 48 hours at room temperature. Compared to previous syntheses, the reaction time was doubled to ensure a quantitative conversion of phenyltrichlorosilane to phenyltrifluorosilane. The suspension was filtered and added to a solution of [IPrH][F] in acetonitrile. The reaction mixture was stirred for a further 24 hours. The volatiles were removed under vacuum and crystals of $[IPrH][PhSiF_4]$ (**5**) were formed. The complete synthesis procedure is shown in Scheme 4.5. Only a small amount of the crystals was collected and used for X-ray structural analysis. The amount was not sufficient for NMR spectroscopy, Raman spectroscopy and mass spectroscopy. *In situ* ^{19}F NMR of (**5**) showed no signals, likely due to low solubility of the compound.

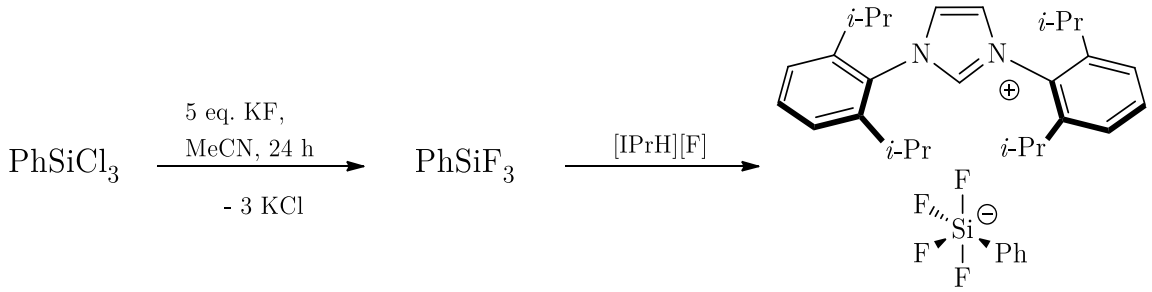

Scheme 4.5: The synthetic procedure for preparation of $[IPrH][PhSiF_4]$ (**5**).

Single crystals of $[IPrH][PhSiF_4]$ (**5**) were formed by slow evaporation of the acetonitrile solvent under static vacuum conditions. It crystallises in the triclinic space group $P\bar{1}$. The crystal structure is shown in Figure 4.5.

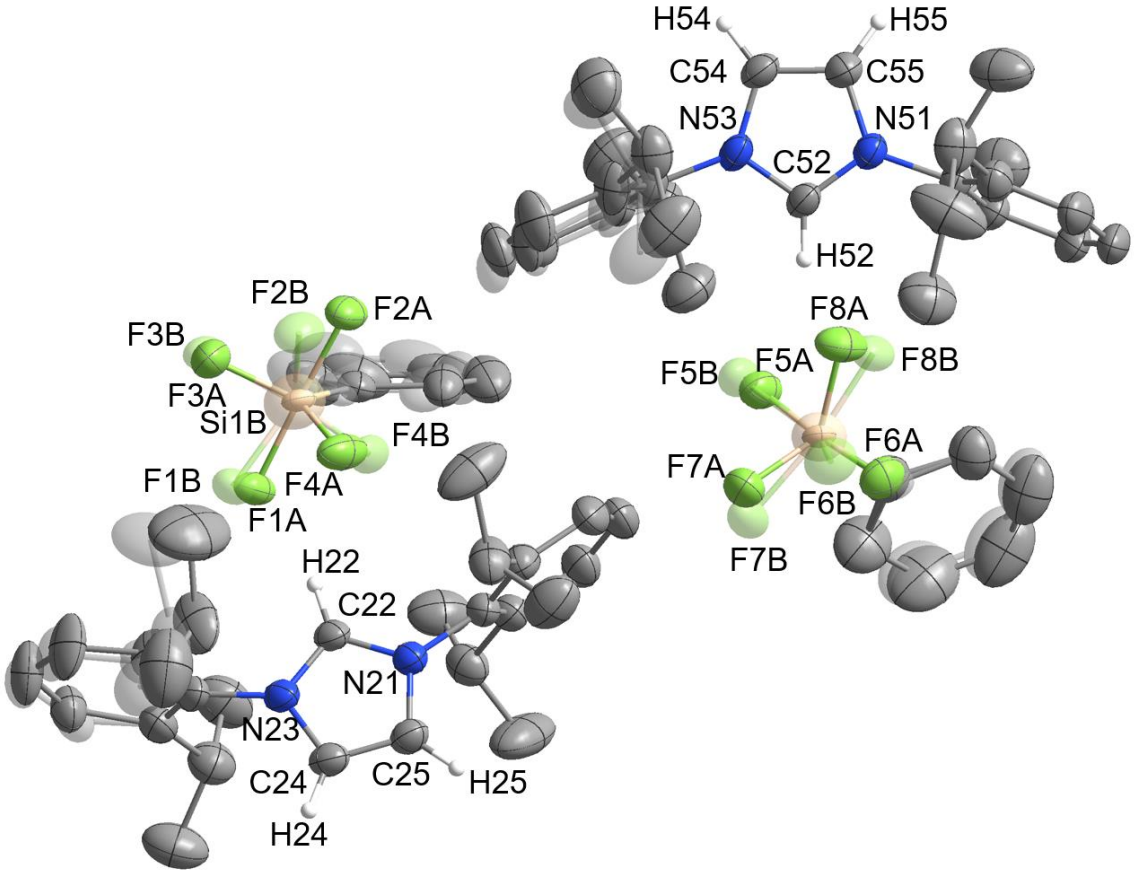

Figure 4.5: Crystal structure of the asymmetric unit of [IPrH][$PhSiF_4$] (**5**). The ellipsoids are drawn at 50% probability. The positions of disordered atoms are shown in domains A and B. For clarity, domain B is shaded, and all hydrogen atoms are omitted except for those on the imidazolium ring.

The asymmetric unit of **5** contains two ion pairs of two imidazolium $[IPrH]^+$ cations and two $[PhSiF_4]^-$ anions. The anions adopt a trigonal bipyramidal structure, with the axial positions occupied by fluorine atoms with the remaining two fluorine atoms and the phenyl group arranged around the silicon centre in the equatorial plane. The positions of the fluorine atoms in **5** of the two anions are highly disordered. Two preferred orientations were modelled, with domain A having 70% occupancy for the first anion and 56% for the second anion. Domain B has an occupancy of 30% for the first anion and 44% for the second anion. The disorder of the fluorine atoms is the result of two possible positions of the fluorine atoms in the anion due to the rotation of the fluorine atoms around the C–Si axis. The atoms in domain B are rotated by 90° compared to those in domain A. Due to the high disorder in **5**, the bond lengths and angles are too imprecise to draw any insights and conclusions.

4.1.1.6 [IPrH][$EtSiF_4$] (6)

In the first step, $EtSiCl_3$ was added to the acetonitrile suspension of 5 equivalents of KF to ensure the exchange of chlorine with fluorine and to generate $EtSiF_3$. The reaction mixture was stirred for 48 hours at room temperature. Like with phenyltrichlorosilane synthesis, the reaction time was doubled to ensure a quantitative conversion of ethyltrichlorosilane to ethyltrifluorosilane. The suspension was filtered and added to a solution of [IPrH][F] in acetonitrile. The reaction mixture was stirred for a further 24 hours.

The volatiles were removed under vacuum and crystals of [IPrH][EtSiF$_4$] (**6**) were formed. The complete synthesis procedure is shown in Scheme 4.6.

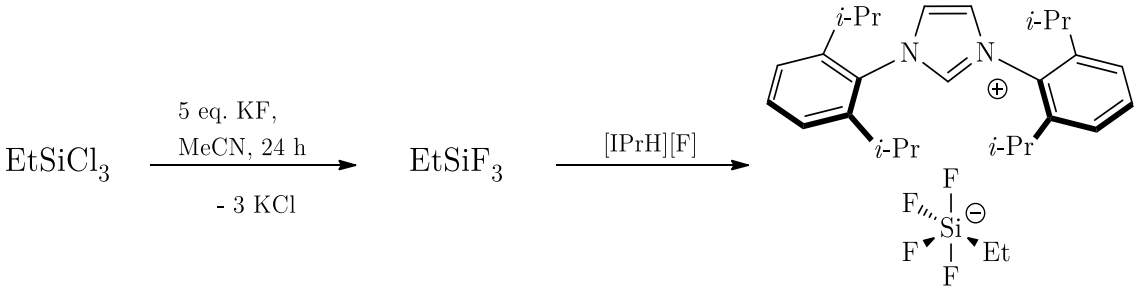

Scheme 4.6: The synthetic procedure for preparation of [IPrH][EtSiF$_4$] (**6**).

Single crystals of [IPrH][EtSiF$_4$] (**6**) were formed by slow evaporation of the acetonitrile solvent under static vacuum conditions. It crystallises in the monoclinic space group *I*2*a*. The crystal structure is shown in Figure 4.6.

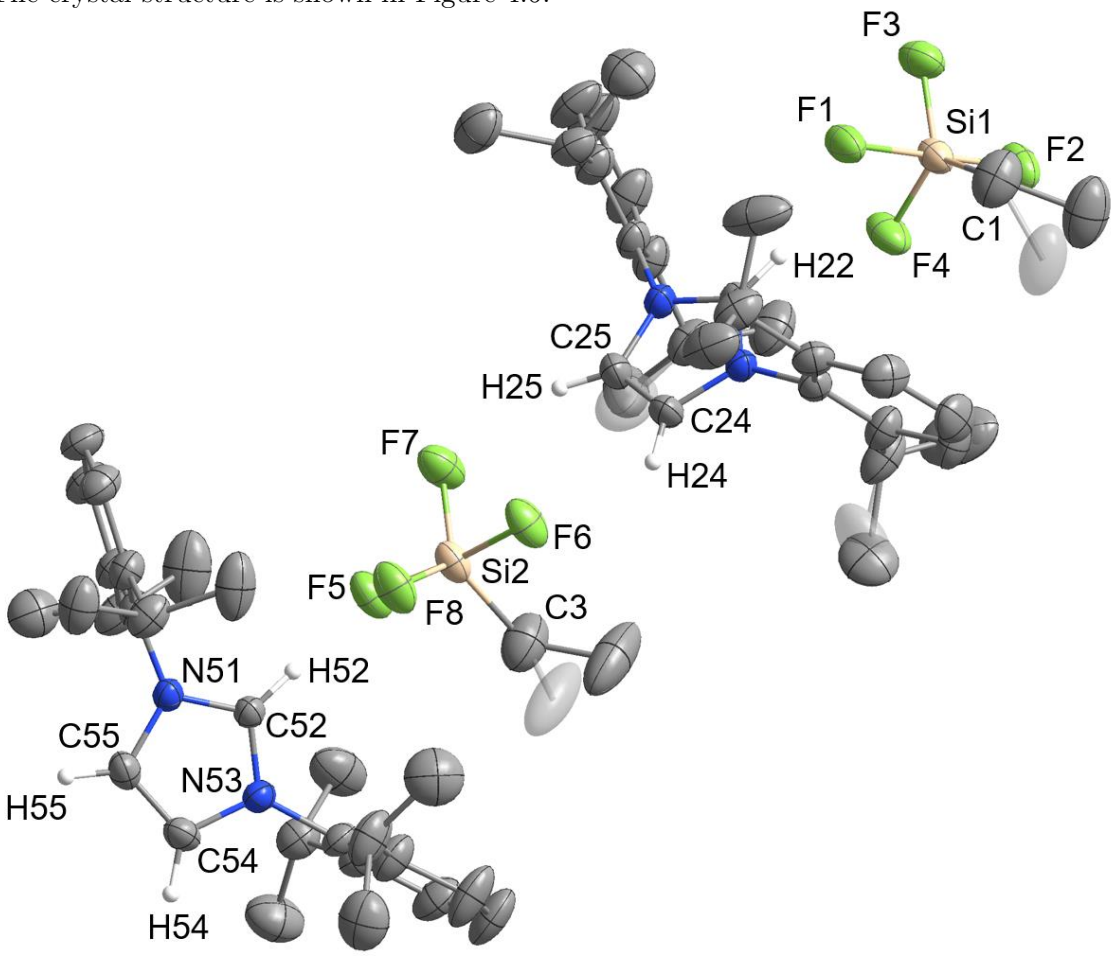

Figure 4.6: Crystal structure of the asymmetric unit of [IPrH][EtSiF$_4$] (**6**). The ellipsoids are drawn at 50% probability. The positions of disordered atoms are shown in domains A and B. For clarity, domain B is shaded and all hydrogen atoms are omitted except for those on the imidazolium ring.

The asymmetric unit of **6** contains two ion pairs of two imidazolium [IPrH]$^+$ cations and two [EtSiF$_4$]$^-$ anions. Compared to the related [IPrH][PhSiF$_4$], the [EtSiF$_4$]$^-$ anions do

not exhibit disorder in the positions of the fluorine atoms, but rather in the ethyl groups. As expected, the anions adopt a trigonal bipyramidal structure, with the axial positions occupied by fluorine atoms. The remaining two fluorine atoms and the phenyl group are arranged around the silicon centre in the equatorial plane. The crystal structure of **6** shows that the Si–F bonds at the axial positions Si(1)–F(1) 1.701(1) Å, Si(1)–F(2) 1.672(1) Å, of the first anion and Si(2)–F(5) 1.698(1) Å, Si(2)–F(6) 1.670(1) Å of the second anion are longer than those in the equatorial position Si(1)–F(3) 1.618(1) Å, Si(1)–F(4) 1.614(1) of the first anion, and Si(2)–F(7) 1.621(1) Å, Si(2)–F(8) 1.617(1) Å of the second anion. This type of behaviour has already been observed in the structures of **3** and **4** and is consistent with literature data for the related $[MeSiF_4]^-$ anion [87].

The $[EtSiF_4]^-$ anion forms five interactions with three different imidazolium $[IPrH]^+$ cations. In both anions of the asymmetric unit, the two closest fluorine atoms (one in the axial and one in the equatorial position) form hydrogen bonds with the hydrogen in the C2 position of the imidazolium cation (anion 1: F(1)···H(22) 2.050(1) Å and F(4)···H(22) 2.379(1) Å, anion 2: F(5)···H(52) 2.105(1) Å and F(8)···H(52) 2.317(1) Å). The remaining two fluorine atoms form interactions with hydrogen atoms on the backbone of the neighbouring imidazolium ring (anion 1: F(2)···H(55) 2.162(1) Å and F(3)···H(54) 2.280(1) Å, anion 2: F(6)···H(24) 2.200(1) Å and F(7)···H(25) 2.229(1) Å). The last interaction observed takes place between the fluorine atom in the axial position and the hydrogen atoms of the neighbouring phenyl rings of the symmetrically generated unit (anion 1: F(2)···H(72) 2.460(1) Å, anion 2: F(6)···H(28) 2.478(1) Å).

4.1.1.7 [IPrH][Ph_3GeF_2] (7)

In the first step, Ph_3GeCl was added to the acetonitrile suspension of 5 equivalents of KF to ensure the exchange of chlorine with fluorine and generate Ph_3GeF. The reaction mixture was stirred for 24 hours at room temperature. The suspension was filtered and added to a solution of [IPrH][F] in acetonitrile. The reaction mixture was stirred for a further 24 hours. The volatiles were removed under vacuum and crystals of [IPrH][Ph_3GeF_2] (**7**) were formed. The complete synthesis procedure is shown in Scheme 4.7. The crystals were collected and used for X-ray structural analysis, NMR spectroscopy, Raman spectroscopy and mass spectroscopy.

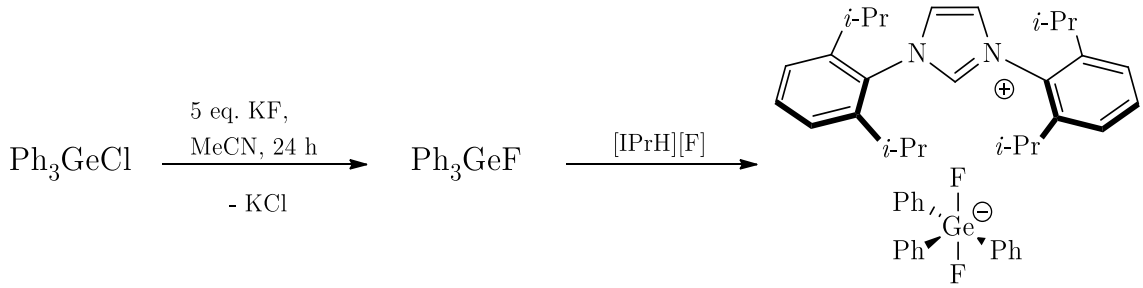

Scheme 4.7: The synthetic procedure for preparation of [IPrH][Ph_3GeF_2] (**7**).

The crystallisation of [IPrH][Ph_3GeF_2] (**7**), which was synthesised according to the procedure described above, resulted in three different crystal structures, all of which were formed under the same crystallisation conditions. The single crystals were formed by slow evaporation of the acetonitrile solvent under static vacuum conditions. The first crystal structure contains only the two [IPrH][Ph_3GeF_2] ion pairs, which crystallised in the triclinic space group $P\bar{1}$. The crystal structure is shown in Figure 4.7. The other two structures **7a** and **7b** crystallised in the form of solvates with acetonitrile, each containing an ion pair

of [IPrH][Ph_3GeF_2] and a single molecule of acetonitrile. Compound **7a** crystallises in the triclinic space group $P\bar{1}$ while **7b** crystallises in the orthorhombic space group $P2_12_12_1$. The crystal structures of **7a** and **7b** are shown in Figure 4.8 and Figure 4.9, respectively.

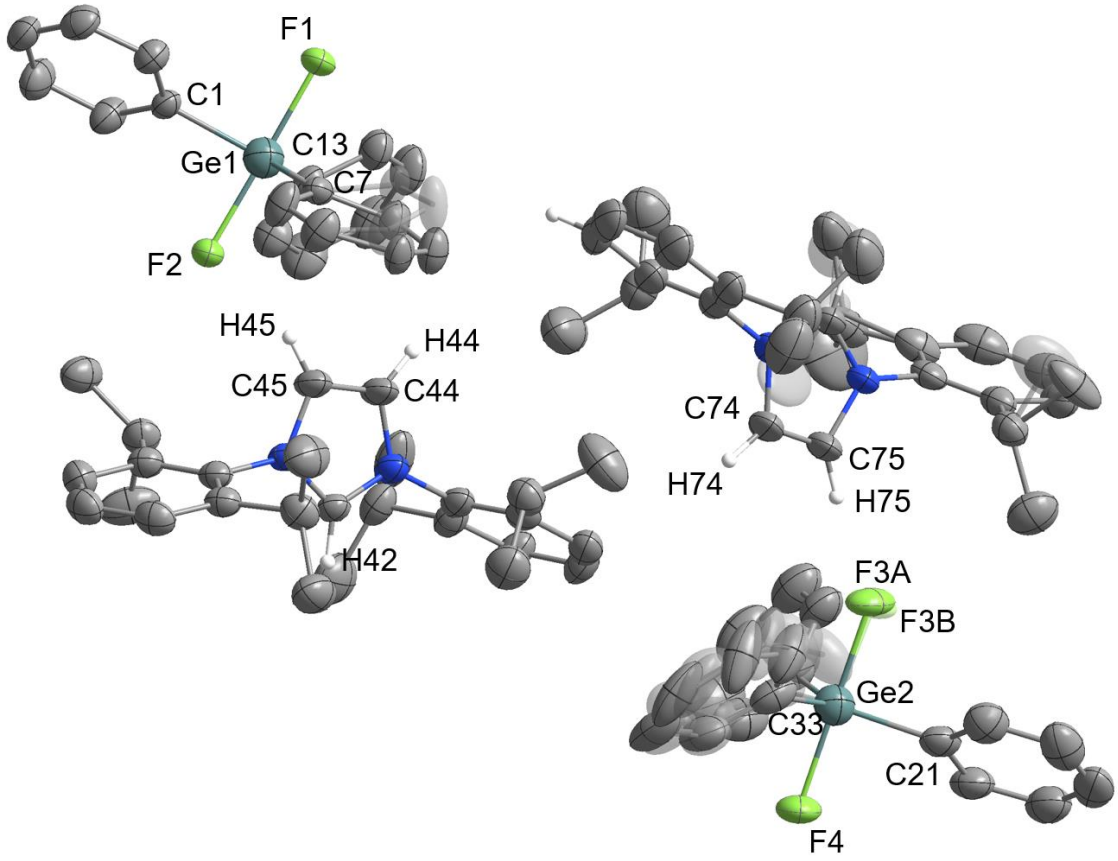

Figure 4.7: Crystal structure of the asymmetric unit of [IPrH][Ph_3GeF_2] (**7**). The ellipsoids are drawn at 50% probability. The positions of disordered atoms are shown in domains A and B. For clarity, domain B is shaded, and all hydrogen atoms are omitted except for those on the imidazolium ring.

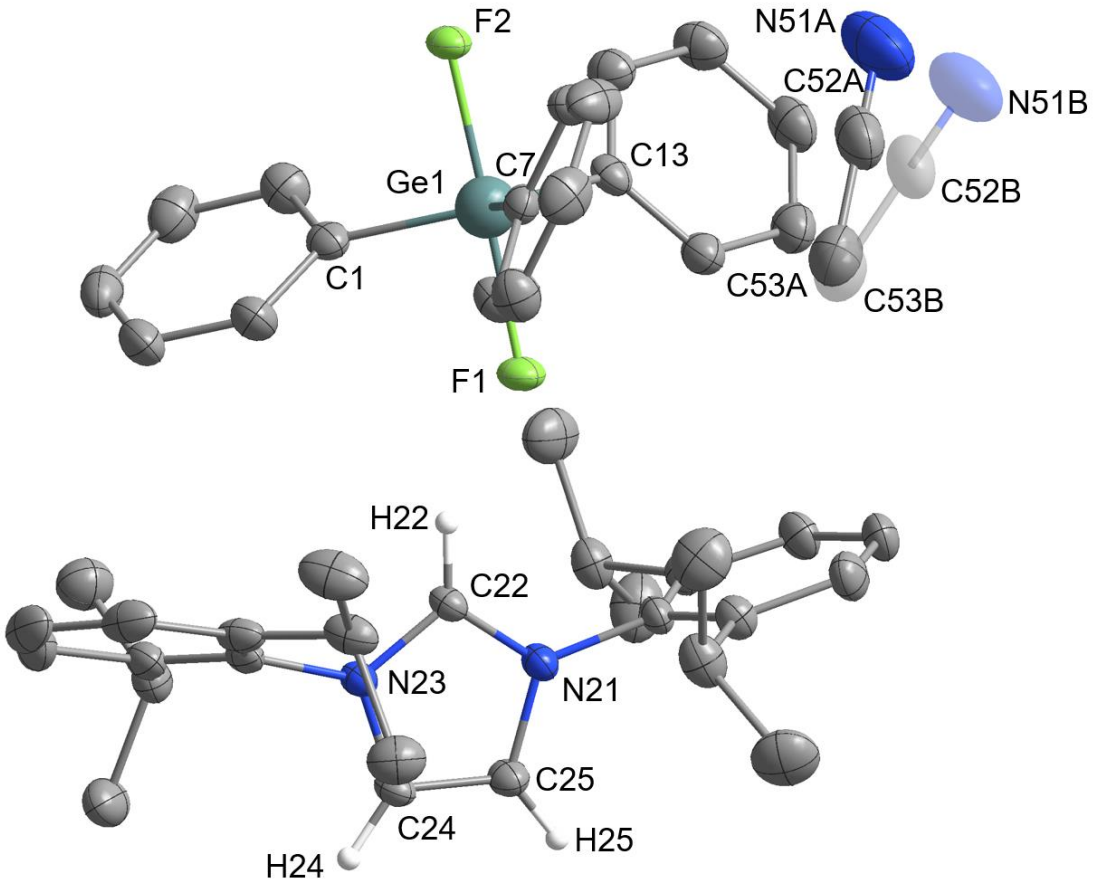

Figure 4.8: Crystal structure of the asymmetric unit of [IPrH][Ph_3GeF_2]·MeCN (**7a**). The ellipsoids are drawn at 50% probability. The positions of disordered atoms are shown in domains A and B. For clarity, domain B is shaded, and all hydrogen atoms are omitted except for those on the imidazolium ring.

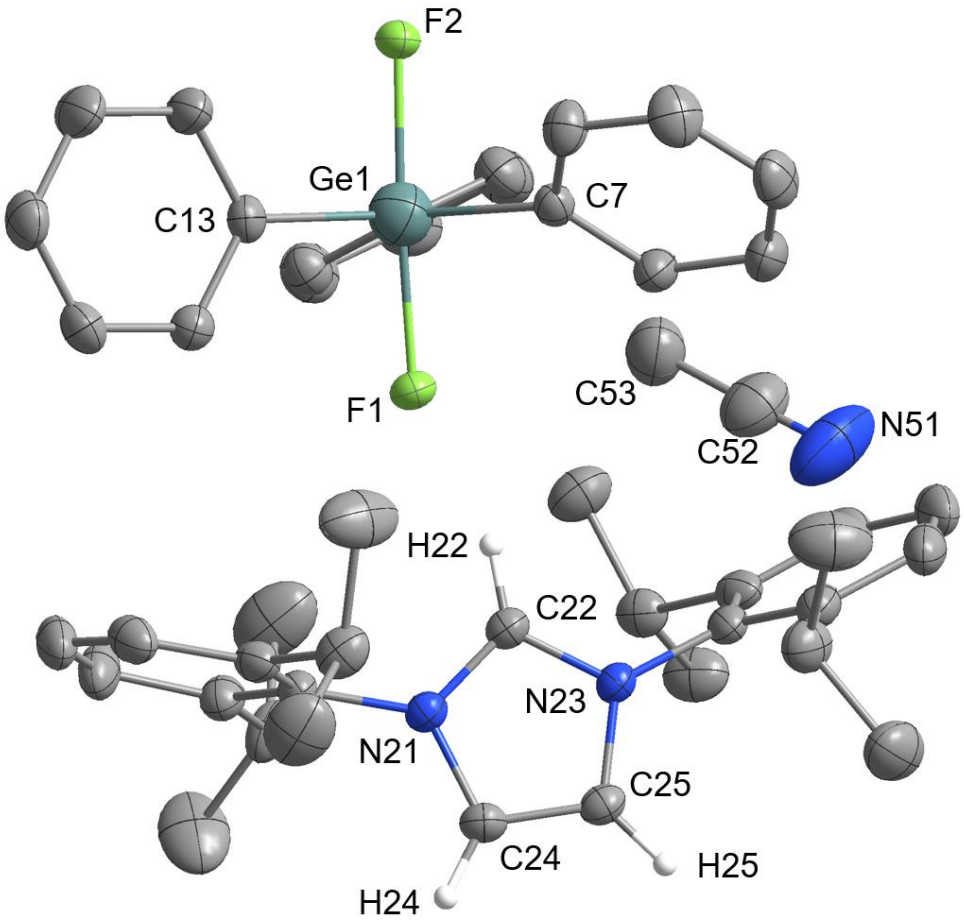

Figure 4.9: Crystal structure of the asymmetric unit of [IPrH][Ph_3GeF_2]·MeCN (**7b**). The ellipsoids are drawn at 50% probability. For clarity, all hydrogen atoms are omitted except for those on the imidazolium ring.

Due to the similar structural characteristics of the anions, only structure **7** is discussed. Similar to the related [Ph_3SiF_2]$^-$ anion, the [Ph_3GeF_2]$^-$ anion retains the trigonal bipyramidal geometry with the fluorine atoms occupying the axial positions. Although [IPrH][Ph_3SiF_2] **1** and [IPrH][Ph_3GeF_2] **7** have the same geometry of the anion, the structures are not isostructural and crystallise in different space groups of $P\bar{1}$ and $P2_1/c$, respectively. The [Ph_3GeF_2]$^-$ anion has an average Ge–F bond length of 1.920 Å, which is significantly longer compared to the other two structurally characterised organofluorogermanate anions [$(C_2F_5)_3GeF_2$]$^-$ and [$(CF_3)_3GeF_2$]$^-$, which have an average Ge–F bond length of 1.834 Å and 1.810 Å, respectively [66], [65]. The difference in bond distances is most likely due to the strong electron-withdrawing groups that are bound to the germanium centre and strongly influence the Ge–F bond length. The [Ph_3GeF_2]$^-$ anion forms three interactions with the two neighbouring [IPrH] cations. First hydrogen bond is formed between the first fluorine atom and the hydrogen atom at the C2 position of the symmetrically generated unit (anion 1: F(1)···H(72) 1.982(2) Å, anion 2: F(4)···H(42) 1.921(2) Å), while the second hydrogen bond is formed between the other fluorine atom and the hydrogen atom on the backbone of the imidazolium ring (anion 1: F(2)···H(45) 2.078(2) Å, anion 2: F(3A)···H(75) 1.93(1) Å and F(3B)···H(75) 2.07(2) Å). Unlike [IPrH][Ph_3SiF_2] **1**, in [IPrH][Ph_3GeF_2] **7** an additional interaction is formed between the fluorine atom F(2) and the hydrogen atom on the neighbouring phenyl ring (F(2)···H(79) 2.373(2) Å).

4.1.1.8 [IPrH][Ph_2GeF_3] (8)

In the first step, Ph_2GeCl_2 was added to the acetonitrile suspension of 5 equivalents of KF to ensure the exchange of chlorine with fluorine and generate Ph_2GeF_2. The reaction mixture was stirred for 24 hours at room temperature. The suspension was filtered and added to a solution of [IPrH][F] in acetonitrile. The reaction mixture was stirred for a further 24 hours. The volatiles were removed under vacuum and crystals of [IPrH][Ph_2GeF_3]·MeCN (**8**) were formed. The complete synthesis procedure is shown in Scheme 4.8. The crystals were collected and used for X-ray structural analysis.

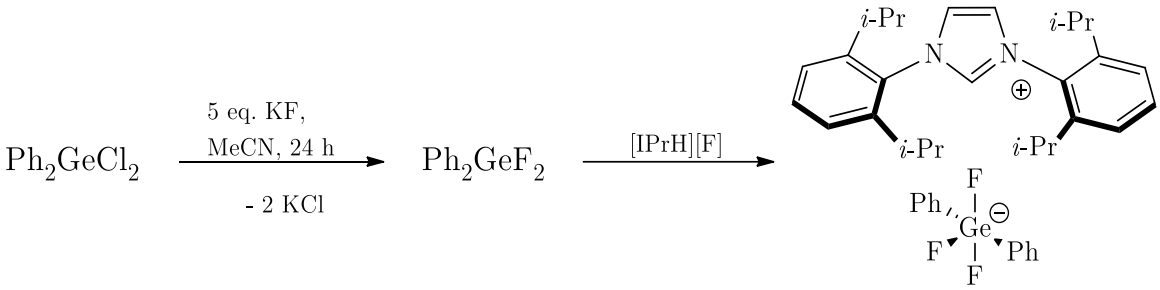

Scheme 4.8: The synthetic procedure for preparation of [IPrH][Ph_2GeF_3]·MeCN (**8**).

Single crystals of [IPrH][Ph_2GeF_3]·MeCN (**8**) were formed by slow evaporation of the acetonitrile solvent under static vacuum conditions. It crystallises in the triclinic space group $P\bar{1}$. The crystal structure is shown in Figure 4.10.

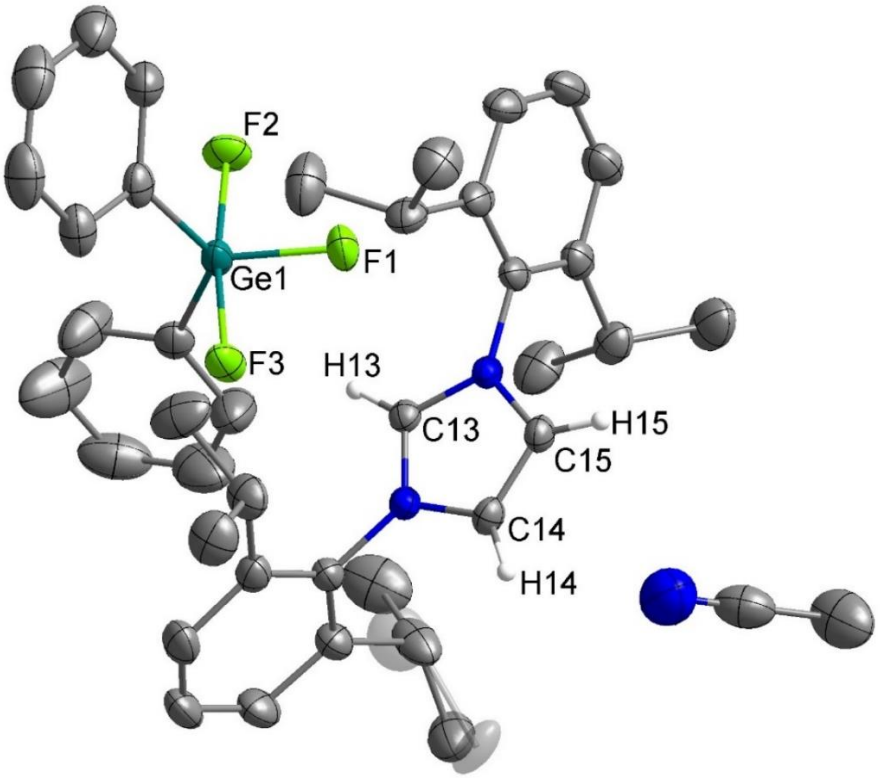

Figure 4.10: Crystal structure of the asymmetric unit of [IPrH][Ph_2GeF_3] (**8**). The ellipsoids are drawn at 50% probability. The positions of disordered atoms are shown in domains A and B. For clarity, domain B is shaded, and all hydrogen atoms are omitted except for those on the imidazolium ring.

The asymmetric unit of **8** contains $[IPrH]^+$ imidazolium cation and $[Ph_2GeF_3]^-$ anion, together with a single molecule of acetonitrile. The $[Ph_2GeF_3]^-$ anion adopts a trigonal bipyramidal geometry, with axial positions occupied by fluorine atoms, which is in accordance with **7** and other structurally characterised organofluorogermanates [66], [65]. The remaining fluorine atom and the two phenyl groups are arranged around the silicon centre in the equatorial plane. As expected, the axial fluorine atoms are more weakly bonded and have longer bonds Ge(1)–F(2) 1.861(1) Å and Ge(1)–F(3) 1.882(1) Å than the equatorially bound equivalent Ge(1)–F(1) 1.758(1) Å. The $[Ph_2GeF_3]^-$ forms two hydrogen bonds, one with each axial fluorine atom. The first interaction is formed between the axial fluorine atom F3 and the hydrogen at the C2 position of the imidazolium ring F(3)···H(13) 2.019(1) Å. The other hydrogen interaction is formed between the second axial fluorine atom and the hydrogen atom on the backbone of the symmetrically structured imidazolium ring F(2)···H(14) 1.981(1) Å. The remaining equatorially positioned fluorine does not form any significant interactions with surrounding molecules.

4.1.2 NMR spectroscopy

All synthesised organofluorosilicate and organofluorogermanate salts, with the exception of [IPrH][$PhSiF_4$] (**5**), were characterised by ^{1}H, ^{13}C and ^{19}F NMR spectroscopy. The attempted synthesis of [IPrH][Et_3SiF_2] (**2**) did not result in any conversion, as shown by the ^{19}F spectra of the reaction mixture after 24 hours, as only [Et_2SiF_2] and [IPrH][F] were seen in the spectrum. This showed that the synthesis of [IPrH][Et_3SiF_2] (**2**) was not possible under the reaction conditions described in the previous section. The crystals of [IPrH][$PhSiF_4$] (**5**) were successfully isolated and characterised by X-ray diffraction, but not sufficient material was isolated for NMR analysis. Attempts to record NMR of the reaction mixture of **5** were unsuccessful as only HF^{2-} and F^- anions were observed each time. Regardless of the temperature used for the measurement, the same result was obtained.

In the ^{1}H NMR spectra, characteristic signals for the imidazolium $[IPrH]^+$ cation and signals for the ethyl and phenyl substituents are visible for all compounds. In some cases, the signals of the substituents overlapped with the signals of the $[IPrH]^+$ cation and are integrated together.

The ^{19}F NMR spectra recorded at room temperature showed no fluorine signals in some cases, most likely due to rapid intramolecular transformations. The measurements were repeated at −40 °C (233 K) to slow down the rate of the processes undergone by the anions, whereupon the signals became visible.

The measured ^{19}F NMR peaks of the characterised compounds are listed in Table 4.1 and are compared with reported values of structurally related anions. In cases where data recorded in deuterated acetonitrile were not available, the values in other deuterated solvents were provided. Because ethylfluorosilicates have not yet been characterised by ^{19}F NMR spectroscopy, the data of the related methylfluorosilicates were used.

Table 4.1: Comparison of the ^{19}F NMR signals of characterised organofluorosilicates and organofluorogermanates in acetonitrile-d_3 with similar compounds from the literature.

Compound	δ(^{19}F) Si/Ge–F	δ(^{19}F) Si/Ge–F in literature
[IPrH][Ph_3SiF_2] (**1**)	−97.0 (298 K)	−96.6 ([$(C_4H_9)_4N$][Ph_3SiF_2], $CDCl_3$) [56]
[IPrH][Et_3SiF_2] (**2**)	*not available*	−61.9 ([PNP][Me_3SiF_2], MeCN-d_3, 253 K) [88]
[IPrH][Ph_2SiF_3] (**3**)	−96.6 (233 K) −134.2 (233 K)	−98.0 ([$(C_2H_5)_4N$][Ph_2SiF_3], CD_2Cl_2) [89] −134.0 ([$(C_2H_5)_4N$][Ph_2SiF_3], CD_2Cl_2) [89]
[IPrH][Et_2SiF_3] (**4**)	−86.0 (233 K) −136.2 (233 K)	−66.3 ([PNP][Me_2SiF_3], CH_3CH_2CN, 193 K) [87] −132.9 ([PNP][Me_2SiF_3], CH_3CH_2CN, 193 K) [87]
[IPrH][$PhSiF_4$] (**5**)	*not available*	−116.8 ([$(CH_3)_4N$][$PhSiF_4$], DMSO-d_6) [89]
[IPrH][$EtSiF_4$] (**6**)	−115.8 (233 K)	−110.5 ([$(C_4H_9)_4N$][$MeSiF_4$], CD_2Cl_2, 213 K) [89]
[IPrH][Ph_3GeF_2] (**7**)	−112.9 (233 K) −143.7 (233 K)	−137.6 ([$(CH3)_3N$][$(CF_3)_3GeF_2$], MeCN-d_3) [66]
[IPrH][Ph_2GeF_3] (**8**)	−113.6 (233 K) −146.0 (233 K)	−111.6 ([K][Ph_2GeF_3], MeCN-d_3, 233 K) [83] −139.8 ([K][Ph_2GeF_3], MeCN-d_3, 233 K) [83]

As expected, difluorosilicates exhibit a single peak, since both fluorine atoms are NMR equivalent. Trifluorosilicates and trifluorogermanates, on the other hand, show two signals with an integrated relative intensity of 2 to 1. The two signals are the result of the trigonal bipyramidal geometry of the anion, where the fluorine atoms are coordinated in two different ways. The signal with the higher frequency belongs to the fluorine atoms at the axial positions, while the signal with the lower frequency is attributed to the equatorially

positioned fluorine atom. No ^{19}F–^{19}F coupling between the axial and equatorial fluorine atoms was observed, most likely due to very broad signal peaks. Interestingly, two signals with chemical shifts very similar to those of the trifluorogermanate anion $Ph_2GeF_3^-$ were observed in the ^{19}F NMR spectrum of the difluorogermanate anion $Ph_3GeF_2^-$. This indicates that the two fluorine atoms of the anion are arranged in axial and equatorial positions. This is probably the result of a Berry pseudorotation of the anions, in which axial ligands can alternate with equatorial ligands and vice versa. Theoretically, a similar behaviour with two signals is expected for the tetrafluorosilicate species, but in practise only one signal is usually visible. This is most likely the result of rapid intramolecular transformations of the anion leading to a single peak with an averaged chemical shift. The chemical shifts of the ^{19}F NMR signals of synthesised organofluorosilicates and organofluorogermanates are mostly consistent with the previously reported values. The signals of [IPrH][Ph_3SiF_2] (**1**) (−97.0 compared to −96.6 ppm) [56] and [IPrH][Ph_2SiF_3] (**3**) (−96.6, −134.2 compared to −98.0, −134.0 ppm) [89] are in good agreement with the reported peaks. A slightly larger discrepancy is observed for [IPrH][$EtSiF_4$] (**6**) (−115.8 compared to −110.5 ppm) [89], [IPrH][Ph_3GeF_2] (**7**) (−143.7 compared to −137.6 ppm) [66] and [IPrH][Ph_2GeF_3] (**8**) (−113.6 and −146.0 compared to −111.6 and −139.8 ppm) [83]. The difference in the first two cases can be attributed to the different substituents on the anions. In the case of **6**, it contains ethyl groups instead of the reported methyl group, while **7** contains phenyl groups instead of the strongly electron-withdrawing trifluoromethyl groups. The difference in the chemical shift of **8** compared to the same anion is most likely due to the very broad peaks of **8**, which makes the determination of the exact chemical shift less reliable. The largest disparity between our data and the reported values was observed for [IPrH][Et_2SiF_3] (**4**), which had values of −86.0 and −136.2 ppm, compared to the reported values of −66.3 and −132.9 ppm values of the $[Me_2SiF_3]^-$ anion [87]. While the signals of the equatorially positioned fluorine atoms (−136.2 and −132.9 ppm) show similar chemical shifts, the axial fluorine atom shifts differ by almost 20 ppm. As can be seen from Table 4.1, the choice of substituent seems to mainly influence the chemical shifts of the axial fluorine atoms in the ^{19}F NMR. On the other hand, the choice of solvent has only a minor influence on the chemical shift.

4.1.3 Raman spectroscopy

The compounds [IPrH][Ph_3SiF_2] (**1**), [IPrH][Ph_2SiF_3] (**3**), [IPrH][Et_2SiF_3] (**4**), [IPrH][$EtSiF_4$] (**6**) and [IPrH][Ph_3GeF_2] (**7**) were measured using a Raman spectrometer. The spectra of the ethyl group-containing compounds [IPrH][Et_2SiF_3] (**4**) and [IPrH][$EtSiF_4$] (**6**) were of too low quality to determine signals related to the vibrations of the anions. This is due to the strong fluorescence of the compounds. In other samples, two peaks were identified that were not associated with the $[IPrH]^+$ cation. In the spectrum of compound **7**, a Ge−F vibration at 662 cm^{-1} was attributed to the symmetric stretching of the GeF_2 unit of the $[Ph_3GeF_2]^-$ anion, which is consistent with published data for the vibrations of the $[GeF_5]^-$ anion [90]. The spectra of **1** and **3** contained similar peaks at 667 and 663 cm^{-1}, respectively, which were attributed to the symmetric stretching of the Si–F bonds of the SiF_2 units of the $[Ph_3SiF_2]^-$ and $[Ph_2SiF_3]^-$ anions. Another signal at 999 cm^{-1} was observed for all the above compounds with phenyl groups. The peak is tentatively attributed to Si−C and Ge−C vibrations. In a study on organofluoroaluminates, a comparable signal was attributed to the Al−C vibration [91].

4.1.4 Computational results

Molecular calculations were performed to better understand the thermodynamics and structural properties of the synthesised compounds. For this purpose, the structures of [IPrH][$R_{4-n}SiF_{n+1}$] (n = 1–4, R = Ph, Et) and [IPrH][$R_{4-n}GeF_{n+1}$] (n = 1–4, R = Ph, Et) were used as a starting point for the DFT calculations of the optimised structures, which were then used to compare the corresponding experimentally obtained parameters. The optimised structures of [IPrH][$R_{4-n}SiF_{n+1}$] and [IPrH][$R_{4-n}GeF_{n+1}$] (n = 1–4, R = Ph, Et) are shown in Figures 4.11 and 4.12 respectively.

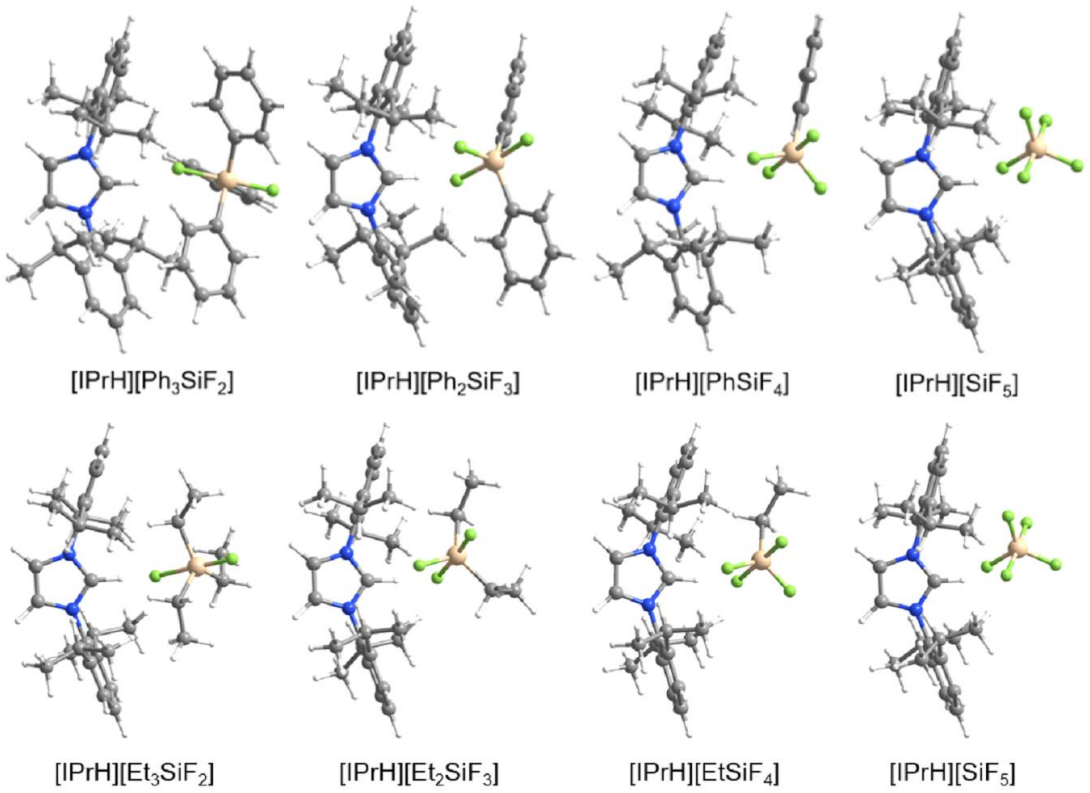

Figure 4.11: Optimised structures of [IPrH][$R_{4-n}SiF_{n+1}$] (n = 1–4, R = Ph, Et).

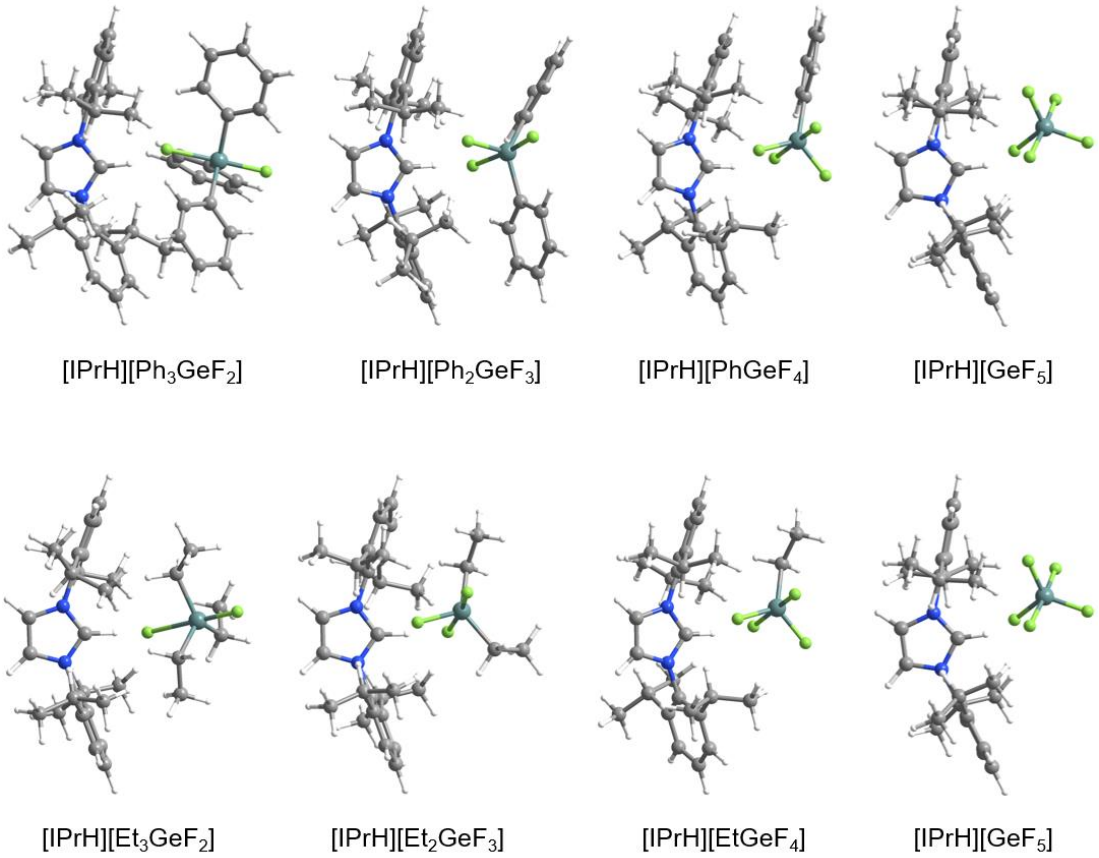

Figure 4.12: Optimised structures of [IPrH][$R_{4-n}GeF_{n+1}$] (n = 1–4, R = Ph, Et).

Tables 4.2 and 4.3 list the experimental and calculated data for Si–C, Si–F and Ge–C, Ge–F bond distances of [IPrH][$R_{4-n}SiF_{n+1}$] and [IPrH][$R_{4-n}GeF_{n+1}$] (n = 1–4, R = Ph, Et) respectively.

Table 4.2: Experimental and calculated bond distances of [IPrH][$R_{4-n}SiF_{n+1}$] (R = Ph, Et, n = 1–4).

Compound	d(Si–C)/Å			d(Si–F)/Å		
	Experimental		Calculated	Experimental		Calculated
[IPrH][Ph_3SiF_2] (**1**)	1.907(2)		1.92	1.746(1)[a]		1.85[a,b]
	1.906(2)		1.92	1.743(1)[a,b]		1.71[a]
	1.898(2)		1.91			
[IPrH][Et_3SiF_2] (**2**)	NA		1.92	NA		2.04[a,b]
			1.91			1.71[a]
			1.91			
[IPrH][Ph_2SiF_3] (**3**)	1.901(2)	1.898(2)	1.91	1.711(1)[a,b]	1.710(1)[a,b]	1.81[a,b]
	1.897(2)	1.897(2)	1.90	1.691(1)[a]	1.689(1)[a]	1.69[a]
				1.645(1)[b]	1.646(1)[b]	1.68
[IPrH][Et_2SiF_3] (**4**)	1.875(2)		1.90	1.733(1)[a,b]		1.87[a,b]
	1.885(2)		1.90	1.729(1)[a]		1.70[a]
				1.648(1)[b]		1.69
[IPrH][$PhSiF_4$] (**5**)	1.901(5)[c]	1.852(7)[c]	1.90	1.718(2)[b,c]	1.751(3)[b,c]	1.77[a,b]
				1.660(2)[a,c]	1.656(3)[a,c]	1.68[a]
				1.654(4)[a,b,c]	1.625(4)[a,b,c]	1.67
				1.584(3)[c]	1.574(5)[c]	1.63

[IPrH][$EtSiF_4$] (**6**)	1.862(3)		1.90	1.701(1)[a,b]		1.80[a,b]
				1.672(1)[a]		1.68[a]
				1.618(1)		1.68
				1.614(1)[b]		1.63
[IPrH][SiF_5][d]				1.62(1)[a,b,c]		1.74[a,b]
				1.644(4)[a,c]		1.66[a]
				1.59(1)[b,c]		1.66
				1.594(4)[c]		1.64
				1.585(4)[c]		1.62

[a] Axial position of fluorine atoms.
[b] Si–F distances, where fluorine atoms form the strongest interactions with the hydrogen atom at C2 position.
[c] Si–C and Si–F distances for domain A, where the anions are disordered.
[d] Values reported in [90].

The calculated data in Table 4.2 show that the calculated distances of the Si–C bonds have similar values to the experimentally determined data. Overall, the calculated bond distances are slightly longer compared to the experimental values, with the exception of [IPrH][$PhSiF_4$] (**5**), where one Si–C bond is significantly shorter (calc. 1.90 Å, exp. 1.852(7) Å). This effect is probably caused by disorder of the anion in the crystal structure. The calculated Si–F bonds, on the other hand, do not follow the same trend. In general, the calculated Si–F bonds agree very well with the experimental values for both axially and equatorially positioned atoms, with the exception of the fluorine atoms where additional interactions with the hydrogen atoms of the cation are present. In these cases, the calculated Si–F bond distances are significantly longer than the experimentally determined bond distances. This effect is probably due to the limitations of the calculations, which were performed in the gas phase and in which the effect of crystal packing was ignored. The DFT calculations thus show the strong effect of the $[IPrH]^+$ cation interactions on the elongation of the Si–F bonds of the organofluorosilicate anions. As with the Si–C bonds, the experimental values for the Si–F bond distances are less reliable for comparison with the calculated data when the anions are disordered.

Table 4.3: Experimental and calculated bond distances of [IPrH][$R_{4-n}GeF_{n+1}$] (R = Ph, Et, n = 1–4).

Compound	d(Ge–C)/Å			d(Ge–F)/Å		
	Experimental		Calculated	Experimental		Calculated
[IPrH][Ph_3GeF_2] (**7**)	1.946(3)	1.958(4)	1.99	1.930(1)[a,b]	1.939(9)[a,b,c]	2.07[a,b]
	1.949(3)	1.970(5)	1.99	1.923(1)[a]	1.935(2)[a]	1.87[a]
	1.963(3)	1.955(4)	1.98			
[IPrH][Et_3GeF_2]	NA		1.99	NA		2.35[a,b]
			1.99			1.85[a]
			1.98			
[IPrH][Ph_2GeF_3] (**8**)	1.936(2)		1.97	1.882(1)[a,b]		1.99[a,b]
	1.939(2)		1.97	1.861(1)[a]		1.84[a]
				1.758(1)		1.82
[IPrH][Et_2GeF_3]	NA		1.99	NA		2.35[a,b]
			1.99			1.85[a]
			1.98			
[IPrH][$PhGeF_4$]	NA		1.97	NA		1.91[a,b]
						1.82[a]
						1.81
						1.76
[IPrH][$EtGeF_4$]	NA		1.97	NA		1.93[a,b]
						1.82[a]
						1.81
						1.77
[IPrH][GeF_5][d]				1.773(4)[a,b,c]		1.85[a,b]
				1.758(1)[c]		1.78[a]
				1.742(4)[b,c]		1.80
				1.716(2)[c]		1.76
				1.703(2)[c]		1.75

[a] Axial position of fluorine atoms.
[b] Ge–F distances, where fluorine atoms form the strongest hydrogen bonds with the hydrogen atom at C2 position.
[c] Ge–C and Ge–F distances for domain A, where the anions are disordered.
[d] Values reported in [90].

Table 4.3 shows similar trends observed for the organofluorosilicate compounds in Table 4.2. The calculated Ge–F bond distances are slightly longer compared to the experimentally determined Ge–F bond lengths. On the other hand, the calculated Ge–F bond distances are very rarely in agreement with the experimental values. While the calculated bond distances of the axially positioned fluorine atoms are in reasonable agreement with the experimental values, the equatorially positioned fluorine atom of [IPrH][Ph_2GeF_3] (**8**) exhibits a significantly shorter Ge–F bond (1.758(1) Å) than the calculated structure (1.82 Å). As with the organofluorosilicate compounds mentioned above, the effects of packing were not considered in the organofluorogermanate calculations, so the $[IPrH]^+$ cation interactions have an exaggerated effect on Ge–F bond lengthening.

In addition to the calculations of the structural parameters, the calculations of the energy released during the formation of the organofluorosilicate and organofluorogermanate salts were carried out on the following chemical reactions in order to better understand the thermodynamic stability of the compounds:

$[R_{4-n}SiF_n] + [IPrH][F] \rightarrow [IPrH][R_{4-n}SiF_{n+1}]$ (R = Et, Ph, n = 1−4),

$[R_{4-n}GeF_n] + [IPrH][F] \rightarrow [IPrH][R_{4-n}GeF_{n+1}]$ (R = Et, Ph, n = 1−4).

Table A.6 in the Appendix A lists the calculated electronic energies of the optimised compounds and the energies of the above-mentioned reactions. As expected, the electron-withdrawing effect of the fluorine atoms helps to disperse the negative charge of organofluorosilicates and organofluorogermanates, increasing their stability as the number of fluorine atoms increases. This is confirmed by calculations showing that reactions with more fluorine atoms are more exothermic. Organic substituents also have a significant influence on the stability of the compounds. In both the organofluorosilicate and organofluorogermanate series, the compounds with less electron-donating phenyl groups formed more stable products.

4.1.5 Summary

This chapter presents a comprehensive study on the reactivity of organofluorosilanes and organofluorogermanes with [IPrH][F] fluoride reagent. This fluoride reagent was used as it has been shown in the past to be capable of stabilising various discrete anions [90]–[93].

The starting materials were prepared by reacting commercially available organochlorosilanes and organochlorogermanes with potassium fluoride. The resulting organofluorosilane and organofluorogermane compounds were further reacted with [IPrH][F] to form new organofluorosilicate $[IPrH][R_{4-n}SiF_{n+1}]$ (R = Ph, Et, n = 1−3) (**1**−**6**) and organofluorogermanate $[IPrH][Ph_{4-n}GeF_{n+1}]$ (n = 1,2) (**7**, **8**) species. The compound $[IPrH][Et_3SiF_2]$ (**2**) did not form, even in liquid phase, as determined by ^{19}F NMR spectrometry. All synthesised compounds were characterised by X-ray structure analysis and, as far as possible, also by mass spectrometry, NMR and Raman spectroscopy.

Two previously unknown ethylfluorosilicate anions $[Et_2SiF_3]^-$ and $[EtSiF_4]^-$ were synthesised in this work. The newly synthesised anions formed despite the electron-donating substituents, which reduce the Lewis acidity of the compound and thus its stability. The least stable anion in the series, $[Et_3SiF_2]^-$, was too unstable to form and the synthesis was unsuccessful.

In addition, two new phenylfluorogermanate compounds $[IPrH][Ph_3GeF_2]$ (**7**) and $[IPrH][Ph_2GeF_3]$ (**8**) were prepared, which represent a rare, structurally isolated species, as only a few organofluorogermanates are known [65], [66].

The experimentally determined structural parameters were compared with the numbers obtained by calculations of the computer-optimised structures. The results of the DFT calculations are mostly in agreement with the experimental values, although the effect of intermolecular interactions on the Si−F and Ge−F bonds is strongly exaggerated. Thermal stability calculations also confirm that the compounds in the $[IPrH][R_{4-n}SiF_{n+1}]$ and $[IPrH][R_{4-n}GeF_{n+1}]$ series (R = Ph, Et, n = 1–3) are more stable with increasing number of fluorine atoms. It has also been shown that phenyl substituents give more stable compounds than ethyl substituents.

4.2 Polymeric Alkali Metal Organofluorosilicates and Organofluorogermanates

This chapter is based on the article "Investigation of polymeric organofluorosilicates and organofluorogermanates" in the *Journal of Fluorine Chemistry* from 2024 [83] and other unpublished results.

This chapter presents the reactivity of organofluorosilanes and organofluorogermanes with alkali metal fluorides (LiF, NaF, KF, RbF, CsF). Alkali metal fluorides are commonly used in fluorination reactions of similar halide compounds, but no side reactions have yet been described. To this end, an NMR reactivity study was performed by reacting $R_{4-n}SiCl_n$ (R = Ph, Et, n = 1−3) and $Ph_{4-n}GeCl_n$ (n = 1−3) with all listed alkali metal fluorides in acetonitrile and THF. The results showed not only halide substitution but also the formation of organofluorosilicates and organofluorogermanates. A new organofluorosilicate and two new organofluorogermanate species were isolated and structurally characterised. X-ray structural analysis showed that the compounds formed a polymeric chain structure in the case of the organofluorogermanates and a planar polymeric structure in the case of the newly synthesised organofluorosilicate compound.

4.2.1 Synthesis and crystal structure determination

The detailed synthetic procedures for both compounds are listed in Appendix A.2, along with their characterisation data.

4.2.1.1 [K][Ph_2GeF_3] · 0.75 MeCN (9)

Ph_2GeCl_2 was added to the acetonitrile suspension of 9.9 equivalents of KF. The reaction mixture was stirred at 50 °C for 48 hours. The excess KF and KCl side product were removed through PTFE filter and the solution was slowly evaporated to obtain crystals of [K][Ph_2GeF_3] · 0.75 MeCN (**9**). The complete synthesis procedure is shown in Scheme 4.9. The crystals were collected and used for X-ray structural analysis.

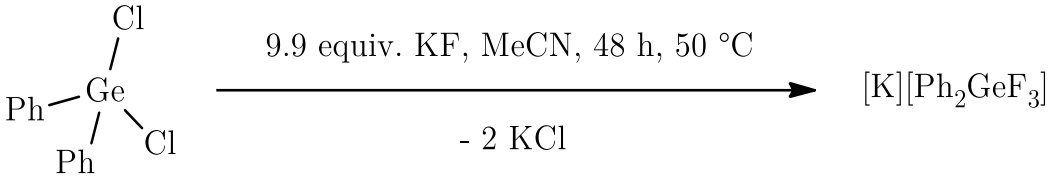

Scheme 4.9: The synthetic procedure for preparation of [K][Ph_2GeF_3] · 0.75 MeCN (**9**).

Single crystals of [K][Ph_2GeF_3] · 0.75 MeCN (**9**) were formed by slow evaporation of the solvent under static vacuum conditions. It crystallises in a monoclinic system with a space group of $P2_1/n$ as a solvate with acetonitrile. The crystal structure of the asymmetric unit is shown in Figure 4.13, while the extended chains from the b- and c-axis are shown in Figures 4.14 and 4.15, respectively.

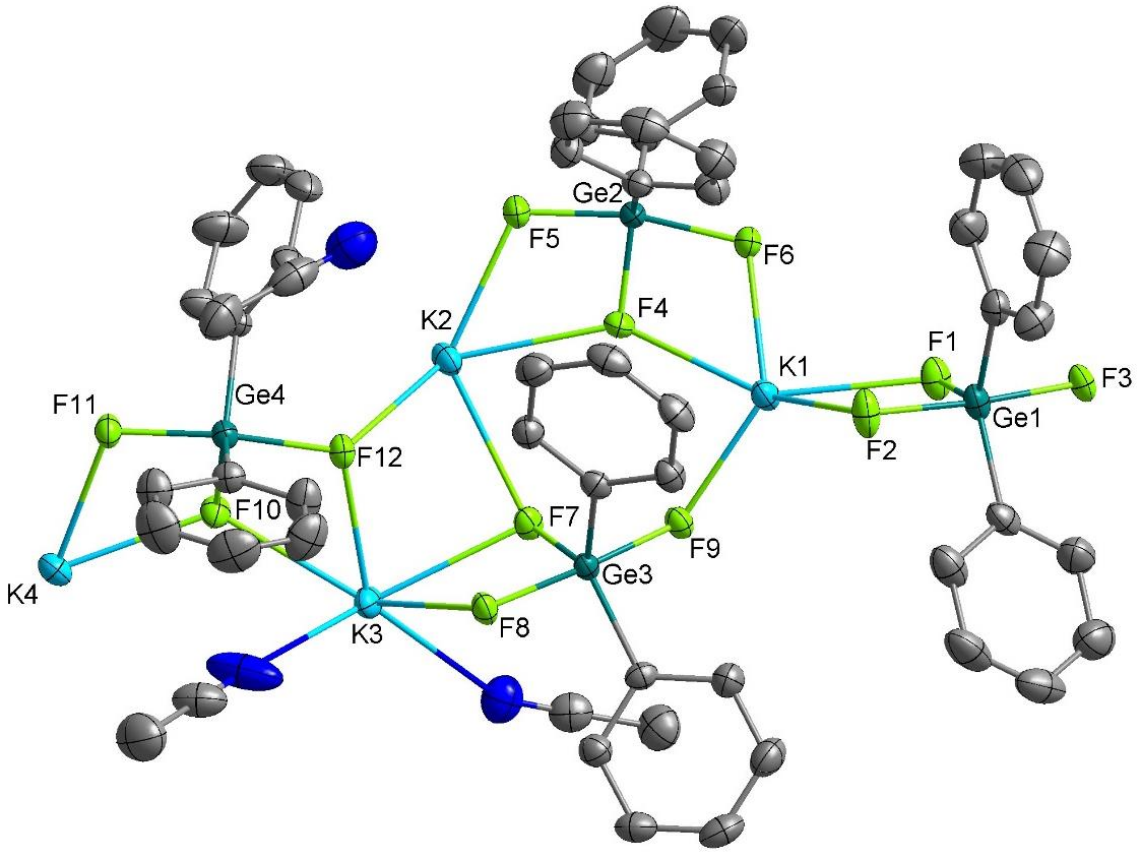

Figure 4.13: The crystal structure of the asymmetric unit of $[K][Ph_2GeF_3] \cdot 0.75$ MeCN, where the thermal ellipsoids are drawn at the 50% probability level. All hydrogen atoms are omitted for clarity.

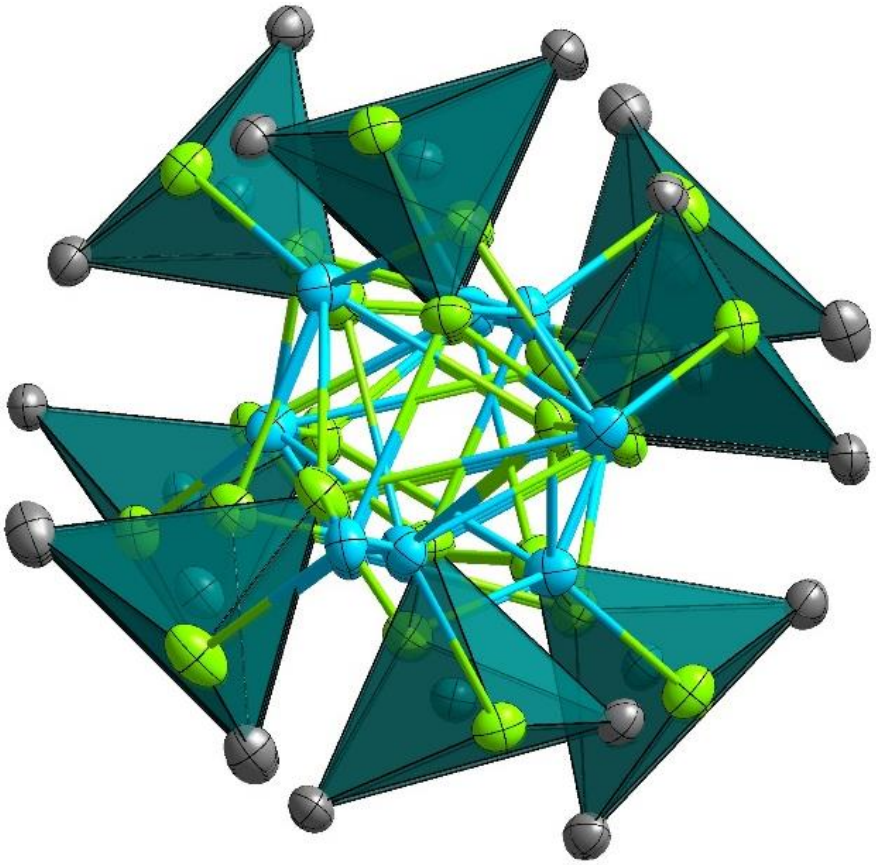

Figure 4.14: The crystal structure of $[K][Ph_2GeF_3] \cdot 0.75$ MeCN along b-axis. The thermal ellipsoids are drawn at the 50% probability level. All hydrogen and ring carbon atoms of the chain structure are omitted for clarity.

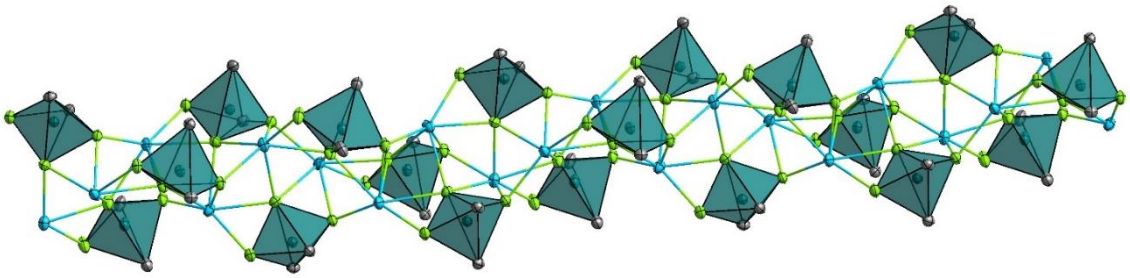

Figure 4.15: The crystal structure of $[K][Ph_2GeF_3] \cdot 0.75$ MeCN along c-axis, where the thermal ellipsoids are drawn at the 50% probability level. All hydrogen and ring carbon atoms are omitted for clarity.

As shown in Figure 4.13, the asymmetric crystal unit contains four ion pairs of $[K][Ph_2GeF_3]$ and three molecules of acetonitrile. The $[Ph_2GeF_3]^-$ anions are all arranged in a trigonal bipyramidal geometry, with the axial positions always occupied by fluorine atoms. The fluorine atoms of the $[Ph_2GeF_3]^-$ anions interact with the potassium cations to form linear K−F−Ge−F−K chains that are twisted into a spiral structure, as shown in Figure 4.15. Figure 4.14 shows that the ionic interactions are contained in the inner part of the one-dimensional structure, while the non-polar phenyl rings form a protective layer on the outside of this structure. While such an organofluorogermanate structure has not been reported, a single similar structure of a polymeric organofluorosilicate exists [64].

Each potassium cation in the asymmetric unit is coordinated to six fluorine atoms of four $[Ph_2GeF_3]^-$ anions, which can act as monodentate or bidentate ligands. In addition, every third potassium cation is coordinated by two acetonitrile molecules. The remaining acetonitrile molecule in the unit cell does not interact with other molecules and is packed together with the organic shell of phenyl groups. In contrast to the organofluorosilicate relative, where π-interactions have been reported, no such interactions were observed in the $[K][Ph_2GeF_3] \cdot 0.75$ MeCN crystal structure, most likely due to the fact that more favourable interactions are preferred.

4.2.1.2 [Cs][Ph₂GeF₃] · THF (10)

Ph_2GeCl_2 was added to the THF suspension of 9.9 equivalents of CsF. The reaction mixture was stirred at 50 °C for 48 hours. The excess CsF and CsCl side product were removed through PTFE filter and the solution was slowly evaporated to obtain crystals of $[Cs][Ph_2GeF_3] \cdot$ THF (**10**). The complete synthesis procedure is shown in Scheme 4.10. The crystals were collected and used for X-ray structural analysis.

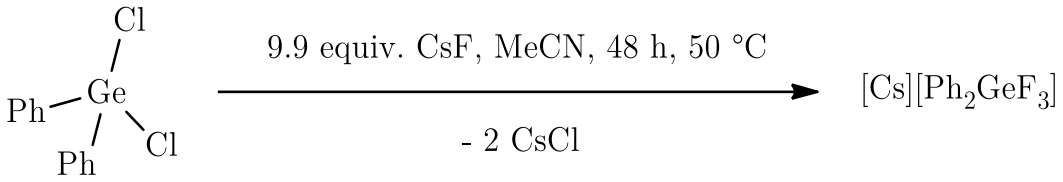

Scheme 4.10: The synthetic procedure for preparation of $[Cs][Ph_2GeF_3] \cdot$ THF (**10**).

Single crystals of $[Cs][Ph_2GeF_3] \cdot$ THF (**10**) were formed by slow evaporation of the solvent under static vacuum conditions. It crystallises in a monoclinic system with a space group of $P2_1/c$ as a solvate with tetrahydrofuran. The crystal structure of the asymmetric unit is shown in Figure 4.16, while the extended chains from the c- and b-axis are shown in Figures 4.17 and 4.18, respectively.

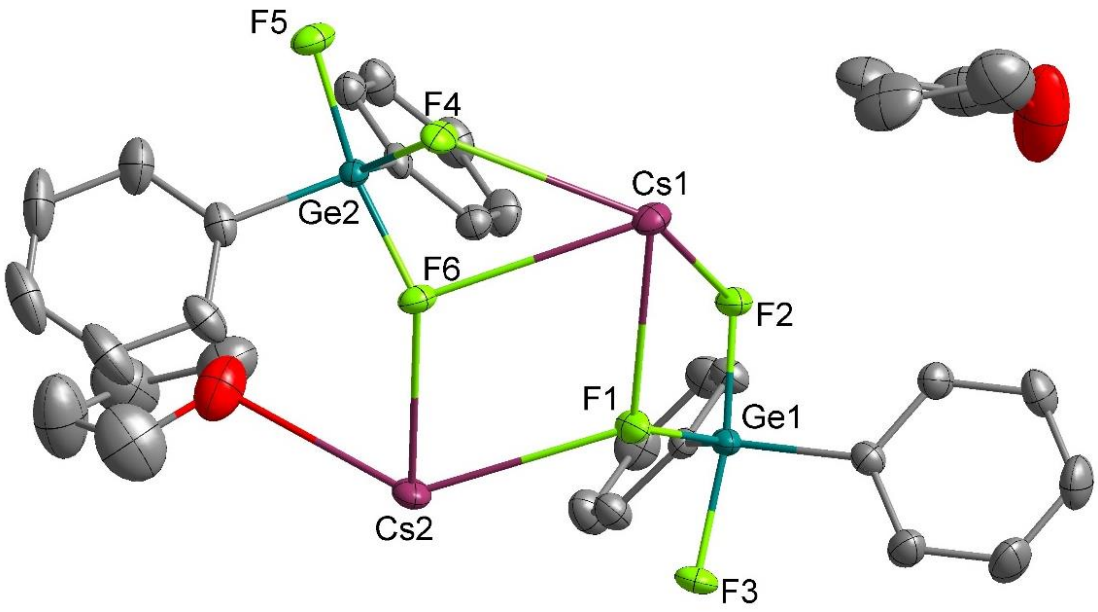

Figure 4.16: The crystal structure of the asymmetric unit of $[Cs][Ph_2GeF_3] \cdot$ THF, where the thermal ellipsoids are drawn at the 50% probability level. All hydrogen atoms are omitted for clarity.

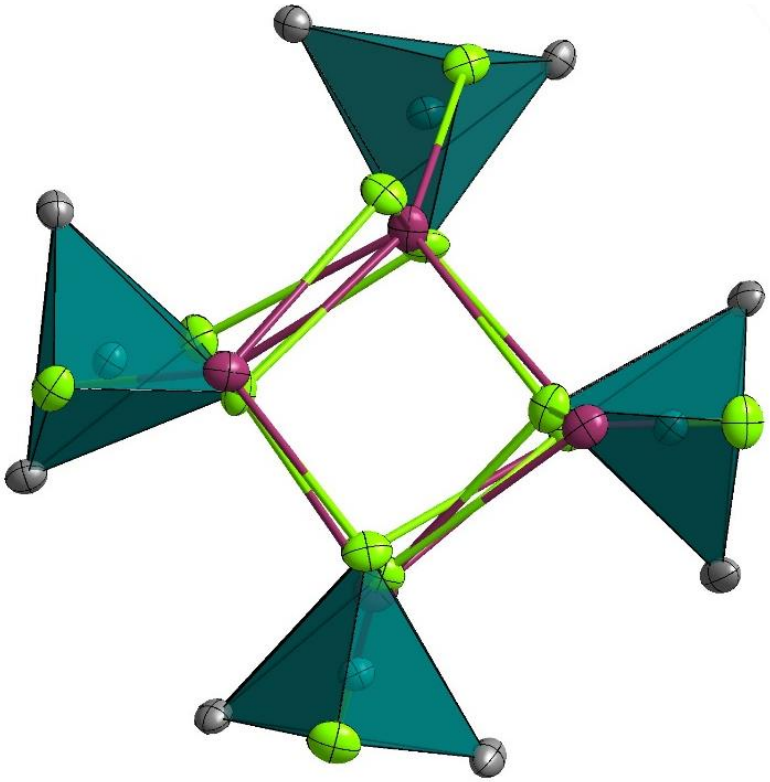

Figure 4.17: The crystal structure of $[Cs][Ph_2GeF_3] \cdot THF$ along c-axis. The thermal ellipsoids are drawn at the 50% probability level. All hydrogen and ring carbon atoms of the chain structure are omitted for clarity.

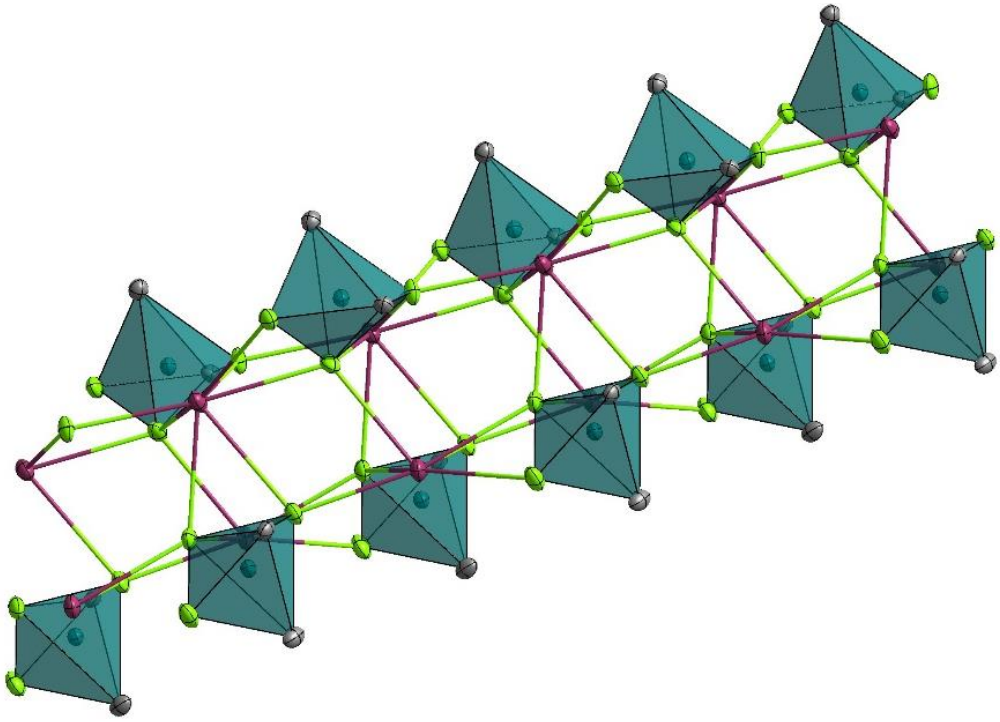

Figure 4.18: The crystal structure of $[Cs][Ph_2GeF_3] \cdot THF$ along b-axis, where the thermal ellipsoids are drawn at the 50% probability level. All hydrogen and ring carbon atoms are omitted for clarity.

The asymmetric crystal unit is shown in Figure 4.16 and contains 2 ion pairs of $[Cs][Ph_2GeF_3]$ together with two molecules of tetrahydrofuran. As in $[K][Ph_2GeF_3] \cdot 0.75$ MeCN, the organofluorogermanate anions are organised in a trigonal bipyramidal structure in which the axial positions are occupied by fluorine atoms and other ligands occupy positions in the equatorial plane. Similar to its potassium counterpart, the cesium atoms interact with fluorine atoms to form a linear Cs−F−Ge−F−Cs chain resulting in a linear polymer structure, which is shown in Figure 4.18. Compared to the previously described polymeric organofluorogermanate $[K][Ph_2GeF_3] \cdot 0.75$ MeCN, the structure is more symmetrical, resulting in a rectangular cavity in the centre of the one-dimensional structure, as shown in Figure 4.17. Non-polar phenyl groups and tetrahydrofuran molecules are arranged around the ionic core of the structure.

The larger cesium cation is expected to be coordinated by more atoms than the smaller potassium, and indeed the first cesium atom of the asymmetric unit is coordinated by seven fluorine atoms compared to the six of potassium. There is a tetrahydrofuran molecule near the first cesium cation, but it does not appear to be coordinated to the cation because the oxygen atom is on the opposite side of the molecule. The second caesium cation, on the other hand, is coordinated by six fluorine atoms together with a tetrahydrofuran molecule. As with its potassium relative, no π-interactions were observed in this crystal structure.

4.2.1.3 $[Cs][Ph_3SiF_2]$ (11)

Ph_3SiCl was added to the acetonitrile suspension of 9.9 equivalents of CsF. The reaction mixture was stirred at 50 °C for 48 hours. The excess CsF and CsCl side product were removed through PTFE filter and the solution was slowly evaporated to obtain crystals of $[Cs][Ph_3SiF_2]$ (**11**). The complete synthesis procedure is shown in Scheme 4.11. The crystals were collected and used for X-ray structural analysis.

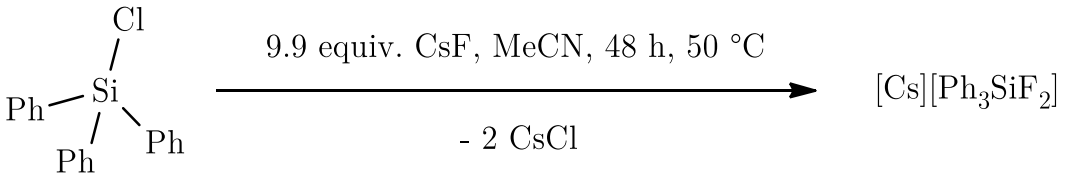

Scheme 4.11: The synthetic procedure for preparation of $[Cs][Ph_3SiF_2]$ (**11**).

Single crystals of $[Cs][Ph_3SiF_2]$ (**11**) were formed by slow evaporation of the solvent under static vacuum conditions. It crystallises in a monoclinic system with a space group of $P2_1/c$. The crystal structure of the asymmetric unit is shown in Figure 4.19, while the extended structures from the a-, c- and b-axis are shown in Figures 4.20, 4.21 and 4.22, respectively.

The asymmetric unit shown in Figure 4.19 contains two ion pairs of $[Cs][Ph_3SiF_2]$. Similar to the previously described polymeric organofluorogermanate species, the anions adopt a trigonal bipyramidal geometry with the fluorine atoms in the axial positions and the phenyl groups in the equatorial positions. As with the germanium counterparts, the alkali metal cations interact with fluorine atoms and form Si−F−Cs−F−Si bonds between different organofluorosilicate anions. However, in contrast to the one-dimensional tubular structures observed in the organofluorogermanates, this organofluorosilicate forms a two-dimensional sheet-like polymer structure, as shown in Figures 4.20, 4.21 and 4.22.

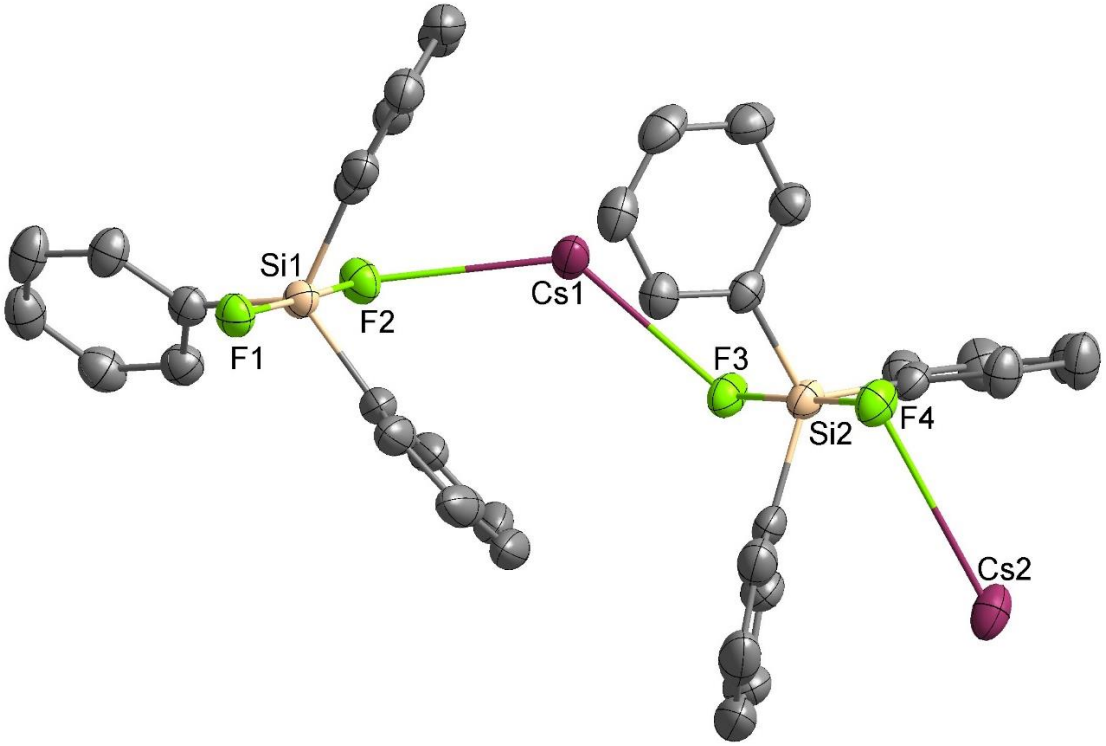

Figure 4.19: The crystal structure of the asymmetric unit of $[Cs][Ph_3SiF_2]$, where the thermal ellipsoids are drawn at the 50% probability level. All hydrogen atoms are omitted for clarity.

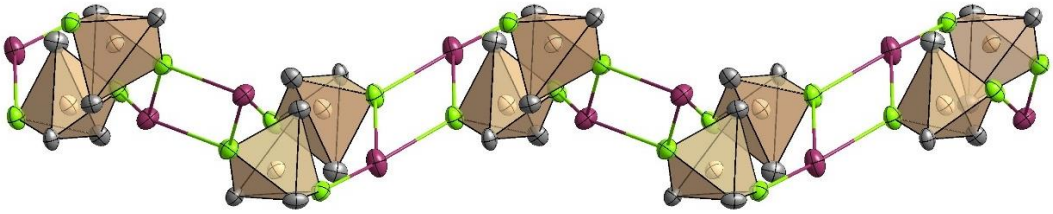

Figure 4.20: The crystal structure of $[Cs][Ph_3SiF_2]$ along a-axis. The thermal ellipsoids are drawn at the 50% probability level. All hydrogen and ring carbon atoms of the chain structure are omitted for clarity.

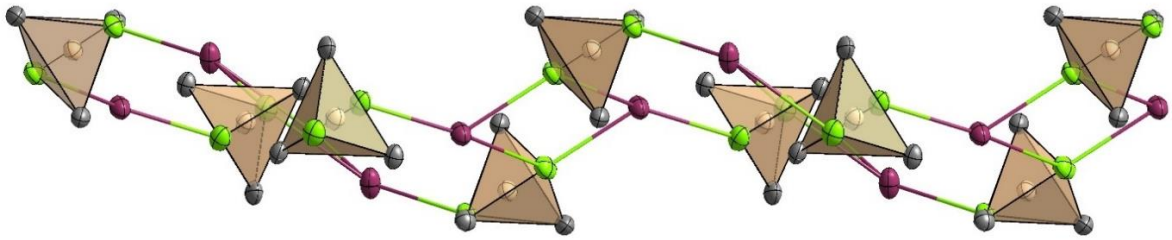

Figure 4.21: The crystal structure of $[Cs][Ph_3SiF_2]$ along c-axis. The thermal ellipsoids are drawn at the 50% probability level. All hydrogen and ring carbon atoms of the chain structure are omitted for clarity.

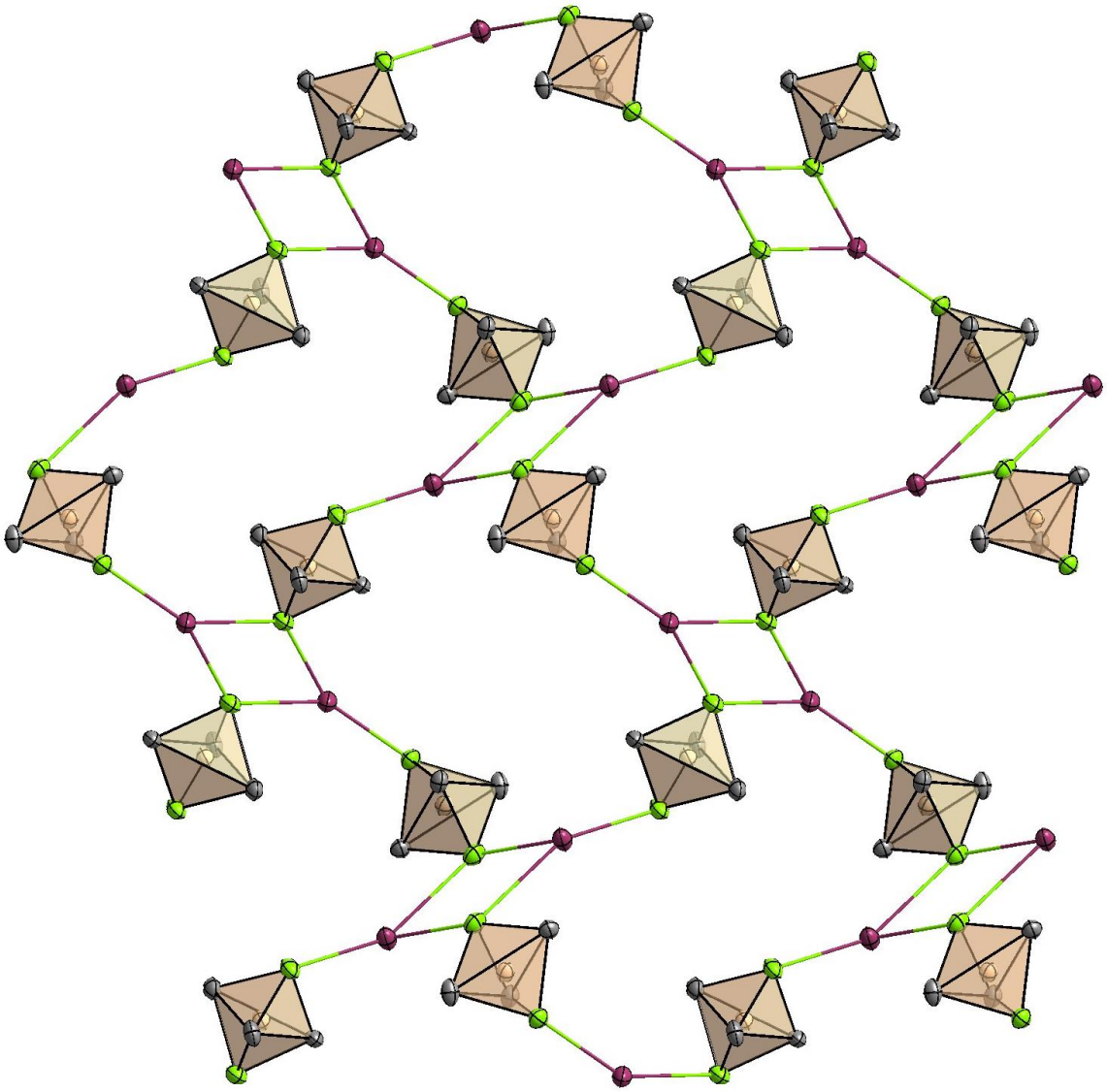

Figure 4.22: The crystal structure of $[Cs][Ph_3SiF_2]$ along b-axis perspective. The thermal ellipsoids are drawn at the 50% probability level. All hydrogen and ring carbon atoms of the chain structure are omitted for clarity.

Due to the lower number of fluorine atoms available for coordination with cesium cations and the steric hindrance by bulky phenyl groups, the cesium cation is only coordinated by three fluorine atoms, which implies a coordination number of only 3. This is significantly lower than the coordination number of 7 observed in $[Cs][Ph_2GeF_3] \cdot THF$. However, the actual coordination number is higher because the nearby phenyl rings are close enough (the Cs−C distances range from 3.4 to 5.7 Å) and have a suitable orientation for the π-cation bonding interaction. As can be seen in Figure 4.23, the cesium cations are coordinated by four phenyl rings, resulting in a coordination number of 7, which is consistent with the previously described $[Cs][Ph_2GeF_3] \cdot THF$.

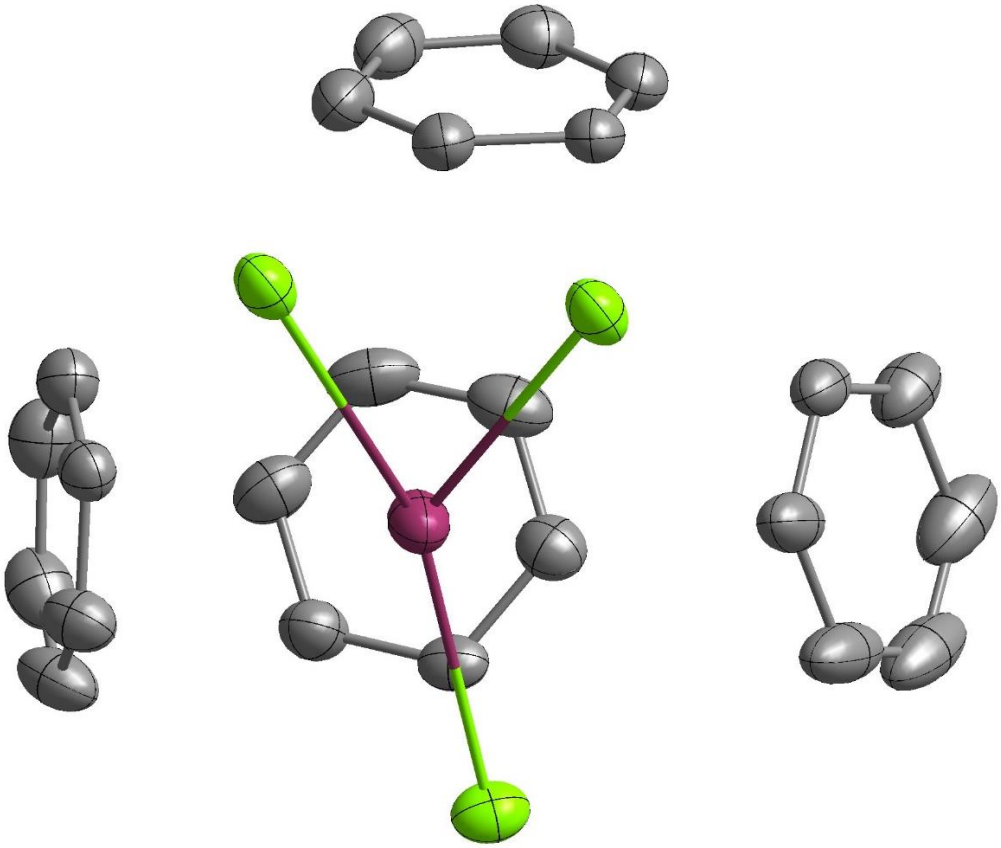

Figure 4.23: Coordination sphere around the cesium atom (Cs1) in the structure $[Cs][Ph_3SiF_2]$. The thermal ellipsoids are drawn at the 50% probability level. For the sake of clarity, only the groups involved in the coordination are shown.

4.2.2 NMR investigations of alkali metal fluoride and organochlorosilane or organochlorogermane reaction mixtures

In an attempt to synthesise imidazolium-based organofluorosilicates and organofluorogermanates described in the previous chapter, some reactants showed the formation of by-products when they underwent a halide exchange reaction with alkali metal fluorides. This anomaly was interesting as alkali metal fluorides are considered harmless reagents with a low propensity for side reactions.

Due to these anomalies, efforts have been made to better understand the reactivity of alkali metal fluorides with organochlorosilanes and organofluorogermanes. The synthetic procedure is outlined in Scheme 4.12.

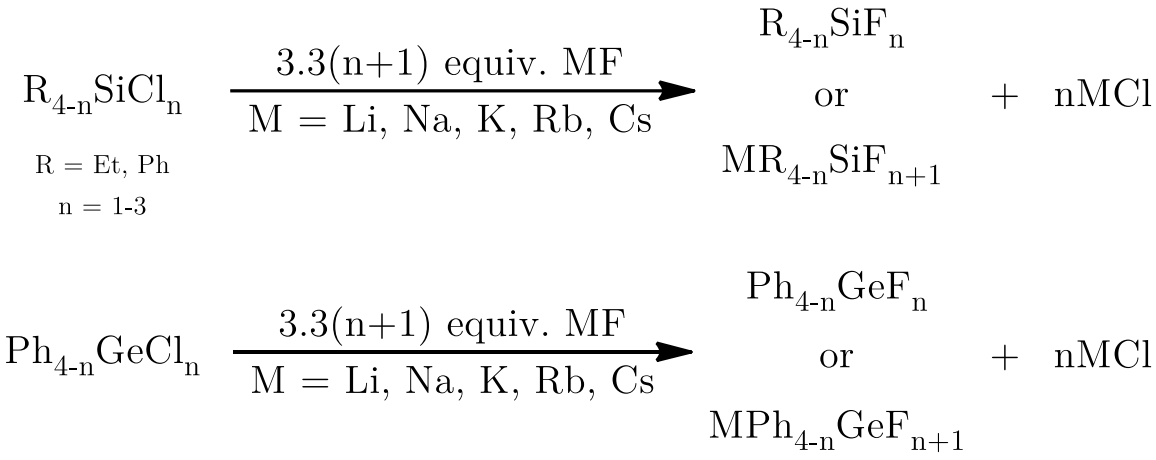

Scheme 4.12: Reaction scheme of various organochlorosilanes and germanes with alkali metal fluorides.

The test reactions were carried out in acetonitrile and THF to maximise the solution of the compounds, as alkali metal fluorides are mostly insoluble in organic solvents. Water was considered but avoided due to the possible hydrolysis of the compounds. To ensure maximum conversion, a 3.3-fold excess of alkali metal fluoride relative to the number of fluorine atoms incorporated into the organochlorine compound was used. Due to the low solubility of the fluoride reagents, the reactions were carried out at 50 °C for 48 hours. After completion of the reactions, the reaction mixtures were analysed by ^{1}H and ^{19}F NMR. The results of the ^{19}F NMR spectra are shown in Tables 4.5 and 4.6 for the reactions in acetonitrile and THF, respectively. Due to the rapid intramolecular transformations undergone by some organofluorosilicate and organofluorogermanate compounds, some signals are not visible in the ^{19}F NMR spectra. In the cases where no signals were present at room temperature, the measurements were repeated at −40 °C.

To identify the products formed in the test reactions, the ^{19}F NMR spectroscopy results were compared with the spectra of known compounds that may have been formed in the reactions. The expected products were neutral organofluorosilanes or organofluorogermanes, or the anionic organofluorosilicate and organofluorogermanate species. Data were available for all silicon-based compounds, with the exception of the $[Et_3SiF_2]^-$ anion, which is unknown. For this reason, the data for the structurally related $[Me_3SiF_2]^-$ anion was used instead. Data for germanium-related compounds, on the other hand, are extremely limited, as only spectral data for Ph_3GeF and the $[Ph_3GeF_2]^-$ anion are available. The ^{19}F NMR literature data are summarised and presented in Table 4.4.

Table 4.4: ^{19}F NMR literature data for selected organofluorosilanes, organofluorogermanes, organofluorosilicates and organofluorogermanates.

	δ (^{19}F) Si/Ge–F		δ (^{19}F) Si/Ge–F
Et_3SiF[94]	−176.5 (C_6D_6)	[PNP][Me_3SiF_2][88]	−61.9 (MeCN-d_3) (253 K)
Et_2SiF_2[94]	−144.3 (C_6D_6)	[IPrH][Et_2SiF_3][82]	−86.0 (MeCN-d_3) (233 K) −136.2 (MeCN-d_3) (233 K)
$EtSiF_3$[95]	−137.7 (C_6D_6)	[IPrH][$EtSiF_4$][82]	−115.8 (MeCN-d_3) (233 K)
Ph_3SiF[96]	−169.4 (THF-d_8)	[IPrH][Ph_3SiF_2][82]	−97.0 (MeCN-d_3)
Ph_2SiF_2[97]	−142.9 (MeCN-d_3)	[IPrH][Ph_2SiF_3][82]	−96.6 (MeCN-d_3) (233 K) −134.2 (MeCN-d_3) (233 K)
$PhSiF_3$[98]	−141.1 ($CDCl_3$)	[$(CH_3)_4N$][$PhSiF_4$][89]	−116.8 (DMSO-d_8)
Ph_3GeF[94]	−203.6 (C_6D_6)	[IPrH][Ph_3GeF_2][82]	−143.7 (MeCN-d_3) (233 K)
Ph_2GeF_2	/	/	/
$PhGeF_3$	/	/	/

Et_3SiCl: The reaction of Et_3SiCl with any alkali metal fluoride gave a single ^{19}F NMR signal at −176.5 ppm in MeCN-d_3 and −176.6 ppm in THF-d_8, which is identical to that of Et_3SiF (−176.5 ppm) [94]. Since the ^{1}H NMR spectrum of the same reaction mixture shows only one set of signals, this indicates a complete conversion of ethylchlorosilane to the fluorinated product. A summary of the reactions with Et_3SiCl is shown in Scheme 4.13.

$$Et_3SiCl \xrightarrow[M = Li, Na, K, Rb, Cs]{6.6 \text{ equiv. MF}} Et_3SiF + MCl$$

Scheme 4.13: Reaction results of Et_3SiCl with alkali metal fluorides.

Et_2SiCl_2: The reaction with Et_2SiCl_2 produced several ^{19}F NMR signals in the range of −142.9 to −144.5 ppm in both solvents. Although this spectral range is consistent with the reported chemical shift for Et_2SiF_2 (−144.3 ppm) [94], a single peak would be expected for this compound. The absence of signals at higher frequencies (above −136 ppm) typically associated with $[Et_2SiF_3]^-$ indicates incomplete chlorine replacement rather than the formation of a fluorosilicate. A summary of the reactions with Et_2SiCl_2 is shown in Scheme 4.14.

$$Et_2SiCl_2 \xrightarrow[M = Li, Na, K, Rb, Cs]{9.9 \text{ equiv. MF}} Et_2SiF_2 + 2MCl$$

Scheme 4.14: Reaction results of Et_2SiCl_2 with alkali metal fluorides.

Table 4.5: ^{19}F NMR chemical shifts for test reactions in acetonitrile-d_3.

δ values in ppm, relative intensities in parentheses	LiF	NaF	KF	RbF	CsF
Et_3SiCl	−175.6	−175.6	−175.6	−175.6	−175.6
Et_2SiCl_2	−143.3 (minor) −144.3 (major)	−144.2	−143.3 (minor) −144.3 (major)	−142.9 (0.20) −143.3 (1.00) −144.2 (2.00)	−142.9 (0.20) −143.3 (1.00)
$EtSiCl_3$	−137.4 (0.27) −140.3 (1.00)	−137.4 −138.4	No signals in ^{1}H and ^{19}F spectra (presumed insoluble).	−137.4 (1.00) −138.4 (0.38) −140.3 (1.92)	No signals in ^{1}H and ^{19}F spectra (presumed insoluble).
Ph_3SiCl	−170.3	−170.3	−170.3	−170.3	−94.8
Ph_2SiCl_2	−141.2 (0.10) −143.0 (1.00)	−142.9	−140.3 (1.00) −140.4 (0.97) −140.8 (1.06) −141.2 (0.89)	−141.1 (1.00) −142.9 (1.01)	−97.3 (2.01) −134.3 (1.06)
$PhSiCl_3$	−138.0 (0.14) −141.9 (1.00)	No signals in ^{1}H and ^{19}F spectra (presumed insoluble).	No signals in ^{1}H and ^{19}F spectra (presumed insoluble).	−138.0 (1.21) −138.9 (1.00) −141.9 (2.14)	No signals in ^{1}H and ^{19}F spectra (presumed insoluble).
Ph_3GeCl	No conversion	No conversion	−201.6	−201.7	(233K) −112.8 (1.76) −142.2 (1.00)
Ph_2GeCl_2	No conversion	−166.6	No signals in ^{19}F spectra at 298K and 233K.	−164.2 (minor) −164.6 (1.00) −166.6 (1.91) −168.9 (minor)	(233K) −111.6 (2.01) −139.8 (1.00)
$PhGeCl_3$	No conversion	No signals in ^{1}H and ^{19}F spectra (presumed insoluble).	No signals in ^{1}H and ^{19}F spectra (presumed insoluble).	Only weak signals of starting compound in ^{1}H, no signals in ^{19}F spectra	No signals in ^{1}H and ^{19}F spectra (presumed insoluble).

$EtSiCl_3$: The reactivity of $EtSiCl_3$ with metal fluorides varied depending on both the solvent and the cation. In acetonitrile, LiF, NaF and RbF gave several ^{19}F NMR resonances ranging from −137.4 to −140.3 ppm, which corresponds approximately to the reported chemical shift for $EtSiF_3$ (−137.7 ppm) [95]. However, the absence of the characteristic peak for $[EtSiF_4]^-$ at −115.8 ppm [82] indicates that either no formation of organofluorosilicate salt has occurred or the compound is insoluble. In contrast, KF and CsF in acetonitrile did not produce observable signals in either ^{1}H or ^{19}F NMR, suggesting the formation of insoluble polymeric organofluorosilicate salts or other by-products.

LiF and RbF showed lower reactivity in THF compared to other alkali metal fluorides. Their ^{19}F NMR spectra showed peaks near −137.7 ppm, consistent with the formation of $EtSiF_3$. Reactions with NaF, KF and CsF in THF led to more complex product mixtures, as evidenced by additional unidentified ^{19}F NMR resonances between −122.1 and −125.4 ppm. Of note, the KF and CsF reactions also produced a small peak at −115.4 ppm, consistent with the expected signal for the target compound, $[EtSiF_4]^-$, suggesting partial conversion of the starting material to the target organofluorosilicate. A summary of the reactions with $EtSiCl_3$ is shown in Scheme 4.15.

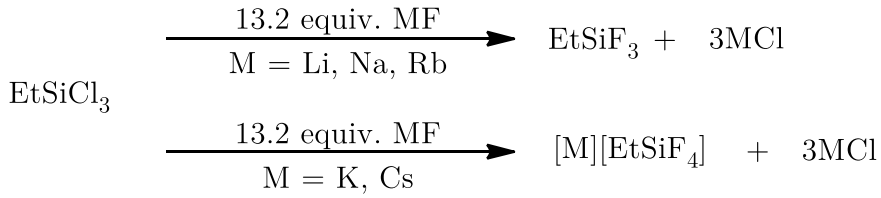

Scheme 4.15: Reaction results of $EtSiCl_3$ with alkali metal fluorides.

Ph_3SiCl: Treatment with LiF, NaF, KF and RbF in acetonitrile gave a single ^{19}F NMR signal at −170.3 ppm, consistent with the chemical shift of Ph_3SiF (−169.4 ppm) [96], indicating complete conversion to the fluorosilane. In contrast, CsF produced a unique peak at −94.8 ppm, consistent with literature values for the $[Ph_3SiF_2]^-$ difluorosilicate anion (−97.0 ppm) [82], indicating complete conversion to the desired organofluorosilicate. While no product formation was observed by NMR in the reaction of LiF in THF, reactions with other alkali metal fluorides in this solvent gave a single peak at −170.7 ppm, consistent with the formation of Ph_3SiF. A summary of the reactions with Ph_3SiCl is shown in Scheme 4.16.

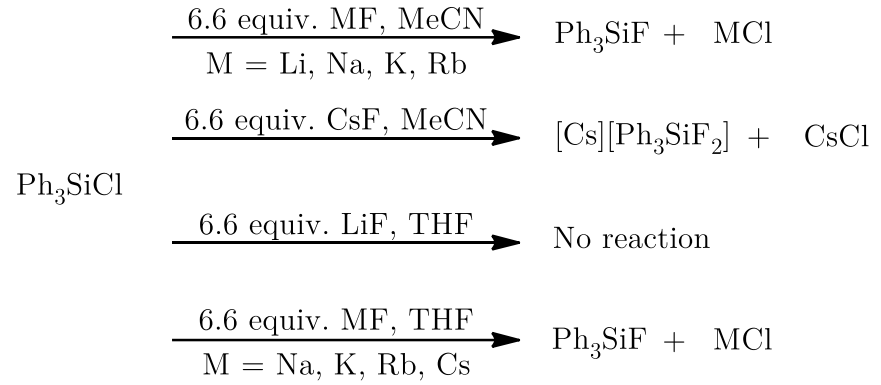

Scheme 4.16: Reaction results of Ph_3SiCl with alkali metal fluorides.

Ph_2SiCl_2: The ^{19}F NMR spectra of almost all reactions in both acetonitrile and THF showed signals centred around −142 ppm, which is consistent with the reported chemical shift for Ph_2SiF_2 (−142.9 ppm) [97]. However, the presence of multiple peaks instead of a single resonance indicates incomplete halogen substitution. In particular, the reactions carried out in THF gave more complex ^{19}F NMR spectra than those in acetonitrile, indicating the formation of additional fluorine-containing compounds in the THF reaction mixture. An important exception was the reaction between Ph_2SiCl_2 and CsF in acetonitrile, which gave two signals at −97.3 and −134.3 ppm with an integrated intensity ratio of 2:1. These values agree well with the reported chemical shifts for $[IPrH][Ph_2SiF_3]$ (−96.6 and −134.2 ppm at 233 K) [10], strongly suggesting successful formation of the $[Ph_2SiF_3]^-$ anion. A summary of the reactions with Ph_2SiCl_2 is shown in Scheme 4.17.

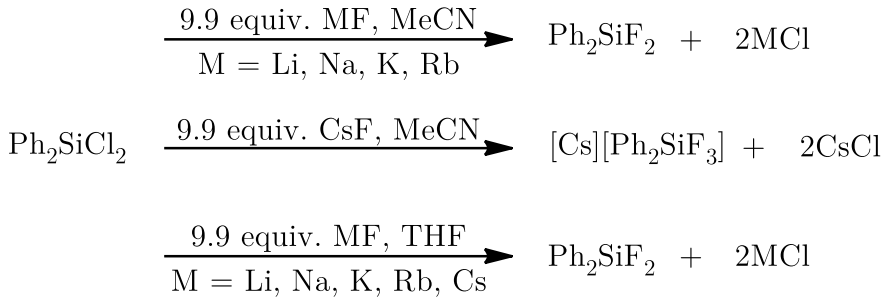

Scheme 4.17: Reaction results of Ph_2SiCl_2 with alkali metal fluorides.

Table 4.6: ^{19}F NMR chemical shifts for test reactions in tetrahydrofuran-d_8.

δ values in ppm relative intensities in parentheses	LiF	NaF	KF	RbF	CsF
Et_3SiCl	−176.7	−176.6	−176.6	−176.6	−176.6
Et_2SiCl_2	−143.6 −144.5	−143.4	−143.3 (2.00) −144.5 (1.26)	−143.3 (0.35) −143.5 (0.09) −144.5 (1.00)	−143.3 (0.11) −144.5 (1.00)
$EtSiCl_3$	−134.5 (1.00) −137.6 (0.13) −138.5 (0.06)	−122.1 (0.13) −122.4 (0.36) −122.5 (1.00) −125.4 (0.29) −137.2 (0.25)	−115.4 (0.64) −122.4 (0.88) −137.5 (1.58) −141.0 (1.00)	−134.3 (0.28) −137.7 (1.00)	−115.4 (0.11) −122.5 (0.16) −125.0 −137.5 (0.48) −141.0 (1.00)
Ph_3SiCl	No conversion	−170.8	−170.7	−170.7	−170.7
Ph_2SiCl_2	−141.1 (0.09) −142.1 (0.21) −143.3 (1.00)	−140.2 (1.98) −140.6 (2.25) −141.1 (1.00) −142.1 (1.95) −143.2 (4.11)	−140.7 (0.89) −142.1 (1.23) −143.3 (1.00)	−140.4 (0.05) −141.1 (0.10) −142.1 (0.48) −143.2 (1.00)	−140.3 (0.05) −140.5 (0.12) −140.7 (0.30) −141.1 (0.95) −142.1 (1.00) −143.2 (0.84)
$PhSiCl_3$	−138.3 (0.13) −138.9 (0.06) −142.5 (1.00)	(233K) −121.2 (1.00) −132.5 (1.17) −137.2 (0.68)	−114.0 (0.16) −122.0 (0.26) −125.4 (0.05) −133.9 (0.09) −138.3 (1.00) −139.0 (0.07) −142.5 (0.20)	−133.9 (0.90) −138.0 (1.00)	−138.3 (0.94) −142.5 (3.00)
Ph_3GeCl	No conversion	−204.8	−204.8	−164.5 (1.00) −204.8 (0.98)	−204.8
Ph_2GeCl_2	−156.6 (1.00) −196.2 (0.23) −197.0 (0.23)	−168.1 (1.00) −171.0 (0.09) −196.2 (0.12) −197.0 (0.12)	−130.0 (0.26) −166.2 (1.00)	(233K) −164.8 (0.36) −192.3 (0.99) −193.5 (1.00)	−112.2 (2.11) −127.6 (1.00)
$PhGeCl_3$	−138.5 (1.00) −138.7 (0.41)	−138.5 (1.00) −138.7 (0.58)	−130.0 (2.56) −136.6 (0.62) −141.3 (1.00)	No signals in ^1H and ^{19}F spectra (presumed insoluble).	−130.0 (2.86) −136.6 (1.38) −141.3 (1.00) −144.5 (0.06) −145.0 (0.21) −146.4 (0.36)

$PhSiCl_3$: Reactions of $PhSiCl_3$ with LiF and RbF in acetonitrile gave several ^{19}F NMR resonances between −138 and −142 ppm, which is in a range consistent with the formation of $PhSiF_3$ (−141.1 ppm) [98], although only one signal is expected. In contrast, reactions with other alkali metal fluorides gave no recognisable signals in either ^{1}H or ^{19}F NMR, probably due to the formation of insoluble organofluorosilicate salts or unidentified by-products.

Reactions carried out in THF showed more complex results compared to those in acetonitrile. LiF and CsF reactions produced a dominant peak at −142.5 ppm, consistent with $PhSiF_3$ (−141.1 ppm) [98], but also contained smaller, unidentified peaks around −138 ppm. NaF and RbF reactions gave two distinct signals at −133 and −138 ppm, possibly representing intermediates or unidentified by-products. The NaF reaction also showed an uncharacterised peak at −122 ppm. The KF reaction produced the most complex mixture, which contained all of the previously mentioned peaks and a smaller peak at −114 ppm. This peak corresponds closely to the value reported for the $[PhSiF_4]^-$ anion (−116.8 ppm) [89], suggesting limited formation of the expected fluorosilicate product. A summary of the reactions with $PhSiCl_3$ is shown in Scheme 4.18.

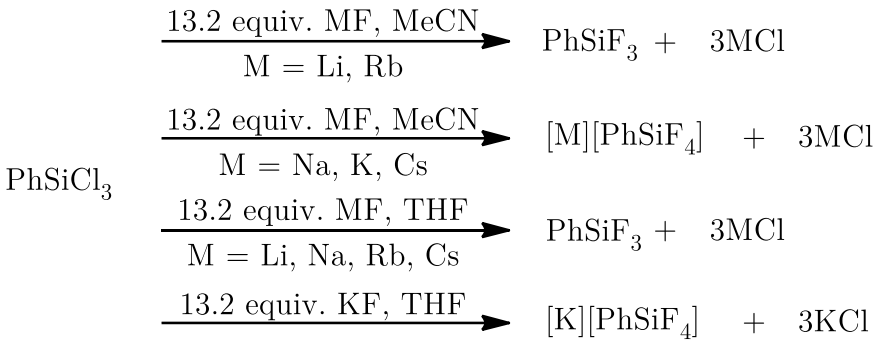

Scheme 4.18: Reaction results of $PhSiCl_3$ with alkali metal fluorides.

Ph_3GeCl: The reactivity of Ph_3GeCl in acetonitrile varied greatly depending on the alkali metal fluoride used in the reaction. LiF and NaF showed no ^{19}F signals and only Ph_3GeCl was observed in ^{1}H NMR, indicating negligible Ph_3GeCl conversion. Reactions with KF and RbF gave a single ^{19}F resonance at −201.6 ppm, consistent with the reported chemical shift for Ph_3GeF (−203.6 ppm) [94]. CsF yielded a more complex product mixture with two new fluorine signals. A peak at −142.2 ppm agrees well with the reported value for the $[Ph_3GeF_2]^-$ anion (−143.7 ppm) [82] and confirms the formation of this organofluorogermanate anion. The peak at −112.8 ppm probably also belongs to the $[Ph_3GeF_2]^-$ anion, but to a different isomer of the same anion. A similar peak was observed in an $[IPrH][Ph_3GeF_2]$ ^{19}F NMR spectrum, but due to the low integral ratio it was thought to be a fluorine-containing impurity or by-product. Interestingly, the ^{19}F NMR spectrum of the $Ph_2GeF_3^-$ anion contains signals at −111.6 ppm and −139.8 ppm, which are very similar to those of the $Ph_3GeF_2^-$ anion. Since these peaks correspond to the axial and equatorial fluorine atoms, respectively, it is very likely that the two signals in the reaction mixture of Ph_3GeCl and CsF belong to the two isomers of the same compound. This phenomenon is probably the result of a Berry pseudorotation in which the two axial ligands can swap positions with the two equatorial ligands.

Similar to acetonitrile, LiF in THF showed no conversion of the starting material. Other alkali metal fluorides produced a signal at −204.8 ppm, consistent with Ph_3GeF (−203.6 ppm) [94]. Remarkably, the RbF reaction yielded an additional, unidentified peak at −164.5 ppm, which probably represents a by-product. Unfortunately, no suitable crystals

could be obtained for X-ray analysis to determine the identity of the compound. A summary of the reactions with Ph_3GeCl is shown in Scheme 4.19.

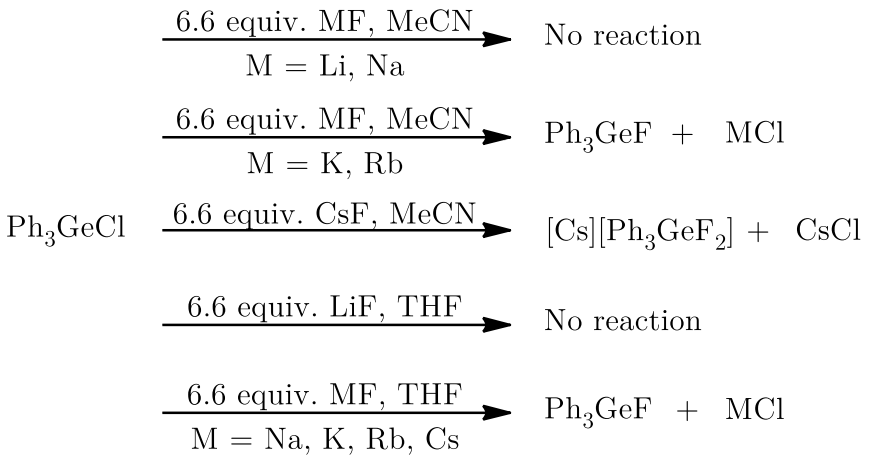

Scheme 4.19: Reaction results of Ph_3GeCl with alkali metal fluorides.

Ph_2GeCl_2: Since the field of organofluorogermanates is little explored, the reference data for the ^{19}F NMR spectra of Ph_2GeF_2 and the $[Ph_2GeF_3]^-$ anion are not available, which prevents a definitive signal assignment. However, some insights can be gained from the general trends observed in silicon analogues. In acetonitrile, LiF was found to be non-reactive, while NaF and RbF produced peaks near −166 ppm. KF did not give ^{19}F signals at either 298 or 233 K, although the formation of new species was detected in ^1H NMR. The lack of fluorine signals, even at low temperatures, could be due to rapid fluctuations in the $[Ph_2GeF_3]^-$ anion geometry. Interestingly, the CsF reaction produced a doublet at −111.6 ppm (integration 2) and a triplet at −139.8 ppm (integration 1), coupled by $^2J(F_{ax}–F_{eq})$ = 16.2 Hz. This pattern is consistent with the $[Ph_2GeF_3]^-$ anion, where the doublet represents axial fluorines and the triplet represents the equatorial fluorine. The peak at −166 ppm probably represents Ph_2GeF_2, but has yet to be confirmed. THF reactions showed increased complexity. LiF gave a major peak at −156.6 ppm with two smaller peaks at −196 ppm. RbF gave a similar spectrum with a smaller peak at −164.8 ppm and larger peaks at −192.3 and −193.5 ppm. NaF produced several low intensity peaks and an intense peak at −168.1 ppm. KF produced a low intensity peak at −130 ppm and an intense peak at −166 ppm. Interestingly, the CsF reaction in THF mirrored the results in acetonitrile, with two singlets at −112.2 and −127.6 ppm (integration 2 and 1, respectively), strongly suggesting the formation of a $[Ph_2GeF_3]^-$ anion. In this case, no coupling was observed. A summary of the reactions with Ph_3GeCl is shown in Scheme 4.20.

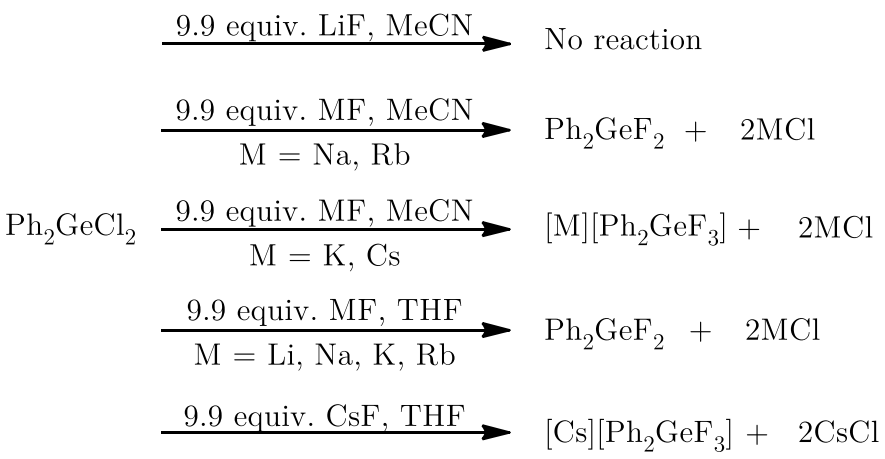

Scheme 4.20: Reaction results of Ph_2GeCl_2 with alkali metal fluorides.

$PhGeCl_3$: Analogous to Ph_2GeCl_2, the lack of reference data for $PhGeF_3$ and the $[PhGeF_4]^-$ anion limits the definitive assignment of the ^{19}F NMR signals. In acetonitrile, LiF did not succeed in converting the starting material. Other alkali metal fluorides produced no discernible signals in either ^1H or ^{19}F NMR, suggesting the formation of insoluble organofluorogermanate salts or other fluorinated species. An exception was RbF, which retained a small amount of unreacted starting material.

In contrast, THF reactions with alkali metal fluorides gave more variable results. LiF and NaF produced a simple spectrum with two peaks at −138.5 and −138.7 ppm. KF produced a more complex spectrum with a dominant peak at −130.0 ppm and two smaller peaks at −136.6 and −141.3 ppm. RbF again produced no detectable signals, indicating the formation of an insoluble product. CsF produced a spectrum with a major peak at −130.0 ppm, similar to KF, accompanied by several minor peaks between −136.6 and −146.4 ppm.

Given the limited reference data, the main peak at −130.0 ppm is tentatively attributed to a $[PhGeF_4]^-$ anion, while signals at lower chemical shifts (−136.6 to −146.4 ppm) could correspond to neutral fluorogermane species. However, further investigation is required for definitive confirmation. A summary of the reactions with $PhGeCl_3$ is shown in Scheme 4.21.

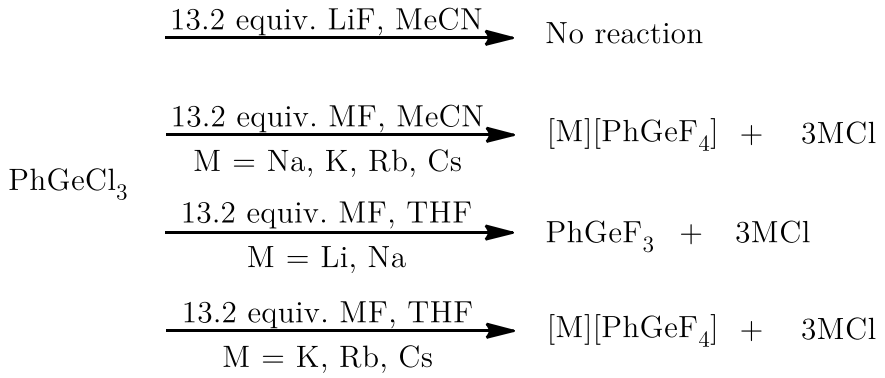

Scheme 4.21: Reaction results of $PhGeCl_3$ with alkali metal fluorides.

In view of the frequent formation of insoluble products in the solvents acetonitrile and THF, alternative solvents for $PhGeCl_3$ reactions were investigated: DMSO, acetone, methanol and tert-butanol. None of these solvents gave new ^{19}F NMR peaks that would indicate the presence of an organofluorogermanate product. However, methanol and *tert-*

butanol each exhibited a single ^{19}F peak at −147.7 and −91.1 ppm, respectively. The reported value for $[N(CH_3)_4][F]$ in methanol-d_3 is −148 ppm [99], strongly suggesting that the observed peak in methanol corresponds to the fluoride anion. Although no reference for the chemical shift of the fluoride ion ^{19}F NMR in *tert*-butanol could be found, repeated reactions of $PhSiCl_3$ and CsF in *tert*-butanol gave the same peak at −91.1 ppm, confirming its assignment to the fluoride anion. Water was excluded as a solvent due to the hydrolysis of the reactants and products.

This screening study of organochlorosilanes and organofluorogermanes with alkali metal fluorides shows how important the choice of reagent and solvent is for a successful conversion to the neutral or anionic species. It has been shown that acetonitrile leads to fewer side reactions and facilitates the formation of organofluorosilicate and organofluorogermanate salts compared to tetrahydrofuran. Compared to other alkali metal fluorides, cesium fluoride proved to be the most successful in the formation of anionic silicon and germanium species.

4.2.3 Summary

This chapter presents a comprehensive study on the reactivity of organofluorosilanes and organofluorogermanes with alkali metal fluorides in acetonitrile and tetrahydrofuran. In this study it was shown that the alkali metal fluorides are not only able to exchange the halogens of organochlorosilanes and organochlorogermanes for fluorine, but also, if present in sufficient quantities, to form new organochlorosilicate and organochlorogermanate species. It has been shown that the choice of alkali metal fluoride reagent and solvent is crucial depending on the final product that is the target of the synthesis.

Using the synthesis procedure described in this chapter, two new polymeric organofluorogermanate structures $[K][Ph_2GeF_3] \cdot 0.75$ MeCN (**9**) and $[Cs][Ph_2GeF_3] \cdot$ THF (**10**) were successfully synthesised and structurally characterised by X-ray structure analysis. The two compounds represent a valuable addition to the little-studied organofluorogermanate chemistry and are the only two organofluorogermanate compounds that form linear polymeric structures.

Chapter 5

Conclusions

This doctoral dissertation presents a comprehensive study on the reactivity of organochlorosilanes and organochlorogermanes with the alkali metal fluorides (LiF, NaF; KF, RbF, CsF) and the reactivity of the corresponding organofluorosilanes and organofluorogermanes with the sterically demanding fluoride reagent [IPrH][F].

The first part of the study focussed on the synthesis and structure determination of new organofluorosilicate and organofluorogermanate salts. The fluorination reagent used was the imidazolium fluoride reagent, which was chosen for its ability to stabilise otherwise unstable discrete anions and was expected to stabilise related discrete organofluorosilicate and organofluorogermanate anion species. Starting materials were commercially available organochlorosilanes [$R_{4-n}SiCl_n$] (n = 1–3, R = Ph, Et) and organochlorogermanes [$Ph_{4-n}GeCl_n$] (n = 1–2), which were first reacted with alkali metal fluorides to obtain the corresponding organofluorosilanes or organofluorogermanes. The reactions were filtered to remove excess insoluble alkali metal fluoride and alkali metal chloride by-products, while the filtrates of these reactions were added to the imidazolium fluoride reagent to synthesise the organofluorosilicate and organofluorogermanate species. Five new organofluorosilicates ([IPrH][Ph_3SiF_2] (**1**), [IPrH][Ph_2SiF_3] (**3**), [IPrH][Et_2SiF_3] (**4**), [IPrH][$PhSiF_4$] (**5**) and [IPrH][$EtSiF_4$] (**6**)) and 2 new organofluorogermanates ([IPrH][Ph_3GeF_2] (**7**) and [IPrH][Ph_2GeF_3] (**8**)) were successfully synthesised and characterised by X-ray crystallography, mass spectrometry, NMR and Raman spectroscopy. The synthesis of [IPrH][Et_3SiF_2] (**2**) was attempted, but no formation of the compound was detected, not even in solution. To gain insight into this chemical system, DFT calculations were performed. The calculations agree with the experimental results as they indicate that the stability of the compound increases with the number of fluorine atoms in the [IPrH][$R_{4-n}MF_n$] (M = Si, Ge; n = 1−3; R = Ph, Et) series.

In particular, this work introduced ethyl-substituted organofluorosilicates (**4**, **6**), which were previously unknown. Despite their weaker Lewis acidity due to the electron-donating substituents, these compounds formed stable organofluorosilicate salts. In addition, organofluorogermanates **7** and **8** represent rare examples of organofluorogermanate salts and are the first structurally characterised compounds of this type with aromatic substituents. This study demonstrates that [IPrH][F] is a suitable reagent for the formation of novel organofluorogermanate and organofluorosilicate species.

Second part of the study presents an extensive and comprehensive study on the reactivity of organochlorosilanes and organochlorogermanes with alkali metal fluorides. Even though alkali metal fluorides are commonly used for halogen exchange of group 14 halides, no previous study reported their side reactions which produce polymeric organofluorosilicate or organofluorogermanate compounds. To date only one related polymeric organofluorosilicate species has been previously reported.

In this study, excess amounts of alkali metal fluorides (LiF, NaF, KF, RbF, CsF) were reacted with commercially available organochlorosilanes [$R_{4-n}SiCl_n$] (n = 1–3, R = Ph, Et) and organochlorogermanes [$Ph_{4-n}GeCl_n$] (n = 1–3) in acetonitrile and tetrahydrofuran. ^{1}H and ^{19}F NMR spectroscopies were performed to analyse the reaction mixtures. It has been shown that alkali metal fluorides are not only capable of exchanging the halogens of

organochlorosilanes and organochlorogermanes for fluorine, but also, if present in sufficient quantities, to form new organochlorosilicate and organochlorogermanate species. Furthermore, it has been shown that the choice of alkali metal fluoride reagent and solvent is crucial depending on the final product that is the target of the synthesis. Lighter alkali metal fluorides are demonstrably less reactive, as they generally only undergo halogen exchange reactions and, in some cases, LiF does not react at all. Cesium fluoride has shown the highest reactivity and has formed the most organofluorosilicate or organofluorogermanate species. Trichlorosilanes and trichlorogermanes were found to be particularly reactive compounds, forming insoluble species that could not be further analysed.

Using the synthetic methods described in this work, two new polymeric organofluorogermanate structures $[K][Ph_2GeF_3] \cdot 0.75$ MeCN (**9**) and $[Cs][Ph_2GeF_3] \cdot$ THF (**10**) and a single polymeric organofluorosilicate $[Cs][Ph_3SiF_2]$ (**11**) were successfully synthesised and structurally characterised by X-ray structure analysis. The two organofluorogermanate compounds represent a valuable addition to the little-studied organofluorogermanate chemistry and are the only two organofluorogermanate compounds that form linear polymeric structures. In contrast, organofluorosilicate **11** forms a two-dimensional layered structure.

More importantly, contrary to expectations, CsF often led to the formation of polymeric species, resulting in little or no yield. In contrast, LiF or NaF proved to be more effective in avoiding these side reactions, which were previously unknown.

Appendix A

A.1 Synthesis and Characterisation of Products

A.1.1 [IPrH][Ph_3SiF_2] (1)

After KF (0.291 g, 2.50 mmol) and Ph_3SiCl (0.147 g, 0.50 mmol) were added to an FEP tube, acetonitrile (5 mL) was added and the resulting suspension was stirred at room temperature for 24 hours. The suspension was then filtered through a PTFE filter and the filtrate was added to a solution of [IPrH][F] (0.204 g, 0.50 mmol) in 5 mL of acetonitrile. The reaction mixture was stirred for a further 24 hours at room temperature. After completion of the reaction, the volatiles were removed by slow evaporation under static vacuum conditions. [IPrH][Ph_3SiF_2] was isolated in the form of yellowish crystals.

^{1}H NMR (MeCN-d_3 , 600 MHz): δ 8.98 (s, 1H, NC*H*N), 7.97 (d, $J = 7.3$, 4H, Ph), 7.84 (s, 1H, NC*H*C*H*N), 7.65 (t, $J = 7.8$, 2H, *p*-C*H*), 7.47 (d, $J = 7.8$, 4H, *m*-C*H*), 7.32 (t, $J = 7.0$, 1H, Ph), 7.22–7.10 (m, 8H, Ph), 2.41 (m, $J = 6.8$, 4H, C*H*CH_3), 1.27 (d, $J = 6.8$, 12H, CHC*H*$_3$), 1.19 (d, $J = 6.8$, 12H, CHC*H*$_3$).

^{13}C NMR (MeCN-d_3 , 151 MHz): δ 146.3, 137.8, 133.1, 127.3, 127.2, 125.7, 29.8, 24.4, 23.8.

^{19}F NMR (MeCN-d_3 , 565 MHz): δ −97.03 (t, $J_{Si–F} = 124.6$).

Raman:ν(Si–F) 667 cm^{-1},ν(Si–C) 1000 cm^{-1}.

HRMS (ESI$^-$): $m/z = 297.0908$ ([Ph_3SiF_2]$^-$ calculated for $C_{18}H_{15}F_2{}^{28}Si$: 297.0911).

A.1.2 [IPrH][Ph_2SiF_3] (3)

After KF (0.581 g, 5.00 mmol) and Ph_2SiCl_2 (0.127 g, 0.50 mmol) were added to an FEP tube, acetonitrile (5 mL) was added and the resulting suspension was stirred at room temperature for 24 hours. The suspension was then filtered through a PTFE filter and the filtrate was added to a solution of [IPrH][F] (0.204 g, 0.50 mmol) in 5 mL of acetonitrile. The reaction mixture was stirred for a further 24 hours at room temperature. After completion of the reaction, the volatiles were removed by slow evaporation under static vacuum conditions. [IPrH][Ph_2SiF_3] was isolated in the form of yellowish crystals.

^{1}H NMR (MeCN-d_3, 600 MHz) δ: 9.15 (s, 1H, NC*H*N), 7.85 (m, 2H, NC*H*C*H*N), 7.78 (m, 4H, Ph), 7.66 (t, $J = 7.8$, 2H, *p*-C*H*), 7.47 (d, $J = 7.8$, 4H, *m*-C*H*), 7.16 (m, 6H, Ph), 2.42 (m, 4H, C*H*CH_3), 1.27 (d, $J = 6.8$ Hz, 12H, CHC*H*$_3$), 1.19 (d, $J = 6.9$ Hz, 12H, CHC*H*$_3$).

^{13}C NMR (MeCN-d_3, 151 MHz,) δ: 146.3, 139.1, 137.8, 135.0, 133.1, 130.9, 128.9, 128.2, 127.4, 127.0, 125.7, 29.9, 24.5, 23.9.

^{19}F NMR (MeCN-d_3, 565 MHz, 233 K) δ: −96.55 (s, axial F), −134.21 (s, equatorial F).

Raman: ν(Si–F) 663 cm^{-1}, ν(Si–C) 999 cm^{-1}.

HRMS (ESI$^-$): $m/z = 239.0511$ ([Ph_2SiF_3]$^-$ calculated for $C_{12}H_{10}F_3{}^{28}Si$: 239.0504).

A.1.3 [IPrH][Et_2SiF_3] (4)

After KF (0.581 g, 5.00 mmol) and Et_2SiCl_2 (0.079 g, 0.50 mmol) were added to an FEP tube, acetonitrile (5 mL) was added and the resulting suspension was stirred at room temperature for 24 hours. The suspension was then filtered through a PTFE filter and the filtrate was added to a solution of [IPrH][F] (0.204 g, 0.50 mmol) in 5 mL of acetonitrile. The reaction mixture was stirred for a further 24 hours at room temperature. After completion of the reaction, the volatiles were removed by slow evaporation under static vacuum conditions. [IPrH][Et_2SiF_3] was isolated in the form of yellowish crystals.

^{1}H NMR (MeCN-d_3, 600 MHz) δ: 9.23 (s, 1H, NC*H*N), 7.90 (s, 2H, NC*H*C*H*N), 7.68 (m, 2H, *p*-C*H*), 7.51 (m, 4H, m-CH), 2.45 (m, 4H, C*H*CH$_3$), 1.30 (d, $J = 5.5$, 12H, CHCH_3), 1.23 (d, $J = 5.5$, 12H, CHCH_3), 0.86 (m, 6H, CH_3), 0.38 (m, 4H, CH_2).

^{13}C NMR (MeCN-d_3 , 151 MHz,) δ: 146.3, 139.3, 133.1, 130.8, 127.0, 125.6, 29.8, 24.4, 23.8, 9.8, 7.8, 6.9.

^{19}F NMR (MeCN-d_3 , 565 MHz, 233 K) δ: −85.99 (s, axial F), −136.17 (s, equatorial F).

HRMS (ESI$^-$): $m/z = 143.0500$ ([Et_2SiF_3]$^-$ calculated for $C_4H_{10}F_3{}^{28}Si$: 143.0504).

A.1.4 [IPrH][$PhSiF_4$] (5)

After KF (0.872 g, 7.50 mmol) and $PhSiCl_3$ (0.106 g, 0.50 mmol) were added to an FEP tube, acetonitrile (5 mL) was added and the resulting suspension was stirred at room temperature for 24 hours. The suspension was then filtered through a PTFE filter and the filtrate was added to a solution of [IPrH][F] (0.204 g, 0.50 mmol) in 5 mL of acetonitrile. The reaction mixture was stirred for a further 24 hours at room temperature. After completion of the reaction, the volatiles were removed by slow evaporation under static vacuum conditions. [IPrH][$PhSiF_4$] was isolated in the form of yellowish crystals. The amount of crystals isolated was sufficient for X-ray diffraction analysis, but not sufficient for NMR, Raman or HRMS spectroscopy.

A.1.5 [IPrH][$EtSiF_4$] (6)

After KF (0.872 g, 7.50 mmol) and $EtSiCl_3$ (0.082 g, 0.50 mmol) were added to an FEP tube, acetonitrile (5 mL) was added and the resulting suspension was stirred at room temperature for 24 hours. The suspension was then filtered through a PTFE filter and the filtrate was added to a solution of [IPrH][F] (0.204 g, 0.50 mmol) in 5 mL of acetonitrile. The reaction mixture was stirred for a further 24 hours at room temperature. After completion of the reaction, the volatiles were removed by slow evaporation under static vacuum conditions. [IPrH][$EtSiF_4$] was isolated in the form of yellowish crystals.

^{1}H NMR (MeCN-d_3, 600 MHz): δ 10.15 (s, 1H, NC*H*N), 7.61 (s, 3H), 7.44 (s, 5H), 2.48 (s, 4H), 1.25 (s, 12H), 1.18 (s, 12H), 0.85 (m, 3H, CH_3), 0.44 (s, 2H, CH_2).

^{13}C NMR (MeCN-d_3, 151 MHz): δ 146.4, 132.7, 125.4, 29.7, 24.5, 23.7, 9.8.

^{19}F NMR (MeCN-d_3, 565 MHz, 233 K): δ −115.75 (t, $J_{Si–F} = 111.6$).

HRMS (ESI$^-$): $m/z = 133.0089$ ([$EtSiF_4$]$^-$ calculated for $C_2H_5F_4{}^{28}Si$: 133.0097).

A.1.6 [IPrH][Ph_3GeF_2] (7)

After KF (0.291 g, 2.50 mmol) and Ph_3GeCl (0.170 g, 0.50 mmol) were added to an FEP tube, acetonitrile (5 mL) was added and the resulting suspension was stirred at room temperature for 24 hours. The suspension was then filtered through a PTFE filter and the filtrate was added to a solution of [IPrH][F] (0.204 g, 0.50 mmol) in 5 mL of acetonitrile. The reaction mixture was stirred for a further 24 hours at room temperature. After

completion of the reaction, the volatiles were removed by slow evaporation under static vacuum conditions. [IPrH][Ph_3GeF_2] was isolated in the form of yellowish crystals.

^{1}H NMR (MeCN-d_3, 600 MHz): δ 10.29 (s, 1H, NC*H*N), 7.86 (s, 2H, NC*H*C*H*N), 7.67 (d, $J = 6.5$, 4H, *m*-C*H*), 7.62 (t, $J = 7.4$, 2H, *p*-C*H*), 7.33–7.55 (m, 13H, Ph), 2.34 (m, 4H, C*H*CH_3), 1.23 (d, $J = 6.1$ Hz, 12H, CHCH_3), 1.13 (d, $J = 6.2$ Hz, 12H, CHCH_3).

^{13}C NMR (MeCN-d_3, 151 MHz): δ 145.8, 139.9, 138.8, 135.0, 132.6, 130.5, 130.4, 128.8, 126.2, 125.1, 29.4, 24.5, 23.1.

^{19}F NMR (MeCN-d_3, 565 MHz, 233 K): δ −143.73 (s).

Raman: ν(Ge–F) 662 cm^{-1}, ν(Ge–C) 999 cm^{-1}.

HRMS (ESI$^-$): $m/z = 343.0364$ ([Ph_3GeF_2]$^-$ calculated for $C_{18}H_{15}F_2{}^{74}Ge$: 343.0354).

A.1.7 [IPrH][Ph_2GeF_3] (8)

After KF (0.291 g, 2.50 mmol) and Ph_2GeCl_2 (0.149 g, 0.50 mmol) were added to an FEP tube, acetonitrile (5 mL) was added and the resulting suspension was stirred at room temperature for 24 hours. The suspension was then filtered through a PTFE filter and the filtrate was added to a solution of [IPrH][F] (0.204 g, 0.50 mmol) in 5 mL of acetonitrile. The reaction mixture was stirred for a further 24 hours at room temperature. After completion of the reaction, the volatiles were removed by slow evaporation under static vacuum conditions. [IPrH][Ph_2GeF_3] was isolated in the form of yellowish crystals.

^{1}H NMR (MeCN-d_3, 600 MHz): δ 9.48 (s, 1H, NC*H*N), 7.88 (s, 2H, NC*H*C*H*N), 7.83 (d, $J = 7.5$ Hz, 4H, $Ph_2GeF_3^-$), 7.65 (t, $J = 7.8$ Hz, 2H, *p*-C*H*), 7.46 (d, $J = 7.8$ Hz, 4H, *m*-C*H*), 7.26 (m, 6H, $Ph_2GeF_3^-$), 2.43 (m, $J = 13.7$ Hz, 4H, C*H*CH_3), 1.26 (d, $J = 6.8$ Hz, 12H, CHCH_3), 1.19 (d, $J = 6.9$ Hz, 12H, CHCH_3).

^{13}C NMR (MeCN-d_3, 151 MHz): δ 146.8, 145.5, 140.4, 137.1, 133.3, 131.5, 130.0, 128.6, 127.4, 126.1, 30.3, 24.9, 24.4.

^{19}F NMR (MeCN-d_3, 565 MHz, 233 K): δ −113.6 (broad singlet, 2F). δ −146.1 (broad singlet, 1F).

A.1.8 [K][Ph_2GeF_3] · 0.75 MeCN (9)

Ph_2GeCl_2 (74 mg, 0.25 mmol) and KF (144 mg, 2.48 mmol) were added to an FEP vessel and suspended in acetonitrile (5 mL). The suspension was stirred at 50 °C for 48 hours. The resulting mixture was filtered with a PTFE filter and the volatiles were removed by slow evaporation under static vacuum conditions to obtain colourless crystals.

A.1.9 [Cs][Ph_2GeF_3] · THF (10)

Ph_2GeCl_2 (74 mg, 0.25 mmol) and CsF (376 mg, 2.48 mmol) were added to an FEP vessel and suspended in tetrahydrofuran (5 mL). The suspension was stirred at 50 °C for 48 hours. The resulting mixture was filtered with a PTFE filter and the volatiles were removed by slow evaporation under static vacuum conditions to obtain colourless crystals.

A.1.10 [Cs][Ph_3SiF_2] (11)

Ph_3SiCl_2 (74 mg, 0.25 mmol) and CsF (376 mg, 2.48 mmol) were added to an FEP vessel and suspended in acetonitrile (5 mL). The suspension was stirred at 50 °C for 48 hours. The resulting mixture was filtered with a PTFE filter and the volatiles were removed by slow evaporation under static vacuum conditions to obtain colourless crystals.

A.2 Crystal Structure Data

Table A.1: Selected crystal data for [IPrH][Ph_3SiF_2] (**1**) and [IPrH][Ph_2SiF_3] (**3**).

	[IPrH][Ph_3SiF_2] (**1**)	[IPrH][Ph_2SiF_3] (**3**)
CCDC No.	2240916	2240917
Chemical formula	$C_{27}H_{37}N_2 \cdot C_{18}H_{15}F_2Si$	$C_{27}H_{37}N_2 \cdot C_{12}H_{10}F_3Si$
F_W (g/mol)	686.97	628.87
T (K)	150	150
λ (Å)	1.54184	1.54184
Crystal size (mm)	0.95 × 0.57 × 0.46	0.59 × 0.46 × 0.25
Crystal system	Monoclinic	Monoclinic
Space group	$P2_1/c$	$P2_1/c$
a (Å)	12.4227(3)	18.4493(2)
b (Å)	18.0014(3)	19.9096(2)
c (Å)	18.7170(4)	20.1610(3)
α (°)	90	90
β (°)	108.699(3)	107.3070(10)
γ (°)	90	90
V (Å^3)	3964.67(16)	7070.21(15)
Z	4	8
ρ_{calc} (g/cm^3)	1.151	1.182
μ (mm^{-1})	0.847	0.944
$F(000)$	1472	2688
Θ range (°)	3.5−72.3	2.8−72.4
Index ranges	$-15 \le h \le 15$ $-21 \le k \le 22$ $-20 \le l \le 22$	$-20 \le h \le 22$ $-24 \le k \le 17$ $-24 \le l \le 24$
Reflections collected	41128	40383
Independent reflections	7763	13662
Reflections with ($I > 2\sigma(I)$)	6558	10288
R_{int}	0.0688	0.0326
Data/restraints/parameters	7763 / 0 / 459	13662 / 0 / 827
S[a]	1.047	1.030
R_1[b], wR_2[c] ($I > 2\sigma(I)$)	0.0480, 0.1266	0.0431, 0.1119
R_1[b], wR_2[c] (all data)	0.0568, 0.1362	0.0608, 0.1242
$\Delta\rho_{min}$, $\Delta\rho_{max}$ (eÅ^{-3})	−0.412, 0.657	−0.345, 0.337

[a] $S = [\Sigma(w(F_o^2-F_c^2)^2)/(N_o-N_p)]^{1/2}$.

[b] $R_1 = ||F_o|-|F_c||/\Sigma|F_o|$.

[c] $wR_2 = [\Sigma(w(F_o^2-F_c^2)^2)/\Sigma(w(F_o^2)^2)]^{1/2}$.

Table A.2: Selected crystal data for [IPrH][Et_2SiF_3] · MeCN (**4**·MeCN) and [IPrH][$PhSiF_4$] (**5**).

	[IPrH][Et_2SiF_3] · MeCN (**4**·MeCN)	[IPrH][$PhSiF_4$] (**5**)
CCDC No.	2240918	2240919
Chemical formula	$C_{27}H_{37}N_2$ · $C_4H_{10}F_3Si$ · C_2H_3N	$C_{27}H_{37}N_2 \cdot C_6H_5F_4Si$
F_W (g/mol)	573.85	570.77
T (K)	150	150
λ (Å)	1.54184	1.54184
Crystal size (mm)	0.76 × 0.48 × 0.34	0.80 × 0.62 × 0.28
Crystal system	Monoclinic	Triclinic
Space group	$P2_1/n$	$P\bar{1}$
a (Å)	10.54523(9)	9.8511(2)
b (Å)	16.13628(15)	17.6141(3)
c (Å)	19.75591(16)	20.1066(3)
α (°)	90	69.107(2)
β (°)	91.4592(8)	82.0820(10)
γ (°)	90	88.7690(10)
V (Å^3)	3360.59(5)	3226.95(11)
Z	4	4
ρ_{calc} (g/cm^3)	1.134	1.175
μ (mm^{-1})	0.950	1.029
$F(000)$	1240	1216
Θ range (°)	3.5–72.3	2.7–72.3
Index ranges	$-13 \le h \le 12$ $-19 \le k \le 19$ $-24 \le l \le 24$	$-12 \le h \le 12$ $-21 \le k \le 21$ $-24 \le l \le 24$
Reflections collected	114300	111155
Independent reflections	6630	12537
Reflections with ($I > 2\sigma(I)$)	5722	10696
R_{int}	0.0649	0.0575
Data/restraints/parameters	6630 / 0 / 398	12537 / 0 / 1006
S[a]	1.051	1.014
R_1[b], wR_2[c] ($I > 2\sigma(I)$)	0.0499, 0.1334	0.0484, 0.1302
R_1[b], wR_2[c] (all data)	0.0565, 0.1423	0.0564, 0.1389
$\Delta\rho_{min}$, $\Delta\rho_{max}$ (eÅ^{-3})	−0.219, 0.474	−0.296, 0.379

[a] $S = [\Sigma(w(F_o^2 - F_c^2)^2)/(N_o - N_p)]^{1/2}$.

[b] $R_1 = ||F_o| - |F_c||/\Sigma|F_o|$.

[c] $wR_2 = [\Sigma(w(F_o^2 - F_c^2)^2)/\Sigma(w(F_o^2)^2)]^{1/2}$.

Table A.3: Selected crystal data for [IPrH][$EtSiF_4$] (**6**) and [IPrH][Ph_3GeF_2] (**7**).

	[IPrH][$EtSiF_4$] (**6**)	[IPrH][Ph_3GeF_2] (**7**)
CCDC No.	2240920	2240921
Chemical formula	$C_{27}H_{37}N_2 \cdot C_2H_5F_4Si$	$C_{27}H_{37}N_2 \cdot C_{18}H_{15}F_2Ge$
F_W (g/mol)	522.73	731.47
T (K)	150	150
λ (Å)	1.54184	1.54184
Crystal size (mm)	0.38 × 0.29 × 0.18	0.52 × 0.23 × 0.06
Crystal system	Monoclinic	Triclinic
Space group	$I2a$	$P\bar{1}$
a (Å)	17.5233(1)	10.6533(3)
b (Å)	39.6998(4)	18.5885(5)
c (Å)	17.5322(1)	20.6911(5)
α (°)	90	94.715(2)
β (°)	90.1310(10)	97.195(2)
γ (°)	90	95.184(2)
V (Å^3)	12196.62(16)	4030.37(19)
Z	16	4
ρ_{calc} (g/cm^3)	1.139	1.205
μ (mm^{-1})	1.042	1.351
$F(000)$	4480	1544
Θ range (°)	2.7−72.3	3.0−72.1
Index ranges	$-21 \leq h \leq 21$ $-42 \leq k \leq 47$ $-21 \leq l \leq 21$	$-12 \leq h \leq 12$ $-22 \leq k \leq 22$ $-25 \leq l \leq 22$
Reflections collected	97660	33630
Independent reflections	11993	15341
Reflections with ($I > 2\sigma(I)$)	11069	11878
R_{int}	0.0337	0.0345
Data/restraints/parameters	11993 / 0 / 709	15341 / 0 / 1033
S[a]	1.020	1.033
R_1[b], wR_2[c] ($I > 2\sigma(I)$)	0.0384, 0.1032	0.0520, 0.1292
R_1[b], wR_2[c] (all data)	0.0430, 0.1073	0.0697, 0.1415
$\Delta\rho_{min}$, $\Delta\rho_{max}$ (eÅ^{-3})	−0.308, 0.344	−0.349, 1.134

[a] $S = [\Sigma(w(F_o^2-F_c^2)^2)/(N_o-N_p)]^{1/2}$.

[b] $R_1 = ||F_o|-|F_c||/\Sigma|F_o|$.

[c] $wR_2 = [\Sigma(w(F_o^2-F_c^2)^2)/\Sigma(w(F_o^2)^2)]^{1/2}$.

Table A.4: Selected crystal data for [IPrH][Ph_3GeF_2] · MeCN (**7a**) and [IPrH][Ph_3GeF_2] · MeCN (**7b**).

	[IPrH][Ph_3GeF_2] · MeCN (**7a**)	[IPrH][Ph_3GeF_2] · MeCN (**7b**)
CCDC No.	2240922	2240923
Chemical formula	$C_{27}H_{37}N_2 \cdot C_{18}H_{15}F_2Ge \cdot C_2H_3N$	$C_{27}H_{37}N_2 \cdot C_{18}H_{15}F_2Ge \cdot C_2H_3N$
F_W (g/mol)	772.53	772.53
T (K)	150	150
λ (Å)	1.54184	1.54184
Crystal size (mm)	0.75 × 0.20 × 0.09	0.44 × 0.29 × 0.2
Crystal system	Triclinic	Orthorhombic
Space group	$P\bar{1}$	$P2_12_12_1$
a (Å)	11.3519(3)	14.4757(1)
b (Å)	12.0229(3)	15.3732(2)
c (Å)	15.6446(4)	18.8377(2)
α (°)	89.256(2)	90
β (°)	81.538(2)	90
γ (°)	80.477(2)	90
V (Å^3)	2082.73(9)	4192.10(7)
Z	2	4
ρ_{calc} (g/cm^3)	1.232	1.224
μ (mm^{-1})	1.341	1.333
$F(000)$	816	1632
Θ range (°)	3.7−72.3	2.8−72.4
Index ranges	$-13 \leq h \leq 13$ $-14 \leq k \leq 14$ $-19 \leq l \leq 19$	$-17 \leq h \leq 17$ $-18 \leq k \leq 18$ $-23 \leq l \leq 23$
Reflections collected	32767	34996
Independent reflections	8068	8093
Reflections with ($I > 2\sigma(I)$)	7139	7783
R_{int}	0.0418	0.0338
Data/restraints/parameters	8068 / 0 / 498	8093 / 0 / 487
S[a]	1.056	1.053
R_1[b], wR_2[c] ($I > 2\sigma(I)$)	0.0354, 0.0851	0.0274, 0.0679
R_1[b], wR_2[c] (all data)	0.0419, 0.0900	0.0293, 0.0692
$\Delta\rho_{min}$, $\Delta\rho_{max}$ (eÅ^{-3})	−0.276, 0.481	−0.229, 0.370

[a] $S = [\Sigma(w(F_o^2 - F_c^2)^2)/(N_o - N_p)]^{1/2}$.

[b] $R_1 = ||F_o| - |F_c||/\Sigma|F_o|$.

[c] $wR_2 = [\Sigma(w(F_o^2 - F_c^2)^2)/\Sigma(w(F_o^2)^2)]^{1/2}$.

Table A.5: Selected crystal data for [K][Ph_2GeF_3] · 0.75 MeCN (**9**) and [Cs][Ph_2GeF_3] · THF (**10**).

	[K][Ph_2GeF_3] · 0.75 MeCN (**9**)	[Cs][Ph_2GeF_3] · THF (**10**)
CCDC Number	2361550	2361556
Chemical formula	$C_{52}H_{46}F_{12}Ge_4K_4N_2 \cdot C_2H_3N$	$C_{16}H_{18}CsF_3GeO$
F_W (g/mol)	1414.72	488.80
T (K)	150	150
λ (Å)	1.54184	0.71073
Crystal size (mm)	0.51 × 0.4 × 0.22	0.79 × 0.46 × 0.33
Crystal system	Monoclinic	Monoclinic
Space group	$P2_1/n$	$P2_1/c$
a (Å)	13.84093 (6)	16.3858 (4)
b (Å)	18.42034 (12)	25.4411 (7)
c (Å)	23.03378 (9)	8.3040 (2)
α (°)	90	90
β (°)	98.0282 (4)	92.022 (2)
γ (°)	90	90
V (Å^3)	5815.01 (5)	3459.56 (15)
Z	4	8
ρ_{calc} (g/cm^3)	1.616	1.877
μ (mm^{-1})	5.623	3.872
F(000)	2824	1888
Θ range (°)	3.0–72.4	2.5–28.7
Index ranges	$-17 \leq h \leq 17$ $-20 \leq k \leq 21$ $-28 \leq l \leq 28$	$-21 \leq h \leq 22$ $-33 \leq k \leq 33$ $-11 \leq l \leq 11$
Reflections collected	158465	66842
Independent reflections	11407	8231
Reflections with ($I > 2\sigma(I)$)	10377	6901
R_{int}	0.0465	0.0914
Data/restraints/parameters	11407 / 0 / 697	8231 / 0 / 406
S[a]	1.043	1.119
R_1[b], wR_2[c] ($I > 2\sigma(I)$)	0.0303, 0.0774	0.0420, 0.0838
R_1[b], wR_2[c] (all data)	0.0344, 0.0803	0.0553, 0.0902
$\Delta\rho_{min}$, $\Delta\rho_{max}$ (eÅ^{-3})	−0.334, 0.702	-1.225, 1.121

[a] $S = [\Sigma(w(F_o^2 - F_c^2)^2)/(N_o - N_p)]^{1/2}$.

[b] $R_1 = ||F_o| - |F_c||/\Sigma|F_o|$.

[c] $wR_2 = [\Sigma(w(F_o^2 - F_c^2)^2)/\Sigma(w(F_o^2)^2)]^{1/2}$.

Table A.6: Selected crystal data for [Cs][Ph_3SiF_2] (**11**).

	[Cs][Ph_3SiF_2] (**11**)
CCDC Number	
Chemical formula	$C_{36}H_{30}Cs_2F_4Si_2$
F_W (g/mol)	860.60
T (K)	150
λ (Å)	1.54184
Crystal size (mm)	0.46 × 0.42 × 0.18
Crystal system	Monoclinic
Space group	$P2_1/c$
a (Å)	13.8001 (2)
b (Å)	18.7711 (3)
c (Å)	13.0331 (3)
α (°)	90
β (°)	95.910 (2)
γ (°)	90
V (Å^3)	3358.19(11)
Z	4
ρ_{calc} (g/cm^3)	1.702
μ (mm^{-1})	18.008
F(000)	1680
Θ range (°)	3.4–76.3
Index ranges	$-16 \leq h \leq 17$ $-23 \leq k \leq 23$ $-16 \leq l \leq 16$
Reflections collected	34792
Independent reflections	6936
Reflections with ($I > 2\sigma(I)$)	6114
R_{int}	0.0658
Data/restraints/parameters	6936 / 0 / 397
S[a]	1.051
R_1[b], wR_2[c] ($I > 2\sigma(I)$)	0.0451, 0.1104
R_1[b], wR_2[c] (all data)	0.0517, 0.1182
$\Delta\rho_{min}$, $\Delta\rho_{max}$ (eÅ^{-3})	-0.641, 1.915

[a] $S = [\Sigma(w(F_o^2-F_c^2)^2)/(N_o-N_p)]^{1/2}$.

[b] $R_1 = ||F_o|-|F_c||/\Sigma|F_o|$.

[c] $wR_2 = [\Sigma(w(F_o^2-F_c^2)^2)/\Sigma(w(F_o^2)^2)]^{1/2}$.

A.3 Molecular Calculations

Table A.7: Calculated electronic energies (E) at the PBE/def2TZVP level of theory and calculated energies of reactions ΔE in a.u. and kJ/mol.

Compound	E / a.u.	Reaction	ΔE / a.u.	ΔE / kJ/mol
[IPrH][F]	−1259.4111232			
Et_3SiF	−626.67114995			
Et_2SiF_2	−647.39000789			
$EtSiF_3$	−668.10336467			
SiF_4	−688.81168744			
Ph_3SiF	−1083.5715290			
Ph_2SiF_2	−951.98720139			
$PhSiF_3$	−820.40216887			
Et_3GeF	−2413.9706465			
Et_2GeF_2	−2434.6670501			
$EtGeF_3$	−2455.3540030			
GeF_4	−2476.0264617			
Ph_3GeF	−2870.8679849			
Ph_2GeF_2	−2739.2614349			
$PhGeF_3$	−2607.6499366			
[IPrH][Et_3SiF_2] (**2**)	−1886.0989692	Et_3SiF + [IPrH][F] → [IPrH][Et_3SiF_2]	−0.0166960	**−44**
[IPrH][Et_2SiF_3] (**4**)	−1906.8287845	Et_2SiF_2 + [IPrH][F] → [IPrH][Et_2SiF_3]	−0.0276534	**−73**
[IPrH][$EtSiF_4$] (**6**)	−1927.5507372	$EtSiF_3$ + [IPrH][F] → [IPrH][$EtSiF_4$]	−0.0362493	**−95**
[IPrH][SiF_5]	−1948.2696837	SiF_4 + [IPrH][F] → [IPrH][SiF_5]	−0.0468731	**−123**
[IPrH][Ph_3SiF_2] (**1**)	−2343.0148273	Ph_3SiF + [IPrH][F] → [IPrH][Ph_3SiF_2]	−0.0321751	**−84**
[IPrH][Ph_2SiF_3] (**3**)	−2211.4377454	Ph_2SiF_2 + [IPrH][F] → [IPrH][Ph_2SiF_3]	−0.0394208	**−103**
[IPrH][$PhSiF_4$] (**5**)	−2079.8560493	$PhSiF_3$ + [IPrH][F] → [IPrH][$PhSiF_4$]	−0.0427572	**−112**
[IPrH][SiF_5]	−1948.2696837	SiF_4 + [IPrH][F] → [IPrH][SiF_5]	−0.0468731	**−123**
[IPrH][Et_3GeF_2] (**7**)	−3673.4042062	Et_3GeF + [IPrH][F] → [IPrH][Et_3GeF_2]	−0.0224365	**−59**
[IPrH][Et_2GeF_3]	−3694.1140978	Et_2GeF_2 + [IPrH][F] → [IPrH][Et_2GeF_3]	−0.0359245	**−94**
[IPrH][$EtGeF_4$]	−3714.8103514	$EtGeF_3$ + [IPrH][F] → [IPrH][$EtGeF_4$]	−0.0452252	**−119**
[IPrH][GeF_5]	−3735.5005421	GeF_4 + [IPrH][F] → [IPrH][GeF_5]	−0.0629572	**−165**

[IPrH][Ph_3GeF_2]	−4130.3124792	Ph_3GeF + [IPrH][F] → [IPrH][Ph_3GeF_2]	−0.0333711	**−88**
[IPrH][Ph_2GeF_3]	−3998.7176148	Ph_2GeF_2 + [IPrH][F] → [IPrH][Ph_2GeF_3]	−0.0450567	**−118**
[IPrH][$PhGeF_4$]	−3867.1121370	$PhGeF_3$ + [IPrH][F] → [IPrH][$PhGeF_4$]	−0.0510772	**−134**
[IPrH][GeF_5]	−3735.5005421	GeF_4 + [IPrH][F] → [IPrH][GeF_5]	−0.0629572	**−165**

References

[1] K. Müller, C. Faeh, and F. Diederich, "Fluorine in pharmaceuticals: Looking beyond intuition," *Science*, vol. 317, no. 5846, pp. 1881–1886, Sep. 2007, doi: 10.1126/SCIENCE.1131943.

[2] S. Purser, P. R. Moore, S. Swallow, and V. Gouverneur, "Fluorine in medicinal chemistry," *Chem. Soc. Rev.*, vol. 37, no. 2, pp. 320–330, Jan. 2008, doi: 10.1039/B610213C.

[3] T. Fujiwara and D. O'Hagan, "Successful fluorine-containing herbicide agrochemicals," *J. Fluor. Chem.*, vol. 167, pp. 16–29, Nov. 2014, doi: 10.1016/J.JFLUCHEM.2014.06.014.

[4] N. A. Meanwell, "Fluorine and Fluorinated Motifs in the Design and Application of Bioisosteres for Drug Design," *J. Med. Chem.*, vol. 61, no. 14, pp. 5822–5880, Jul. 2018, doi: 10.1021/ACS.JMEDCHEM.7B01788.

[5] B. E. Smart, "Fluorine substituent effects (on bioactivity)," *J. Fluor. Chem.*, vol. 109, no. 1, pp. 3–11, Jun. 2001, doi: 10.1016/S0022-1139(01)00375-X.

[6] M. Morgenthaler *et al.*, "Predicting and Tuning Physicochemical Properties in Lead Optimization: Amine Basicities," *ChemMedChem*, vol. 2, no. 8, pp. 1100–1115, Aug. 2007, doi: 10.1002/CMDC.200700059.

[7] M. A. Massa *et al.*, "Novel heteroaryl replacements of aromatic 3-tetrafluoroethoxy substituents in trifluoro-3-(tertiaryamino)-2-propanols as potent inhibitors of cholesteryl ester transfer protein," *Bioorg. Med. Chem. Lett.*, vol. 11, no. 13, pp. 1625–1628, Jul. 2001, doi: 10.1016/S0960-894X(01)00244-X.

[8] J. P. Bégué and D. Bonnet-Delpon, "Recent advances (1995–2005) in fluorinated pharmaceuticals based on natural products," *J. Fluor. Chem.*, vol. 127, no. 8, pp. 992–1012, Aug. 2006, doi: 10.1016/J.JFLUCHEM.2006.05.006.

[9] C. Isanbor and D. O'Hagan, "Fluorine in medicinal chemistry: A review of anti-cancer agents," *J. Fluor. Chem.*, vol. 127, no. 3, pp. 303–319, Mar. 2006, doi: 10.1016/J.JFLUCHEM.2006.01.011.

[10] K. L. Kirk, "Fluorine in medicinal chemistry: Recent therapeutic applications of fluorinated small molecules," *J. Fluor. Chem.*, vol. 127, no. 8, pp. 1013–1029, Aug. 2006, doi: 10.1016/J.JFLUCHEM.2006.06.007.

[11] Q. Wang *et al.*, "FDA approved fluorine-containing drugs in 2023," *Chinese Chem. Lett.*, vol. 35, no. 11, p. 109780, Nov. 2024, doi: 10.1016/J.CCLET.2024.109780.

[12] A. P. Lea and D. McTavish, "Atorvastatin. A review of its pharmacology and therapeutic potential in the management of hyperlipidaemias," *Drugs*, vol. 53, no. 5, pp. 828–847, Oct. 1997, doi: 10.2165/00003495-199753050-00011.

[13] K. Drlica and M. Malik, "Fluoroquinolones: Action and Resistance," *Curr. Top. Med. Chem.*, vol. 3, no. 3, pp. 249–282, Mar. 2005, doi: 10.2174/1568026033452537.

[14] D. T. Wong, F. P. Bymaster, and E. A. Engleman, "Prozac (fluoxetine, lilly 110140), the first selective serotonin uptake inhibitor and an antidepressant drug: Twenty years since its first publication," *Life Sci.*, vol. 57, no. 5, pp. 411–441, Jun. 1995, doi: 10.1016/0024-3205(95)00209-O.

[15] V. Subbiah *et al.*, "Structural basis of acquired resistance to selpercatinib and pralsetinib mediated by non-gatekeeper RET mutations," *Ann. Oncol.*, vol. 32, no. 2, pp. 261–268, Feb. 2021, doi: 10.1016/J.ANNONC.2020.10.599.

[16] C. F. Xia *et al.*, "[^{18}F]T807, a novel tau positron emission tomography imaging agent for Alzheimer's disease," *Alzheimer's Dement.*, vol. 9, no. 6, pp. 666–676, Nov. 2013, doi: 10.1016/J.JALZ.2012.11.008.

[17] S. Segal-Maurer *et al.*, "Capsid Inhibition with Lenacapavir in Multidrug-Resistant HIV-1 Infection," *N. Engl. J. Med.*, vol. 386, no. 19, pp. 1793–1803, May 2022, doi: 10.1056/NEJMOA2115542.

[18] J. D. Sobel and P. Nyirjesy, "Oteseconazole: An Advance in Treatment of Recurrent Vulvovaginal Candidiasis," *Future Microbiol.*, vol. 16, no. 18, pp. 1453–1461, Dec. 2021, doi: 10.2217/FMB-2021-0173.

[19] M. J. . Welch and C. S. . Redvanly, *Handbook of radiopharmaceuticals : radiochemistry and applications*. J. Wiley, 2003.

[20] *Positron Emission Tomography Basic Sciences*. Springer-Verlag London Limited, 2005.

[21] D. O'Hagan and H. Deng, "Enzymatic fluorination and biotechnological developments of the fluorinase," *Chem. Rev.*, vol. 115, no. 2, pp. 634–649, Jan. 2015, doi: 10.1021/CR500209T.

[22] J. Aigueperse *et al.*, "Fluorine Compounds, Inorganic," *Ullmann's Encycl. Ind. Chem.*, Jun. 2000, doi: 10.1002/14356007.A11_307.

[23] A. Harsanyi and G. Sandford, "Organofluorine chemistry: applications, sources and sustainability," *Green Chem.*, vol. 17, no. 4, pp. 2081–2086, Apr. 2015, doi: 10.1039/C4GC02166E.

[24] S. Caron, "Where Does the Fluorine Come From? A Review on the Challenges Associated with the Synthesis of Organofluorine Compounds," *Org. Process Res. Dev.*, vol. 24, no. 4, pp. 470–480, Apr. 2020, doi: 10.1021/ACS.OPRD.0C00030.

[25] J. G. Speight, *Environmental industrial inorganic chemistry for Engineers*, vol. 1, no. Chapter 3. Butterworth-Heinemann, 2017.

[26] J. C. Bertolini, "Hydrofluoric acid: a review of toxicity," *J. Emerg. Med.*, vol. 10, no. 2, pp. 163–168, 1992, doi: 10.1016/0736-4679(92)90211-B.

[27] P. A. Champagne, J. Desroches, J. D. Hamel, M. Vandamme, and J. F. Paquin, "Monofluorination of Organic Compounds: 10 Years of Innovation," *Chem. Rev.*, vol. 115, no. 17, pp. 9073–9174, Sep. 2015, doi: 10.1021/CR500706A.

[28] W. J. Middleton, "New Fluorinating Reagents. Dialkylaminosulfur Fluorides," *J. Org. Chem.*, vol. 40, no. 5, pp. 574–578, Mar. 1975, doi: 10.1021/JO00893A007.

[29] G. S. Lal, G. P. Fez, R. J. Pesaresi, and F. M. Prozonic, "Bis(2-methoxyethyl)aminosulfur trifluoride: a new broad-spectrum deoxofluorinating

agent with enhanced thermal stability," *Chem. Commun.*, no. 2, pp. 215–216, Jan. 1999, doi: 10.1039/A808517J.

[30] M. K. Nielsen, C. R. Ugaz, W. Li, and A. G. Doyle, "PyFluor: A low-cost, stable, and selective deoxyfluorination reagent," *J. Am. Chem. Soc.*, vol. 137, no. 30, pp. 9571–9574, Aug. 2015, doi: 10.1021/JACS.5B06307.

[31] N. W. Goldberg, X. Shen, J. Li, and T. Ritter, "AlkylFluor: Deoxyfluorination of Alcohols," *Org. Lett.*, vol. 18, no. 23, pp. 6102–6104, Dec. 2016, doi: 10.1021/ACS.ORGLETT.6B03086.

[32] T. Fujimoto and T. Ritter, "PhenoFluorMix: Practical chemoselective deoxyfluorination of phenols," *Org. Lett.*, vol. 17, no. 3, pp. 544–547, Feb. 2015, doi: 10.1021/OL5035518.

[33] S. D. Taylor, C. C. Kotoris, and G. Hum, "Recent advances in electrophilic fluorination," *Tetrahedron*, vol. 55, no. 43, pp. 12431–12477, Oct. 1999, doi: 10.1016/S0040-4020(99)00748-6.

[34] W. J. Middleton and E. M. Bingham, "α-Fluorination of Carbonyl Compounds with CF3OF," *J. Am. Chem. Soc.*, vol. 102, no. 14, pp. 4845–4846, 1980, doi: 10.1021/JA00534A053.

[35] B. L. Shapiro and M. M. Chrysam, "α -Fluoro-3,3,5,5-Tetrasubstituted Cyclohexanones. I. Synthesis and Conformational Analysis," *J. Org. Chem.*, vol. 38, no. 5, pp. 880–893, Mar. 1973, doi: 10.1021/JO00945A008.

[36] S. Rozen and O. Lerman, "Synthesis and Chemistry of Trifluoroacetyl Hypofluorite with Elemental Fluorine. A Novel Method for Synthesis of α-Fluorohydrins," *J. Org. Chem.*, vol. 45, no. 4, pp. 672–678, 1980, doi: 10.1021/JO01292A025.

[37] E. H. Appelman and L. J. Basile, "Fluoroxysulfate: A powerful new oxidant and fluorinating agent," *J. Am. Chem. Soc.*, vol. 101, no. 12, pp. 3384–3385, Jun. 1979, doi: 10.1021/JA00506A046.

[38] B. Zajc and M. Zupan, "Room temperature fluorination of 1,3-diketones and enol acetates with xenon difluoride," *J. Chem. Soc. Chem. Commun.*, no. 16, pp. 759–760, Jan. 1980, doi: 10.1039/C39800000759.

[39] G. S. Lal, G. P. Pez, and R. G. Syvret, "Electrophilic NF fluorinating agents," *Chem. Rev.*, vol. 96, no. 5, pp. 1737–1755, 1996, doi: 10.1021/CR941145P.

[40] A. S. Kiselyov, "Chemistry of *N*-fluoropyridinium salts," *Chem. Soc. Rev.*, vol. 34, no. 12, pp. 1031–1037, Nov. 2005, doi: 10.1039/B509217P.

[41] E. Differding and H. Ofner, "*N*-Fluorobenzenesulfonimide: A Practical Reagent for Electrophilic Fluorinations," *Synlett*, vol. 1991, no. 3, pp. 187–189, Mar. 1991, doi: 10.1055/S-1991-20673/BIB.

[42] P. T. Nyffeler, S. G. Durón, M. D. Burkart, S. P. Vincent, and C. H. Wong, "Selectfluor: Mechanistic Insight and Applications," *Angew. Chem. Int. Ed.*, vol. 44, no. 2, pp. 192–212, Jan. 2005, doi: 10.1002/ANIE.200400648.

[43] S. Stavber, M. Zupan, A. J. Poss, and G. A. Shia, "1-Fluoro-4-hydroxy-1,4-diazoniabicyclo[2.2.2]octane bis(tetrafluoroborate) as a new, effective reagent for selective fluorofunctionalisation of alkenes under mild reaction conditions," *Tetrahedron Lett.*, vol. 36, no. 37, pp. 6769–6772, Sep. 1995, doi: 10.1016/00404-0399(50)1337-H.

[44] M. P. Sibi and Y. Landais, "C_{sp3}-F bond formation: A free-radical approach," *Angew. Chem. Int. Ed.*, vol. 52, no. 13, pp. 3570–3572, Mar. 2013, doi: 10.1002/ANIE.201209583.

[45] V. Grakauskas, "Aqueous Fluorination of Carboxylic Acid Salts," *J. Org. Chem.*, vol. 34, no. 8, pp. 2446–2450, 1969, doi: 10.1021/JO01260A040.

[46] S. Rozen, "Elemental Fluorine as a 'Legitimate' Reagent for Selective Fluorination of Organic Compounds," *Acc. Chem. Res.*, vol. 21, no. 8, pp. 307–312, Aug. 1988, doi: 10.1021/AR00152A004.

[47] T. B. Patrick, S. Khazaeli, S. Nadji, K. Hering-Smith, and D. Reif, "Mechanistic Studies of Fluorodecarboxylation with Xenon Difluoride," *J. Org. Chem.*, vol. 58, no. 3, pp. 705–708, 1993, doi: 10.1021/JO00055A026.

[48] M. Rueda-Becerril *et al.*, "Fluorine transfer to alkyl radicals," *J. Am. Chem. Soc.*, vol. 134, no. 9, pp. 4026–4029, Mar. 2012, doi: 10.1021/JA211679V.

[49] M. Döbele, S. Vanderheiden, N. Jung, and S. Bräse, "Synthesis of Aryl Fluorides on a Solid Support and in Solution by Utilizing a Fluorinated Solvent," *Angew. Chem. Int. Ed.*, vol. 49, no. 34, pp. 5986–5988, Aug. 2010, doi: 10.1002/ANIE.201001507.

[50] D. Meyer, H. Jangra, F. Walther, H. Zipse, and P. Renaud, "A third generation of radical fluorinating agents based on *N*-fluoro-N-arylsulfonamides," *Nat. Commun. 2018 91*, vol. 9, no. 1, pp. 1–10, Nov. 2018, doi: 10.1038/s41467-018-07196-9.

[51] Claire Breliere *et al.*, "Preparation and NMR Studies of Hexacoordinated Fluorosilicates: Nondissociative Fluorine Site Exchange within the Octahedral Complexes in Solution," *Organometallics*, vol. 11, no. 4, pp. 1586–1593, Apr. 1992, doi: 10.1021/OM00040A032.

[52] R. Tacke and M. Mühleisen, "Hexacoordinate Silicon in a Compound with an F_5SiC Unit," *Angew. Chem. Int. Ed.*, vol. 33, no. 13, pp. 1359–1360, Jul. 1994, doi: 10.1002/ANIE.199413591.

[53] M. Pülm, J. Becht, and R. Tacke, "Singly charged λ^6Si-silicate anions with an SiF_5C skeleton: Syntheses and crystal structure analyses of the ionic hexacoordinate silicon compounds $[Me_3NH][F_5SiCH_2NMe_2H] \cdot H_2O$ and $[Me_3NH][F_5SiCH_2NMe_3] \cdot H_2O$," *Zeitschrift fur Naturforsch. - Sect. B J. Chem. Sci.*, vol. 55, no. 1, pp. 60–64, 2000, doi: 10.1515/znb-2000-0111.

[54] J. Harloff, D. Michalik, S. Nier, A. Schulz, P. Stoer, and A. Villinger, "Cyanidosilicates—Synthesis and Structure," *Angew. Chem. Int. Ed.*, vol. 58, no. 16, pp. 5452–5456, Apr. 2019, doi: 10.1002/ANIE.201901173.

[55] William J. Middleton, "Tris(dimethylamino)sulfonium difluorotrimethylsilicate," *Org. Synth.*, vol. 64, p. 221, 1986, doi: 10.15227/ORGSYN.064.0221.

[56] A. S. Pilcher, H. L. Ammon, and P. DeShong, "Utilization of Tetrabutylammonium (Triphenylsilyl)difluorosilicate as a Fluoride Source for Nucleophilic Fluorination," *J. Am. Chem. Soc.*, vol. 117, no. 18, pp. 5166–5167, 1995, doi: 10.1021/JA00123A025.

[57] T. Wang and D. H. Wang, "Potassium Alkylpentafluorosilicates, Primary Alkyl Radical Precursors in the C-1 Alkylation of Tetrahydroisoquinolines," *Org. Lett.*, vol. 21, no. 11, pp. 3981–3985, Jun. 2019, doi: 10.1021/ACS.ORGLETT.9B01124.

[58] J. M. Posz, S. R. Harruff, and R. Van Hoveln, "Practical and scalable synthesis of

bench-stable organofluorosilicate salts," *Chem. Commun.*, vol. 56, no. 86, pp. 13233–13236, Oct. 2020, doi: 10.1039/D0CC05400C.

[59] D. Kost *et al.*, "New zwitterionic pentacoordinate silicates with $SiONFC_2$, $SiONF_2C$, and SiO_2N_2C frameworks: Synthesis, structure, and dynamic stereochemistry," *Organometallics*, vol. 19, no. 6, pp. 1083–1095, Mar. 2000, doi: 10.1021/OM990842A.

[60] L. J. P. Van Der Boon *et al.*, "Chiral Control in Pentacoordinate Systems: The Case of Organosilicates," *Inorg. Chem.*, vol. 57, no. 20, pp. 12697–12708, Oct. 2018, doi: 10.1021/ACS.INORGCHEM.8B01861.

[61] R. O. Day *et al.*, "Anionic Five-Coordinated Cyclic Organofluorosilicates Varying in Ring Size from Five- to Seven-Membered," *Organometallics*, vol. 10, no. 6, pp. 1758–1766, Jun. 1991, doi: 10.1021/OM00052A022.

[62] D. Brondani, F. H. Carré, R. J. P. Corriu, J. J. E. Moreau, and M. W. C. Man, "Synthesis and Dynamic Behavior of the Heptafluorotrisilacyclohexane Anion: A New Fluxional Silicate with Rapid Intramolecular Exchange of Fluoride Ligand," *Angew. Chem. Int. Ed.*, vol. 35, no. 3, pp. 324–326, Feb. 1996, doi: 10.1002/ANIE.199603241.

[63] M. Kira, E. Kwon, C. Kabuto, and K. Sakamoto, "X-ray crystal structure and dynamic behavior of pentafluoro-9,10-disila-9,10-dihydroanthracene anion salts having transannular 1,4-fluorine bridge," *Chem. Lett.*, no. 11, pp. 1183–1184, Nov. 1999, doi: 10.1246/cl.1999.1183.

[64] R. Pietschnig and K. Merz, "The first polymer with a fluorosilicate backbone and a non-polar shell," *Chem. Commun.*, vol. 1, no. 13, pp. 1210–1211, Jan. 2001, doi: 10.1039/B102853G.

[65] S. Pelzer, B. Neumann, H. G. Stammler, N. Ignat'ev, and B. Hoge, "Hypervalent Pentafluoroethylgermanium Compounds, $[(C_2F_5)_nGeX_{5-n}]^-$ and $[(C_2F_5)_3GeF_3]_2^-$ (X=F, Cl; n=2–5)," *Chem. Eur. J*, vol. 22, no. 46, pp. 16460–16466, Nov. 2016, doi: 10.1002/CHEM.201602859.

[66] D. J. Brauer, J. Wilke, and R. Eujen, "Tris- and tetrakis-(trifluoromethyl)fluorogermanates; the structure of an anion with pentacoordinated germanium," *J. Organomet. Chem.*, vol. 316, no. 3, pp. 261–269, Dec. 1986, doi: 10.1016/0022-328X(86)80495-8.

[67] D. J. Brauer, H. Bürger, and R. Eujen, "(Trifluoromethyl)fluorogermanates," *Angew. Chem. Int. Ed.*, vol. 19, no. 10, pp. 836–837, Oct. 1980, doi: 10.1002/ANIE.198008361.

[68] B. Ališ and G. Tavčar, "Reaction of N-heterocyclic carbene (NHC) with different HF sources and ratios – A free fluoride reagent based on imidazolium fluoride," *J. Fluor. Chem.*, vol. 192, pp. 141–146, Dec. 2016, doi: 10.1016/J.JFLUCHEM.2016.11.004.

[69] R. K. Harris, E. D. Becker, S. M. De Cabral Menezes, P. Granger, R. E. Hoffman, and K. W. Zilm, "Further conventions for NMR shielding and chemical shifts (IUPAC Recommendations 2008)," *Magn. Reson. Chem.*, vol. 46, no. 6, pp. 582–598, Jun. 2008, doi: 10.1002/MRC.2225.

[70] "CrysAlisPro Data Collection and Processing Software for Agilent X-ray Diffractometers," *Agilent*. 2013.

[71] R. C. Clark and J. S. Reid, "The analytical calculation of absorption in multifaceted crystals," *Acta Crystallogr. Sect. A*, vol. 51, no. 6, pp. 887–897, Nov. 1995, doi: 10.1107/S0108767395007367.

[72] G. M. Sheldrick, "SHELXT - integrated space-group and crystal-structure determination," *Acta Crystallogr. Sect. A*, vol. 71, no. Pt 1, pp. 3–8, Jan. 2015, doi: 10.1107/S2053273314026370.

[73] G. M. Sheldrick and IUCr, "Crystal structure refinement with SHELXL," *urn:issn:2053-2296*, vol. 71, no. 1, pp. 3–8, Jan. 2015, doi: 10.1107/S2053229614024218.

[74] O. V. Dolomanov, L. J. Bourhis, R. J. Gildea, J. A. K. Howard, and H. Puschmann, "OLEX2: A complete structure solution, refinement and analysis program," *J. Appl. Crystallogr.*, vol. 42, no. 2, pp. 339–341, Jan. 2009, doi: 10.1107/S0021889808042726.

[75] "Diamond - Crystal and Molecular Structure Visualization." http://www.crystalimpact.com/diamond/ (accessed Jan. 13, 2023).

[76] "Gaussian 16 | Gaussian.com." https://gaussian.com/gaussian16/ (accessed Jan. 29, 2023).

[77] J. P. Perdew, K. Burke, and M. Ernzerhof, "Generalized Gradient Approximation Made Simple," *Phys. Rev. Lett.*, vol. 77, no. 18, p. 3865, Oct. 1996, doi: 10.1103/PhysRevLett.77.3865.

[78] S. Grimme, J. Antony, S. Ehrlich, and H. Krieg, "A consistent and accurate ab initio parametrization of density functional dispersion correction (DFT-D) for the 94 elements H-Pu," *J. Chem. Phys.*, vol. 132, no. 15, p. 154104, Apr. 2010, doi: 10.1063/1.3382344.

[79] S. Grimme, S. Ehrlich, and L. Goerigk, "Effect of the damping function in dispersion corrected density functional theory," *J. Comput. Chem.*, vol. 32, no. 7, pp. 1456–1465, May 2011, doi: 10.1002/JCC.21759.

[80] F. Weigend and R. Ahlrichs, "Balanced basis sets of split valence, triple zeta valence and quadruple zeta valence quality for H to Rn: Design and assessment of accuracy," *Phys. Chem. Chem. Phys.*, vol. 7, no. 18, pp. 3297–3305, Aug. 2005, doi: 10.1039/B508541A.

[81] F. Weigend, "Accurate Coulomb-fitting basis sets for H to Rn," *Phys. Chem. Chem. Phys.*, vol. 8, no. 9, pp. 1057–1065, Feb. 2006, doi: 10.1039/B515623H.

[82] J. Gnidovec, E. Gruden, M. Tramšek, J. Iskra, J. Kvíčala, and G. Tavčar, "Synthesis of imidazolium-based pentacoordinated organofluorosilicate and germanate salts," *Dalt. Trans.*, vol. 52, no. 16, pp. 5085–5094, Apr. 2023, doi: 10.1039/D3DT00421J.

[83] J. Gnidovec and G. Tavčar, "Investigation of polymeric organofluorosilicates and organofluorogermanates," *J. Fluor. Chem.*, vol. 278, p. 110332, Aug. 2024, doi: 10.1016/J.JFLUCHEM.2024.110332.

[84] S. Yamaguchi, S. Akiyama, and K. Tamao, "Effect of countercation inclusion by [2.2.2]cryptand upon stabilization of potassium organofluorosilicates," *Organometallics*, vol. 18, no. 15, pp. 2851–2854, Jul. 1999, doi: 10.1021/OM990085G.

[85] P. D. Prince, M. J. Bearpark, G. S. McGrady, and J. W. Steed, "Hypervalent hydridosilicates: synthesis, structure and hydride bridging," *Dalt. Trans.*, no. 2, pp.

271–282, Dec. 2007, doi: 10.1039/B713427D.

[86] A. F. Hill, J. S. Ward, and Y. Xiong, "Synthesis of a Stable Methylidyne Complex," *Organometallics*, vol. 34, no. 20, pp. 5057–5064, Oct. 2015, doi: 10.1021/ACS.ORGANOMET.5B00635.

[87] C. Bolli *et al.*, "Bis(triphenyl-λ^5-phosphanylidene)ammonium fluoride: a reactive fluoride source to access the hypervalent silicates $[Me_nSiF_{5-n}]-$ (n = 0–3)," *Dalt. Trans.*, vol. 43, no. 11, pp. 4326–4334, Feb. 2014, doi: 10.1039/C3DT52617H.

[88] E. Lork, D. Viets, M. Müller, and R. Mews, "Bis(dimethylamino)trifluoromethylsulfonium Salze: $[CF_3S(NMe_2)_2]^+[Me_3SiF_2]^-$, $[CF_3S(NMe_2)_2]^+[HF_2]^-$ und $[CF_3S(NMe_2)_2]^+[CF_3S]^-$," *Z. Anorg. Allg. Chem.*, vol. 630, no. 15, pp. 2692–2696, Dec. 2004, doi: 10.1002/ZAAC.200400242.

[89] F. Klanberg and E. L. Muetterties, "Nuclear Magnetic Resonance Studies on Pentacoordinate Silicon Fluorides," *Inorg. Chem.*, vol. 7, no. 1, pp. 155–160, Jan. 1968, doi: 10.1021/IC50059A032.

[90] B. Ališ, M. Tramšek, A. Kokalj, and G. Tavčar, "Discrete GeF_5^- Anion Structurally Characterized with a Readily Synthesized Imidazolium Based Naked Fluoride Reagent," *Inorg. Chem.*, vol. 56, no. 16, pp. 10070–10077, Aug. 2017, doi: 10.1021/acs.inorgchem.7b01606.

[91] E. Gruden, M. Tramšek, and G. Tavčar, "Discrete Organofluoroaluminate Anions: Synthetic, Structural, and Spectroscopic Aspects," *Organometallics*, vol. 41, no. 1, pp. 41–51, Jan. 2022, doi: 10.1021/ACS.ORGANOMET.1C00601.

[92] Ž. Zupanek, M. Tramšek, A. Kokalj, and G. Tavčar, "Reactivity of VOF_3 with N-Heterocyclic Carbene and Imidazolium Fluoride: Analysis of Ligand-VOF_3 Bonding with Evidence of a Minute π Back-Donation of Fluoride," *Inorg. Chem.*, vol. 57, no. 21, pp. 13866–13879, Nov. 2018, doi: 10.1021/ACS.INORGCHEM.8B02377.

[93] Ž. Zupanek, M. Tramšek, A. Kokalj, and G. Tavčar, "The peculiar case of conformations in coordination compounds of group V pentahalides with N-heterocyclic carbene and synthesis of their imidazolium salts," *J. Fluor. Chem.*, vol. 227, p. 109373, Nov. 2019, doi: 10.1016/J.JFLUCHEM.2019.109373.

[94] G. Meißner, K. Kretschmar, T. Braun, and E. Kemnitz, "Consecutive Transformations of Tetrafluoropropenes: Hydrogermylation and Catalytic C−F Activation Steps at a Lewis Acidic Aluminum Fluoride," *Angew. Chem. Int. Ed.*, vol. 56, no. 51, pp. 16338–16341, Dec. 2017, doi: 10.1002/ANIE.201707759.

[95] E. Schnell and E. G. Rochow, "The nuclear magnetic resonance of fluorine in fluorosilanes," *J. Inorg. Nucl. Chem.*, vol. 6, no. 4, pp. 303–307, Jul. 1958, doi: 10.1016/0022-1902(58)80112-8.

[96] B. Lecachey *et al.*, "Intertwined Analytical, Experimental and Theoretical Studies on the Formation and Structure of a Copper Dienolate," *Chem. Eur. J*, vol. 27, no. 29, pp. 7942–7950, May 2021, doi: 10.1002/CHEM.202100596.

[97] A. Hermannsdorfer and M. Driess, "Isolable Silicon-Based Polycations with Lewis Superacidity," *Angew. Chem. Int. Ed.*, vol. 59, no. 51, pp. 23132–23136, Dec. 2020, doi: 10.1002/ANIE.202011696.

[98] G. A. Molander and L. Iannazzo, "Palladium-catalyzed Hiyama cross-coupling of aryltrifluorosilanes with aryl and heteroaryl chlorides," *J. Org. Chem.*, vol. 76, no.

21, pp. 9182–9187, Nov. 2011, doi: 10.1021/JO201840N.

[99] K. O. Christe, W. W. Wilson, R. D. Wilson, R. Ban, and J. an Feng, "Syntheses, Properties, and Structures of Anhydrous Tetramethylammonium Fluoride and Its 1:1 Adduct with trans-3-Amino-2-butenenitrile," *J. Am. Chem. Soc.*, vol. 112, no. 21, pp. 7619–7625, 1990, doi: 10.1021/JA00177A025.

Bibliography

Publications Related to the Thesis

Journal Articles

J. Gnidovec, E. Gruden, M. Tramšek, J. Iskra, J. Kvíčala, G. Tavčar (2023). Synthesis of imidazolium-based pentacoordinated organofluorosilicate and germanate salts, *Dalt. Trans.*, 52, 5085–5094. DOI: 10.1039/D3DT00421J.

J. Gnidovec, G. Tavčar (2024). Investigation of polymeric organofluorosilicates and organofluorogermanates, *J. Fluor. Chem.*, 278, 1–10. DOI: 10.1016/j.jfluchem.2024.110332.

Conference Paper

J. Gnidovec, G. Tavčar (2022). Preparation of new hypervalent Group 14 based nucleophilic fluorination reagents. *In 14th Jožef Stefan International Postgraduate School Students' Conference*. Kamnik, Slovenia: International Postgraduate School Jožef, Jožef Stefan Institute.

J. Gnidovec, G. Tavčar (2022). Synthesis of hypervalent Group 14 based nucleophilic fluorination reagents. In *20th European Symposium on Fluorine Chemistry*. Berlin, Germany: Humboldt-Universität, Institut für Chemie.

J. Gnidovec, G. Tavčar (2022). Synthesis of hypervalent silicon and germanium fluorides as potential fluorination reagents. In *28th Annual Meeting of the Slovenian Chemical Society*. Portorož, Slovenia: Slovenian Chemical Society.

J. Gnidovec, E. Gruden, M. Tramšek, J. Iskra, J. Kvíčala, G. Tavčar (2023). Synthesis of pentacoordinated organofluorosilicate and germanate salts. In *7th Fluorine Days*. Poznań, Poland: Adam Mickiewicz University.

G. Tavčar, J. Gnidovec, E. Gruden, J. Iskra, J. Kvíčala, M. Tramšek (2023). Imidazolium fluoride as a reagent with compounds of group 14 elements. In *23rd International Symposium on Fluorine Chemistry and the 9th International Symposium on Fluorous Technologies*. Québec City, Canada: University of Lethbridge, Trinity Western University, McMaster University, Université Laval.

G. Tavčar, J. Gnidovec, M. Tramšek (2024). Pentacoordinated organofluorosilicates and organofluorogermanates. In *2nd South African Fluorine Symposium*. Sun City, South Africa: Humboldt-Universität, Philipps-University Marburg, University of Pretoria.

Biography

The author of this thesis, Jan Gnidovec, was born on 22th May 1995 in Ljubljana, Slovenia. After finishing his primary education at the Primary School Rodica in 2010 and his secondary education at the high school Škofijska klasična gimnazija in 2014, he enrolled in the Chemistry study programme at the Faculty of Chemistry and Chemical Technology, University of Ljubljana. Author obtained his bachelor's degree in 2017 by defending his bachelor's thesis with the title "Organocatalyzed reactions of isatin imines with ornithine derived pyrrolone" under the supervision of Prof. Dr. Uroš Grošelj. He obtained his master's degree in 2019 by with thesis titled "Organocatalyzed spiroheterocyclization of arylidene-pyrrolone derivatives with 1,4-dithiane-2,5-diole" also under supervision of Prof. Dr. Uroš Grošelj. In the same year he received the funding from the Slovenian Research Agency and a position as a young researcher at the Department of Inorganic Chemistry and Technology at Jožef Stefan Institute, Ljubljana, Slovenia. Concurrently, he continued his academic education under the supervision of Assoc. Prof. Dr. Gašper Tavčar at the Jožef Stefan International Postgraduate School, Ljubljana, Slovenia. Jan Gnidovec reached the stage of a PhD candidate in his doctoral study in 2024.